

# Rpl12 is a conserved ribophagy receptor

Received: 6 March 2024

Accepted: 12 December 2024

Published online: 11 February 2025

 Check for updates

Yuting Chen<sup>1,2,21</sup>, Jiaxin Hu<sup>3,21</sup>, Pengwei Zhao<sup>1,21</sup>, Jie Fang<sup>4,5,6,21</sup>, Yingqi Kuang<sup>1</sup>, Zhaojie Liu<sup>2,7</sup>, Shuling Dong<sup>1,8</sup>, Weijing Yao<sup>1</sup>, Yuanyuan Ding<sup>9</sup>, Xinhui Wang<sup>10</sup>, Yibin Pan<sup>11,12</sup>, Jianbin Wu<sup>13</sup>, Jingwei Zhao<sup>13</sup>, Jing Yang<sup>14</sup>, Zhenzhong Xu<sup>14,15</sup>, Xiaodi Liu<sup>2</sup>, Yi Zhang<sup>1</sup>, Choufei Wu<sup>8</sup>, Liqin Zhang<sup>8</sup>, Mingzhu Fan<sup>16</sup>, Shan Feng<sup>16</sup>, Zhi Hong<sup>17,18</sup>, Zhangming Yan<sup>19</sup>, Hongguang Xia<sup>1</sup>, Kaiyue Tang<sup>20</sup>, Bing Yang<sup>16,20</sup>, Wei Liu<sup>1</sup>, Qiming Sun<sup>1</sup>, Kunrong Mei<sup>9</sup>✉, Wei Zou<sup>4,5</sup>✉, Yunpeng Huang<sup>3</sup>✉, Du Feng<sup>2,7</sup>✉ & Cong Yi<sup>1</sup>✉

Ribophagy is a selective autophagic process that regulates ribosome turnover. Although NUFIP1 has been identified as a mammalian receptor for ribophagy, its homologues do not exist in yeast and nematodes. Here we demonstrate that Rpl12, a ribosomal large subunit protein, functions as a conserved ribophagy receptor in multiple organisms. Disruption of Rpl12–Atg8s binding leads to significant accumulation of ribosomal proteins and rRNA, while Atg1-mediated Rpl12 phosphorylation enhances its association with Atg11, thus triggering ribophagy during starvation. Ribophagy deficiency accelerates cell death induced by starvation and pathogen infection, leading to impaired growth and development and a shortened lifespan in both *Caenorhabditis elegans* and *Drosophila melanogaster*. Moreover, ribophagy deficiency results in motor impairments associated with ageing, while the overexpression of RPL12 significantly improves movement defects induced by starvation, ageing and A $\beta$  accumulation in fly models. Our findings suggest that Rpl12 functions as a conserved ribophagy receptor vital for ribosome metabolism and cellular homeostasis.

Ribosome turnover is a vital cellular process allowing rapid adaptation to environmental changes for survival in the most efficient manner<sup>1</sup>. During nutrient abundance, ribosome synthesis increases, enabling the translation of numerous proteins to support cell growth and proliferation. Conversely, nutrient deprivation inhibits protein translation, leading to ribosome degradation and subsequent utilization of resulting amino acids and nucleotides for essential protein and RNA synthesis, crucial for cell survival. In this process, autophagy plays a pivotal role in ribosome turnover<sup>2,3</sup>. In *Saccharomyces cerevisiae*, the ubiquitin protease Ubp3p/Bre5p and its partners Cdc48 and Ufd3 have been found to be specifically required for the selective autophagy of the 60S ribosomal subunit but not the 40S ribosomal subunit under nitrogen starvation conditions<sup>4</sup>. However, the receptor for ribophagy in yeast remains unidentified. In mammals, NUFIP1 has been identified as a ribophagy receptor for starvation-induced

ribophagy. During amino acid starvation, NUFIP1 translocates from the nucleus to the autophagosome via binding with LC3B, along with ribosome. Deficiency in NUFIP1–LC3B binding impairs the degradation of ribosomal proteins and rRNAs<sup>5</sup>. Nevertheless, a recent report revealed that NUFIP1 is involved in rRNA degradation, not ribosomal protein degradation, in mouse cancer-associated fibroblast (mCAF) cells under conditions of glutamine deprivation<sup>6</sup>, suggesting the potential involvement of other ribophagy receptor(s) in ribosome turnover.

In this study, we uncovered the critical role of Rpl12 in ribophagy. Rpl12 promotes autophagosome incorporation and ribosome degradation via binding Atg8s. Further research reveals that Rpl12-mediated ribophagy is required for various physiological processes. Our findings demonstrate that Rpl12 is a conserved ribophagy receptor required for ribosome turnover and the maintenance of cellular homeostasis.

A full list of affiliations appears at the end of the paper. ✉e-mail: [kmei@tju.edu.cn](mailto:kmei@tju.edu.cn); [zouwei@zju.edu.cn](mailto:zouwei@zju.edu.cn); [huangyp@ucas.ac.cn](mailto:huangyp@ucas.ac.cn); [Fenglab@gzhmu.edu.cn](mailto:Fenglab@gzhmu.edu.cn); [yiconglab@zju.edu.cn](mailto:yiconglab@zju.edu.cn)

## Results

### Rpl12 binds directly to both Atg8 and Atg11

Given the highly conserved nature of ribophagy from yeast to humans, we aimed to identify potential NUFIP1 homologues across various species. Bioinformatic analysis revealed the absence of a homologue in yeast and *Caenorhabditis elegans*<sup>7</sup>, suggesting the existence of alternative ribophagy receptor(s) in these organisms (Fig. 1a). To identify the yeast ribophagy receptor, we performed in vitro pull-down experiments by incubating purified yeast wild-type (WT) glutathione S-transferase (GST)–Atg8 or GST–Atg8<sup>Y49A-L50A</sup> protein (the latter mutant unable to bind receptors) from *Escherichia coli* with starvation-treated yeast lysates<sup>8</sup> (Fig. 1b). Mass spectrometry (MS) analysis revealed that ribosomal proteins Rpl12, Rpl8, Rpl3, Rps22, Rpl17, Rpl32 and Rps3 bind to WT Atg8 but not to Atg8<sup>Y49A-L50A</sup> (Extended Data Fig. 1a and Supplementary Tables 1–3). Yeast two-hybrid (Y2H) assays were then used to determine which of these proteins could directly interact with Atg8. The results showed that only Rpl12 could directly interact with WT Atg8, failing to do so with Atg8<sup>Y49A-L50A</sup> (Fig. 1c and Extended Data Fig. 1b). Furthermore, a nickel-nitriilotriacetic acid (Ni-NTA) pull-down experiment confirmed that Rpl12 binds directly with WT Atg8, but not with Atg8<sup>Y49A-L50A</sup> (Fig. 1d). In yeast, Rpl12 has two paralogues, Rpl12a and Rpl12b, possessing distinct promoters but encoding identical proteins<sup>9</sup>. In this study, we focused on Rpl12a as the candidate ribophagy receptor. To confirm the Rpl12–Atg8 interaction in yeast cells, we co-expressed haemagglutinin (HA)–Rpl12 along with green fluorescent protein (GFP)–Atg8 or GFP–Atg8<sup>Y49A-L50A</sup> in *atg8Δ* cells. Immunoprecipitation assays consistently showed that GFP–Atg8 binds to Rpl12, with substantially reduced association in the GFP–Atg8<sup>Y49A-L50A</sup> mutant under starvation (Fig. 1e). Another characteristic of receptors involves their interaction with Atg11 through its CC4 domain<sup>10</sup>. Y2H, immunoprecipitation and GST pull-down assays demonstrated that Atg11 directly binds to Rpl12 via its CC4 domain (Fig. 1f,g and Extended Data Fig. 1c–e). Altogether, these findings suggest that Rpl12 interacts directly with both Atg8 and Atg11.

Next, we aimed to explore the specific region(s) on Rpl12 required for its association with Atg8. Previous studies have shown that LC3-interacting region motifs or Atg8-interaction motifs (AIM) are crucial for selective autophagy receptors to bind to the LC3-interacting region docking site of Atg8/LC3 (ref. 11). Bioinformatic analysis identified two potential AIM regions in Rpl12: Y12-LY-L15 and F53-KG-I56 (ref. 12). However, Y2H assay revealed that mutations in these two motifs did not disrupt the Rpl12–Atg8 interactions (Extended Data Fig. 1f), suggesting that the binding of Rpl12 to Atg8 is independent of the classic AIM region. To delineate which regions of Rpl12 are responsible for Atg8 binding, we generated a series of Rpl12 deletion variants (Extended Data Fig. 1g). Y2H assays indicated that the region 2–30 amino acid (aa) of Rpl12 is required for its binding with Atg8 (Extended Data Fig. 1h). Further Y2H analysis using specific deletions within this region demonstrated that both the 2–4aa and the 21–23aa regions are required for Rpl12 binding to Atg8 (Extended Data Fig. 1i–k). We next introduced a series of amino

acid substitutions within the two identified regions for Y2H screening. The results showed that the P3 and E21 residues of Rpl12 are crucial for binding to Atg8 (Fig. 1h and Extended Data Fig. 1l,m). Subsequently, the Rpl12<sup>P3N-E21L</sup> mutant was tested for its Atg8 binding capability using GST pull-down assays. The results revealed a complete loss of Rpl12–Atg8 binding in the His–TF–Rpl12<sup>P3N-E21L</sup> mutant (where TF is trigger factor) (Fig. 1i). To rule out potential artefacts, we expressed WT Rpl12 and Rpl12<sup>P3N-E21L</sup> mutant with a smaller His–small ubiquitin-like modifier (SUMO) tag and performed a Ni-NTA pull-down assay using untagged Atg8. The results confirmed that Rpl12 directly interacts with Atg8 and that this interaction is specifically dependent on the P3 and E21 residues (Fig. 1j). Furthermore, co-immunoprecipitation (co-IP) assays confirmed almost complete inhibition of Rpl12–Atg8 binding in the Rpl12<sup>P3N-E21L</sup> mutants (Fig. 1k).

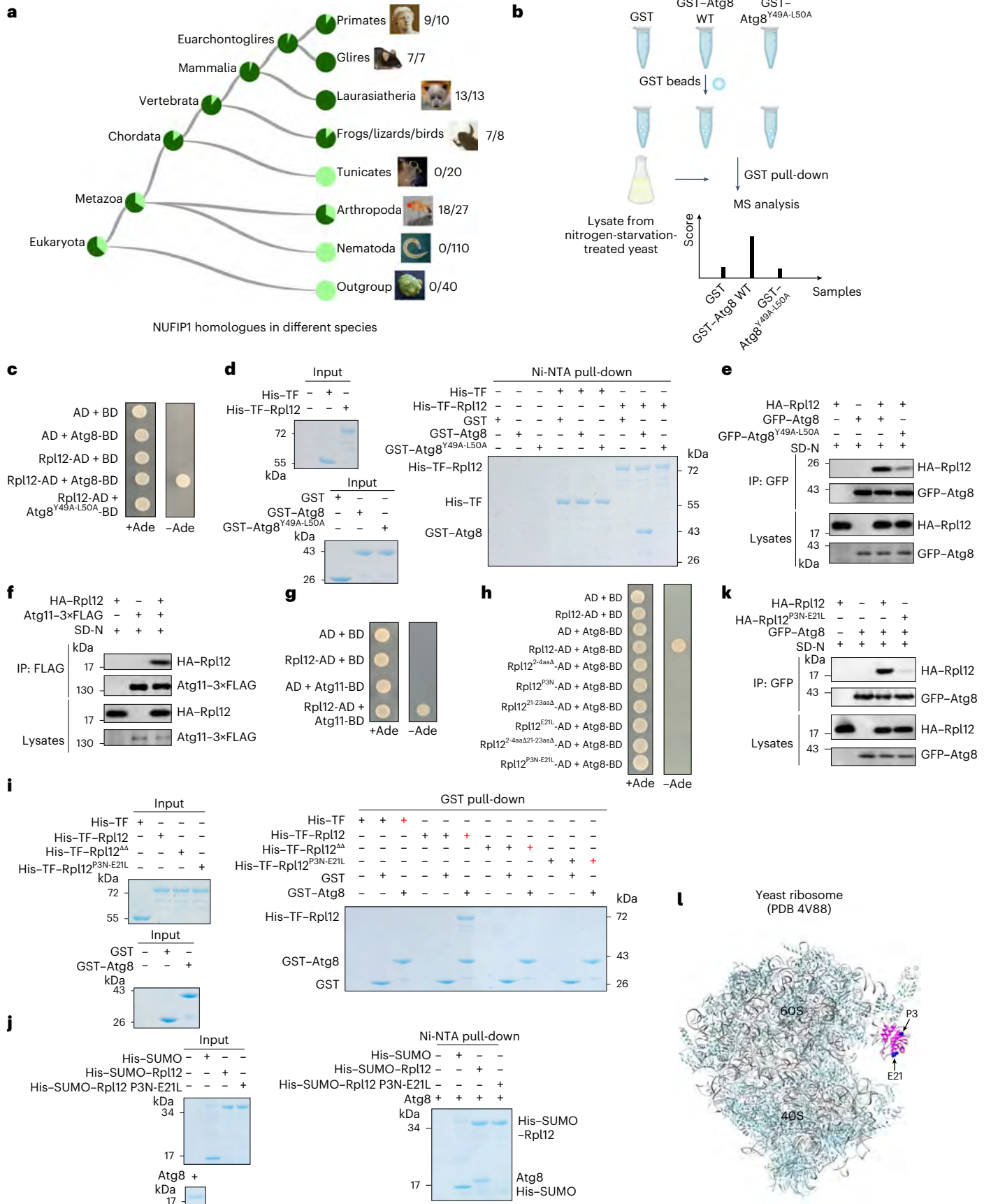
For a protein to function as a ribophagy receptor, it is crucial that it is situated on the ribosome's surface, with its Atg8 binding site exposed and free from interaction with ribosome-associated proteins or rRNA during ribophagy. To assess if Rpl12 meets these prerequisites, we examined the crystal structure of yeast ribosomes. Our analysis revealed that Rpl12 resides on the outer surface of the yeast 80S ribosome, with its N-terminal domain remaining unbound, showing no interaction with ribosome-associated proteins or rRNA (Fig. 1l). Furthermore, using cross-linking MS and genetically encoded chemical cross-linking, we confirmed that the peptide segment containing P3 and E21 directly interacts with Atg8 (Extended Data Fig. 1n,o).

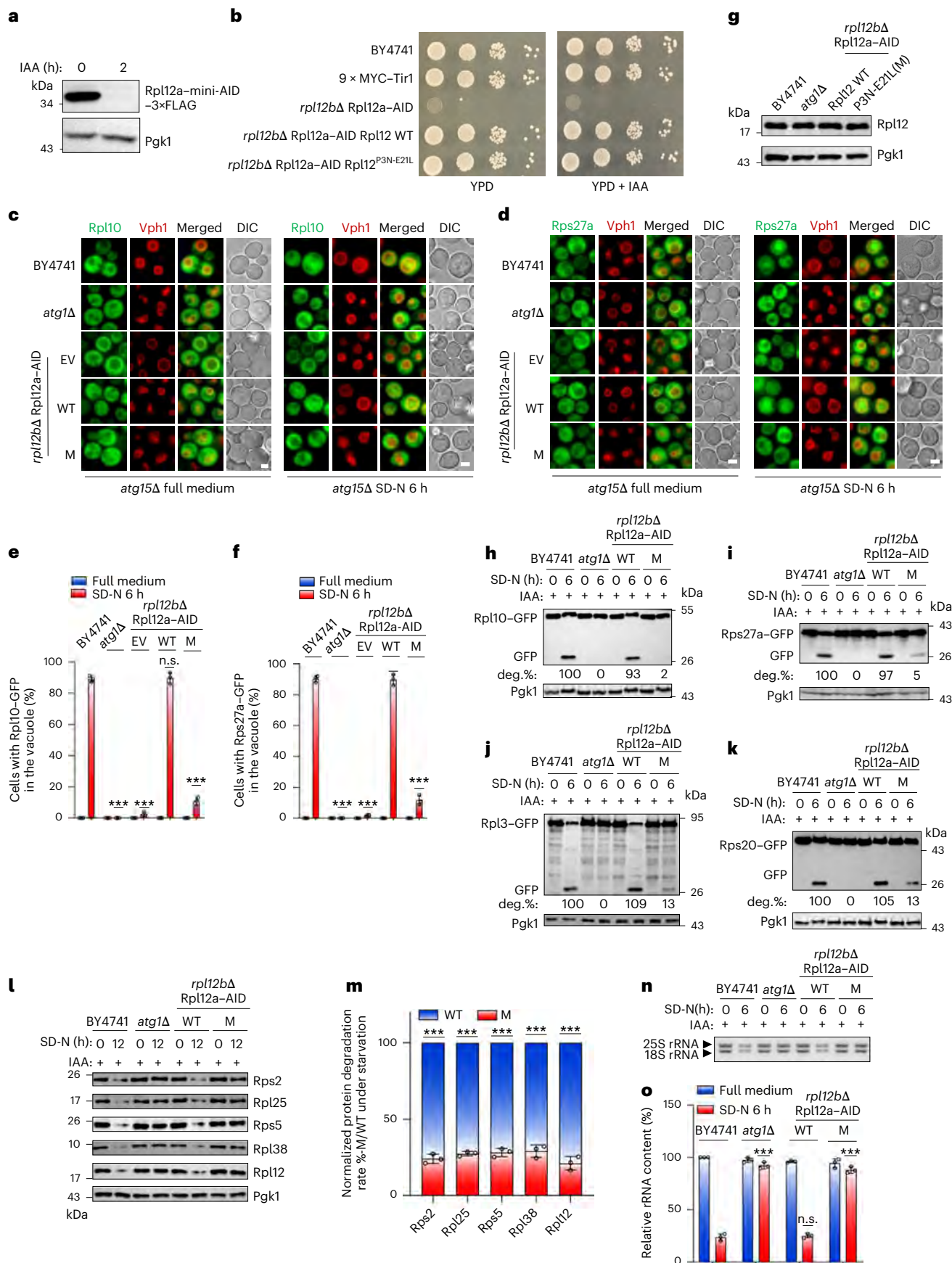
### Rpl12 is a ribophagy receptor in yeast

We next investigated whether Rpl12 functions as a ribophagy receptor. Since double knockout (KO) of *RPL12A* and *RPL12B* is lethal for cell viability, we utilized an auxin-inducible degron system to degrade the endogenous Rpl12a in *rpl12bΔ* yeast cells<sup>13</sup>. As shown in Fig. 2a, the Rpl12a protein degraded rapidly upon treatment with indoleacetic acid (IAA). Nevertheless, a spotting assay showed severely impaired growth in *rpl12bΔ* cells expressing Rpl12a–mini-AID–3×FLAG (hereafter referred to as Rpl12a–AID), regardless of IAA treatment, indicating that the mini-AID–3×FLAG tag at the C-terminal of Rpl12a may affected its structure or its binding to ribosomes (Extended Data Fig. 2a). Using this yeast strain, we investigated whether Rpl12a is degraded under starvation conditions and whether its degradation depends on the activity of vacuolar acid hydrolases. The results demonstrated that Rpl12a–AID is degraded in WT cells during starvation, while its degradation is significantly inhibited in *pep4Δ* cells, indicating that the degradation of Rpl12a–AID relies on the vacuolar pathway (Extended Data Fig. 2b,c). Subsequent tests showed that KO of *RPL12B* with IAA treatment almost completely blocked the cleavage of multiple ribosomal proteins fused with GFP tags (Extended Data Fig. 2d–k), highlighting the importance of Rpl12 in ribophagy. To further confirm the pivotal role of Rpl12 in ribophagy, we generated specific antibodies targeting yeast ribosomal proteins. Western blot analysis showed marked degradation of ribosomal proteins in WT yeast cells under

**Fig. 1 | Rpl12 directly interacts with Atg8 and Atg11.** **a**, Orthologues of human NUFIP1 gene were identified using the PANTHER database (version 17.0). **b**, A flowchart illustrating the process of identifying the yeast ribophagy receptor. **c**, The AH109 strain was transformed with Rpl12-activation domain (AD) and either Atg8-binding domain (BD) or Atg8<sup>Y49A-L50A</sup>-BD, followed by growth on SD–Leu–Trp or SD–Leu–Trp–Ade agar plates at 30 °C for 3 days. **d**, Ni-NTA pull-down assays were performed with purified His-tagged TF or His–TF–Rpl12 protein, and GST, GST–Atg8 or GST–Atg8<sup>Y49A-L50A</sup> from *E. coli*. Protein samples were separated by SDS–PAGE and visualized using Coomassie blue staining. **e**, *atg8Δ* yeast cells co-expressing HA–Rpl12a with either GFP–Atg8 or the GFP–Atg8<sup>Y49A-L50A</sup> were subjected to nitrogen starvation (SD–N) for 1 h. Cell lysates were immunoprecipitated using anti-GFP agarose beads and analysed by western blot with an anti-HA antibody. **f**, Yeast cells co-expressing HA–Rpl12 with Atg11–3×FLAG were subjected to SD–N for 1 h. Cell lysates were immunoprecipitated using anti-FLAG agarose beads and analysed by western blot with an anti-HA

antibody. **g,h**, The AH109 strain was co-transformed with the Rpl12-AD and Atg11-BD (**g**) plasmids or the indicated Rpl12 variants and Atg8-BD (**h**) plasmids, followed by growth on the indicated agar plates at 30 °C for 3 days. Ade, adenine. **i**, GST pull-downs were performed using purified His–TF, His–TF–Rpl12, or its variants with GST or GST–Atg8 from *E. coli*. Protein samples were separated by SDS–PAGE and visualized using Coomassie blue staining. **j**, Ni-NTA pull-downs were performed using purified His-tagged SUMO, His–SUMO–Rpl12 or His–SUMO–Rpl12<sup>P3N-E21L</sup> protein with Atg8 from *E. coli*. Protein samples were separated by SDS–PAGE and detected using Coomassie blue staining. **k**, Yeast cells co-expressing either HA–Rpl12 or HA–Rpl12<sup>P3N-E21L</sup> with GFP–Atg8 were subjected to SD–N for 1 h. Cell lysates were immunoprecipitated using anti-GFP agarose beads and analysed using western blot with an anti-HA antibody. **l**, The spatial positions of the P3 and E21 residues in yeast Rpl12 within the ribosome (PDB 4V88). The data presented in **c–j** are representative of three independent experiments. Unprocessed blots and gels are provided.





starvation, whereas both *ATG1* KO and Rpl12 knockdown (KD) yeast cells exhibited substantial inhibition in ribosomal proteins degradation (Extended Data Fig. 2l,m). Consistently, a significant decrease in rRNA levels was observed in WT cells under starvation, whereas

*ATG1* KO or Rpl12 KD yeast cells exhibited a marked inhibition of rRNA degradation (Extended Data Fig. 2n,o).

To validate the unique role of Rpl12 in ribophagy, we randomly selected a ribosomal large subunit protein, Rpl34, and a small subunit

**Fig. 2 | Rpl12 functions as a ribophagy receptor in yeast.** **a**, *rpl12bΔ* cells expressing Rpl12a–mini-AID–3×FLAG were treated with 0.5 mM IAA treatment for 2 h and the expression of Rpl12a–mini-AID–3×FLAG was detected using an anti-FLAG antibody. The data are representative of two independent experiments. **b**, The indicated yeast cells were grown on Yeast extract Peptone Dextrose (YPD) with or without IAA agar plates for 2 days at 30 °C. **c,d**, The indicated yeast cells co-expressing GFP-tagged Rpl10 (**c**) or Rps27a (**d**) with Vph1–mCherry were treated with IAA for 2 h, followed by SD-N for 0 h or 6 h. Images of cells were obtained using fluorescence microscopy. Scale bars in differential interference contrast (DIC) panels, 2 μm. **e,f**, Cells from **c** (**e**) and **d** (**f**) were quantified for the vacuolar localization of Rpl10–GFP or Rps27a–GFP. *n* = 300 cells were pooled from three independent experiments. **g**, The indicated proteins were detected by anti-Rpl12 antibody. Data are representative of two independent experiments. **h–k**, BY4741, *atg1Δ* and *rpl12bΔ* Rpl12a–AID yeast cells, carrying either WT Rpl12a or the Rpl12a<sup>P3N-E21L</sup> (**m**) mutant and expressing Rpl10–GFP (**h**), Rps27a–GFP (**i**),

Rpl3–GFP (**j**) or Rps20–GFP (**k**), were treated with IAA for 2 h and then subjected to SD-N for 6 h. The ribophagic activity was analysed by western blot for the cleavage of the GFP fusion protein, deg.%, percentage of degradation. The results were quantified (Methods). **l**, The indicated yeast cells were treated with IAA for 2 h and then subjected to SD-N for 12 h. Protein samples were analysed by western blot using the indicated anti-ribosomal protein antibodies. **m**, The degradation ratios of the indicated proteins from **l** were quantified. **n**, The indicated yeast cells were treated with IAA for 2 h and then subjected to SD-N for 6 h. Five OD<sub>600</sub> yeast cells were collected and total RNA was extracted to detect the expression level of yeast rRNA. **o**, Yeast rRNA from **n** was quantified. The data presented in **b–d**, **h–l** and **n** are representative of three independent experiments. Pgk1 served as a loading control. The data in **e**, **f**, **m** and **o** are presented as mean ± s.d. (*n* = 3 biologically independent experiments). \*\*\**P* < 0.001; n.s., no significance; two-tailed Student's *t*-tests were used. Exact *P* values, source numerical data and unprocessed blots or gels are provided.

protein, Rps9, to examine their involvement in this process. Using the auxin-induced protein degradation system, we successfully induced degradation of Rpl34 and Rps9 proteins (Extended Data Fig. 2p,q). However, western blotting and rRNA analysis indicated that Rps9 and Rpl34 did not participate in ribophagy (Extended Data Fig. 2r–t), indicating the specificity and significance of Rpl12 in ribophagy. To investigate whether the reduction of ribosomal proteins and rRNA under starvation is dependent on the vacuole, we conducted a series of experiments, including testing for accelerated turnover, *PEP4* KO<sup>14</sup>, the use of the translation inhibitor cycloheximide (CHX) and the KO of *RNY1* (ref. 15). The results showed that the reduction in ribosomal proteins and rRNA under starvation is indeed primarily due to vacuolar degradation (Extended Data Fig. 3a–j).

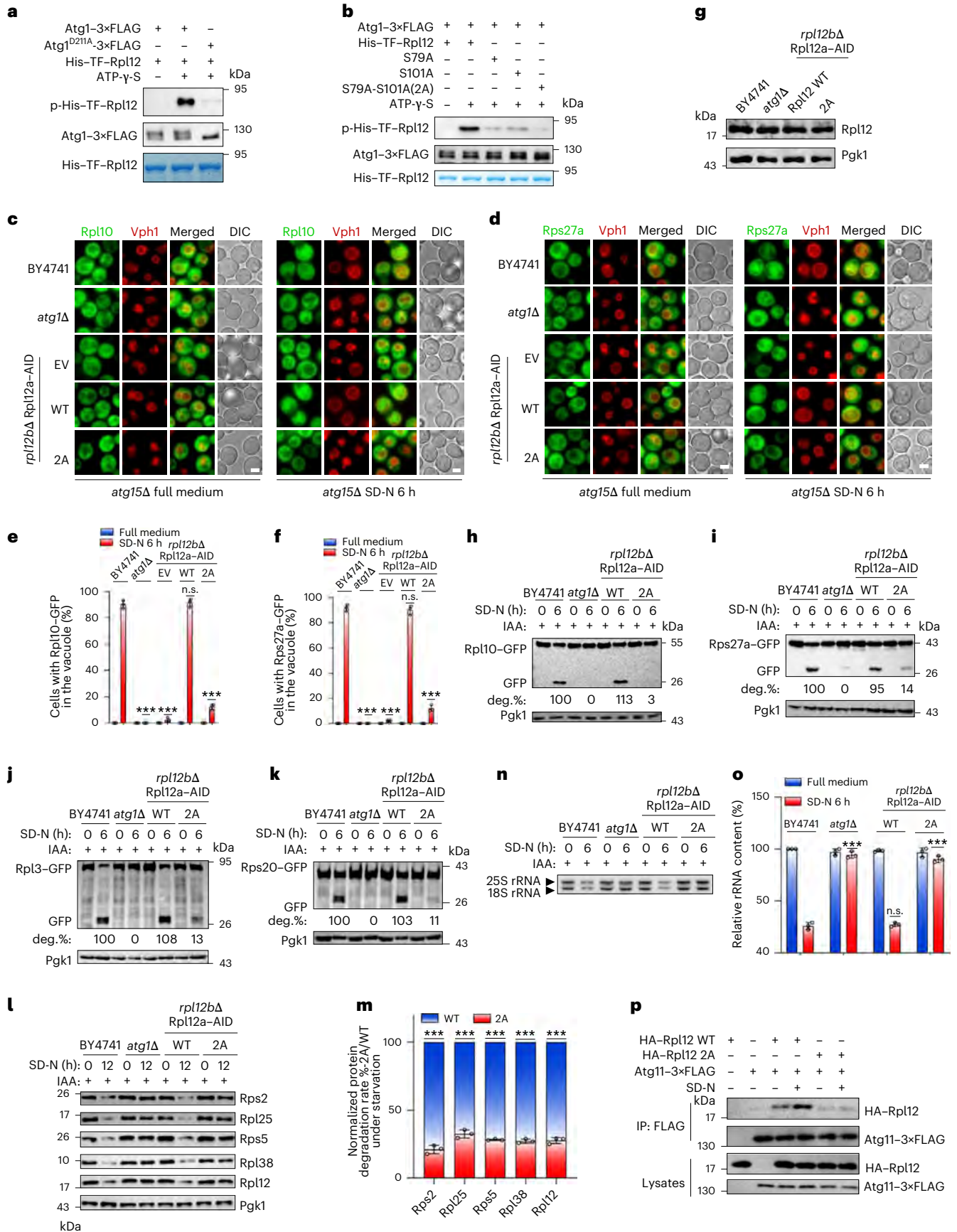
Next, we investigated whether the binding of Rpl12–Atg8 is required for ribophagy. WT Rpl12a, Rpl12a<sup>P3N-E21L</sup> (**m**) or empty vector (EV) plasmids were separately transformed into *rpl12bΔ* Rpl12a–AID yeast cells. A spotting assay showed that the introduction of Rpl12a WT or the P3N-E21L mutant plasmid rescued the growth defect (Fig. 2b). Fluorescence microscopy revealed that, under nitrogen starvation, Rpl10–GFP and Rps27a–GFP failed to enter the vacuoles in *atg1Δ*, Rpl12 KD or the Rpl12<sup>P3N-E21L</sup> mutation cells, whereas a significant amount entered the vacuoles of WT Rpl12 cells (Fig. 2c–f). Correspondingly, GFP cleavage efficiency assays indicated that Rpl12<sup>P3N-E21L</sup> mutant cells generated minimal free GFP, whereas WT Rpl12 cells restored the production of free GFP (Fig. 2g–i). In addition, the Rpl12<sup>P3N-E21L</sup> mutation almost entirely blocked the production of free GFP in other GFP-tagged ribosomal proteins (Fig. 2j,k and Extended Data Fig. 3k–n). Furthermore, the degradation of endogenous ribosomal proteins and rRNA was suppressed in yeast cells with the Rpl12<sup>P3N-E21L</sup> mutation (Fig. 2l–o). Cumulatively, our results suggest that Rpl12 functions as a receptor for yeast ribophagy in response to starvation.

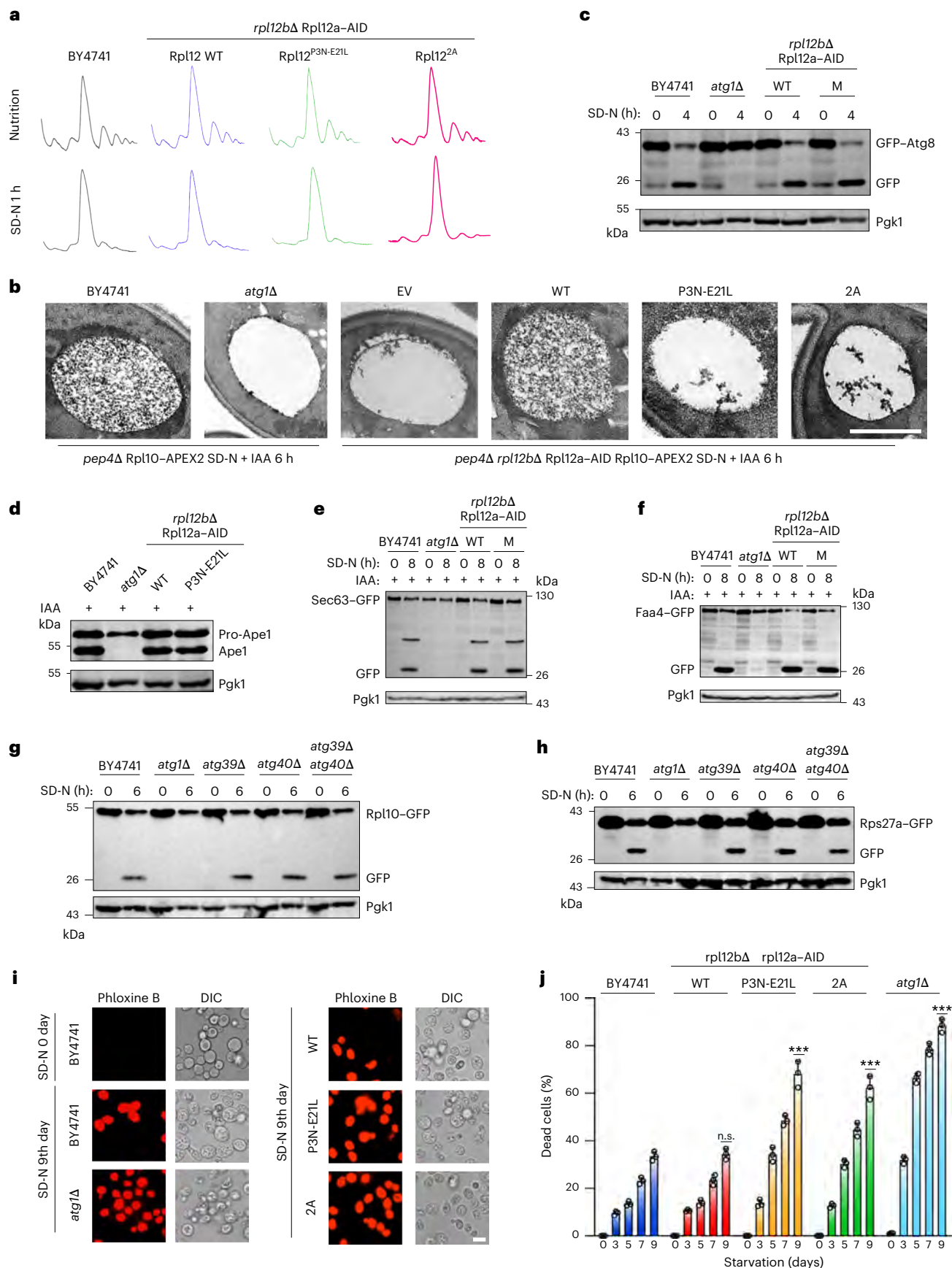
**Fig. 3 | Atg1-mediated Rpl12 phosphorylation triggers yeast ribophagy under starvation.** **a,b**, In vitro kinase assays were performed using His–TF–Rpl12a (**a** and **b**) or its variants (**b**) from *E. coli* as substrates, with purified Atg1–3×FLAG (**a** and **b**) or Atg1–3×FLAG<sup>D211A</sup> (**a**) from nitrogen-starved yeast cells as protein kinases. Phosphorylation of His–TF–Rpl12 was detected using an anti-thioP antibody. **c,d**, The indicated yeast cells co-expressing GFP-tagged Rpl10 or Rps27a with Vph1–mCherry were treated with IAA for 2 h and then subjected to SD-N for 0 h or 6 h. Images of cells were obtained using fluorescence microscopy. Scale bar, 2 μm. **e,f**, Quantification of vacuolar localization of Rpl10–GFP or Rps27a–GFP in **c** (**e**) and **d** (**f**); *n* = 300 cells pooled from three independent experiments. **g**, The indicated proteins were detected by anti-Rpl12 antibody. Data are representative of two independent experiments. **h–k**, BY4741, *atg1Δ* and *rpl12bΔ* Rpl12a–AID yeast cells, carrying either WT Rpl12a or Rpl12a<sup>S79A-S101A</sup> (2A) mutant and expressing Rpl10–GFP (**h**), Rps27a–GFP (**i**), Rpl3–GFP (**j**) or Rps20–GFP (**k**), were treated with IAA for 2 h and subjected to SD-N for 6 h, and were analysed for ribophagic activity via western blot by detecting GFP fusion protein

**Atg1-mediated Rpl12 phosphorylation triggers ribophagy**  
Next, we explored the signalling pathway that initiates ribophagy, focusing on the involvement of TOR, Snf1 and Atg1, the three primary protein kinases known to regulate autophagy in yeast<sup>16–18</sup>. Through in vitro kinase assays<sup>19</sup>, we found that only Atg1 displayed the capability to phosphorylate Rpl12 (Fig. 3a and Extended Data Fig. 4a,b). Subsequent MS analysis identified two specific amino acid residues, namely Ser79 and Ser101, as the targets of Atg1-mediated phosphorylation on Rpl12 (Extended Data Fig. 4c,d). Moreover, purified Rpl12 protein from nitrogen-starved yeast cells also exhibited phosphorylation at these two sites. To confirm these sites as specific targets of Atg1-mediated phosphorylation on Rpl12, we individually purified four proteins—WT Rpl12, S79A, S101A and S79A-S101A (2A) mutants—from *E. coli*. Using these variants as substrates with Atg1–3×FLAG as the kinase, in vitro kinase assays showed that mutations at S79A, S101A and 2A substantially hindered Atg1-mediated phosphorylation of Rpl12 (Fig. 3b). These results provided direct evidence that Rpl12 is a phosphorylation substrate of Atg1 in vitro.

We then investigated the function of Atg1-mediated Rpl12 phosphorylation in ribophagy. WT Rpl12, Rpl12<sup>2A</sup> or EV plasmid were separately transformed into *rpl12bΔ* Rpl12a–AID yeast cells. Spotting assays showed that the introduction of either WT Rpl12a or 2A mutant plasmids rescued the growth defect (Extended Data Fig. 4e). Subsequently, we assessed whether Atg1-mediated Rpl12 phosphorylation is required for ribophagy. Fluorescence microscopy revealed that, under nitrogen starvation, Rpl10–GFP and Rps27a–GFP failed to localize to vacuoles in cells with the Rpl12<sup>2A</sup> mutation (Fig. 3c–f). Western blot analysis further confirmed that Rpl10–GFP and Rps27a–GFP in these cells produced hardly any free GFP, whereas WT Rpl12 restored the generation of free GFP (Fig. 3g–i). Similarly, the Rpl12<sup>2A</sup> mutation inhibited the production of free GFP in other ribosomal proteins tagged with GFP under starvation (Fig. 3j,k and Extended

cleavage. Results were quantified (Methods). **l**, The indicated yeast cells were treated with IAA for 2 h and then subjected to SD-N for 12 h. Ribophagic activity was analysed by western blot using the indicated anti-ribosomal antibodies. **m**, The degradation ratios of the indicated proteins from **l** were quantified. **n,o**, The changes in RNA content presented using different data display types (images (**n**) or statistical graphs (**o**)). The indicated yeast cells were treated with IAA for 2 h and then subjected to SD-N for 6 h. Total RNA of five OD<sub>600</sub> yeast cells was extracted to measure rRNA expression levels. Quantification of rRNAs is shown in **o**. **p**, Yeast cells co-expressing HA–Rpl12 or HA–Rpl12 2A with Atg11–3×FLAG were subjected to SD-N for 1 h. Cell lysates were immunoprecipitated using anti-FLAG beads and analysed by western blot with anti-HA antibody. The data presented in **a–d**, **h–l**, **n** and **p** are representative of three independent experiments. Pgk1 served as a loading control. Data in **e**, **f**, **m** and **o** are shown as mean ± s.d. (*n* = 3 biologically independent experiments). \*\*\**P* < 0.001; two-tailed Student's *t*-tests were used. Exact *P* values, source numerical data and unprocessed blots or gels are provided.





Data Fig. 4f–i). In addition, the degradation of endogenous ribosomal proteins and rRNA was suppressed in yeast cells with the Rpl12<sup>2A</sup> mutation (Fig. 3l–o), indicating that Atg1-mediated Rpl12 phosphorylation is required for ribophagy.

We proceeded to explore the molecular mechanism behind Atg1-mediated Rpl12 phosphorylation and its regulation of ribophagy. Considering that Rpl12 binds directly to both Atg8 and Atg11, we investigated whether Atg1-mediated Rpl12 phosphorylation regulates its

**Fig. 4 | Ribophagy is crucial for maintaining cellular survival during starvation.** **a**, The indicated yeast cells were treated with IAA for 2 h, then subjected to SD-N for 0 h or 1 h. Polysome profiles were analysed. **b**, The indicated yeast cells treated with IAA for 2 h and subjected to SD-N for 6 h were visualized using APEX-TEM. Scale bar, 500 nm. **c**, The indicated yeast cells expressing GFP-Atg8 were treated with IAA for 2 h and subjected to SD-N for 0 h or 4 h. Protein samples were analysed by western blot using the indicated anti-GFP antibody. **d**, The indicated yeast cells were grown to early log phase and then subjected to IAA for 2 h. The activity of the Cvt pathway was analysed by analysing Pro-Ape1 maturation via western blot. **e,f**, The indicated yeast cells expressing Sec63-GFP (ER marker) (**e**) or Faa4-GFP (lipid droplet marker) (**f**) were treated with IAA for 2 h, followed by SD-N for 0 h or 8 h. Different organelles labeled with GFP reflect the occurrence of different types of selective autophagy. Specifically, Sec63 is a marker for the endoplasmic reticulum and Faa4 is a marker for lipid droplets. The cleavage of Sec63-GFP reflects the occurrence level of ER autophagy and the cleavage of Faa4-GFP reflects the occurrence level of lipid droplet autophagy.

association with Atg8 or Atg11 under nutrient-rich and starvation conditions. Co-IP experiments revealed a substantial increase in the binding of Rpl12 to both Atg8 and Atg11 under starvation compared with nutrient-rich conditions. However, the HA-Rpl12<sup>2A</sup> mutation substantially impaired the interaction between Rpl12 and Atg11, without affecting its binding to Atg8 (Fig. 3p and Extended Data Fig. 4j). In addition, in vitro Ni-NTA pull-down assays indicated that the Rpl12<sup>2A</sup> mutant maintained its binding to Atg11 CC4, suggesting that the 2A mutant does not impair the binding of Rpl12 to Atg11 CC4 in vitro (Extended Data Fig. 4k). Furthermore, the phospho-mimic Rpl12<sup>S79D-S101D</sup> (2D) mutant enhanced ribophagy induced by starvation (Extended Data Fig. 5a–f). Taken together, these results suggest that Atg1-mediated Rpl12 phosphorylation triggers ribophagy by enhancing its association with Atg11 under starvation.

### Ribophagy is crucial for cell survival during starvation

Next, we assessed whether the Rpl12<sup>P3N-E21L</sup> mutation affected its ribosomal function. Polysome profiling experiments revealed no notable differences in the polysome profiles between Rpl12<sup>P3N-E21L</sup> and WT Rpl12 under both nutrient-rich and starvation conditions<sup>20</sup> (Fig. 4a). Similarly, the polysome profile of Rpl12<sup>2A</sup> showed no notable differences compared with WT Rpl12 (Fig. 4a). To further confirm the pivotal role of Rpl12 in ribophagy, we performed transmission electron microscopy (TEM) assays and observed that both the Rpl12<sup>P3N-E21L</sup> and 2A mutations almost completely inhibited yeast ribophagy under nitrogen starvation, using Rpl10 and Rps27a tagged with APEX2 as markers<sup>21</sup> (Fig. 4b and Extended Data Fig. 5g). These findings suggest that the Rpl12<sup>P3N-E21L</sup> and 2A mutations block ribophagy by impairing its association with Atg8 or Atg11, rather than affecting its ribosomal function.

We also investigated whether Rpl12 plays a role in bulk autophagy or other selective autophagy. Western blot analysis showed that the Rpl12<sup>P3N-E21L</sup> mutation did not impact bulk autophagy or the maturation of Pro-Ape1, nor the cleavage of marker proteins associated with

Protein samples were analysed by western blot with an anti-GFP antibody. **g,h**, The indicated yeast cells expressing Rpl10-GFP (**g**) or Rps27a-GFP (**h**) were subjected to SD-N for 0 h or 6 h. The components of the ribosomal large (Rpl10) or small (Rps27a) subunits labeled with GFP reflect the degradation of ribosomal subunits. Ribophagic activity was analysed by detecting GFP cleavage via western blot with anti-GFP antibody. **i**, Yeast cells treated with IAA for 2 h, followed by SD-N for varying time periods, were stained with 2.5 µg ml<sup>-1</sup> phloxine B to identify dead cells. Images were obtained using fluorescence microscopy. Scale bar, 2 µm. **j**, Quantification of phloxine B-positive dead cells relative to the total cells observed under bright-field microscopy. *n* = 300 cells were pooled from three independent experiments. The data presented in **a–i** are representative of three independent experiments. Ptk1 served as a loading control. Data are shown as mean ± s.d. (*n* = 3 biologically independent experiments). \*\*\**P* < 0.001; two-tailed Student's *t*-tests were used. Exact *P* values, source numerical data and unprocessed blots are provided.

other types of selective autophagy, including Om45-GFP (mitophagy), Sec63-GFP (endoplasmic reticulum (ER)-phagy), Faa4-GFP (lipophagy) and Pex14-GFP (pexophagy) (Fig. 4c–f and Extended Data Fig. 5h,i). This suggests that Rpl12 is not involved in these processes, emphasizing its specific role as a ribophagy receptor.

Since ribosomes associate with the ER for mRNA translation, we investigated whether ribophagy is influenced by the absence of ER-phagy. Analysis of ribophagy in yeast cells with double KO of the ER-phagy receptors *ATG39* and *ATG40* under nitrogen starvation conditions revealed that ribophagy proceeded unaffected<sup>14</sup> (Fig. 4g,h and Extended Data Fig. 5j–m), indicating that ribophagy is independent of ER-phagy. We then evaluated whether ribophagy contributes to cell survival during such conditions<sup>14,22</sup>. The results indicated that the Rpl12<sup>P3N-E21L</sup> and 2A mutations significantly increased starvation-induced cell death (Fig. 4i,j). Altogether, these data highlight the critical role of ribophagy in maintaining cell survival during starvation.

### RPL-12 is a conserved ribophagy receptor in *C. elegans*

Next, we explored whether Rpl12 functions as a conserved ribophagy receptor across species. Blasting the amino acid sequence of Rpl12 from yeast to human revealed highly conserved proline and glutamine residues at the 3rd and 21st positions (P3 and E21, respectively) (Extended Data Fig. 6a), suggesting a potential conserved role as a ribophagy receptor. We next examined whether RPL-12, the *C. elegans* homologue of yeast Rpl12, regulates ribophagy to control ribosome turnover. We initially investigated whether RPL-12 binds to LGG-1 or LGG-2, the *C. elegans* homologues of Atg8 (ref. 23). In vitro pull-down assays showed that only LGG-1 interacts with RPL-12 (Extended Data Fig. 6b). We then examined the binding capabilities of WT RPL-12 and the P3N-E21L mutant proteins, which were purified from *E. coli*, to LGG-1 using GST pull-down assays. The results demonstrated that WT RPL-12 robustly binds to LGG-1, while the RPL-12 P3N-E21L mutant fails to bind (Fig. 5a).

### Fig. 5 | The function of RPL-12 as a ribophagy receptor is conserved in *C. elegans*.

**a**, GST pull-down assays using purified His-TF-RPL-12 or TF-RPL-12<sup>P3N-E21L</sup> with GST-LGG-1 from *E. coli*. The experiments were repeated independently three times with similar results. **b**, Co-IP between GFP-LGG-1 and either endogenous WT RPL-12 or RPL-12<sup>P3N-E21L</sup> (from *syb7750*[*P3N-E21L*]) using worm lysates. **c**, Western blotting analysis of ribophagic activity in *N*<sub>2</sub>, *rpl-12*(*syb7750*[*P3N-E21L*]) and *atg-3*(*bp412*). Animals were subjected to starvation for 0 h or 24 h. Tubulin served as a loading control. **d**, Quantification of protein degradation ratios from **c**. **e**, Total RNA extracted from the indicated worms starved for 0 h or 24 h, analysed on a formaldehyde agarose gel. Total DNA served as a loading control. **f**, Quantification of rRNAs from **e**. **g**, A flowchart for assessing L1 larvae survival under starvation. **h**, Survival rates of L1 larvae for indicated strains under starvation. *N*<sub>2</sub>: *n* = 287, *atg-3*(*bp412*): *n* = 101, *rpl-12*(*sb7750*): *n* = 126. **i**, The mean lifespan of larvae from **h**. **j**, The survival

rate of each indicated strain exposed to PA14. *N*<sub>2</sub>: *n* = 53, *atg-3*(*bp412*): *n* = 53, *rpl-12*(*sb7750*): *n* = 51, *Ex*[*rpl-12p::rpl-12* WT *cDNA*]: *n* = 50, *Ex*[*rpl-12p::rpl-12* *mut cDNA*]: *n* = 46. **k,l**, Quantification of worm length (**k**) and brood size (**l**) for each indicated strain (*n* = 20). **m**, Lifespan analyses of strains. *N*<sub>2</sub>: *n* = 121, *atg-3*(*bp412*): *n* = 119, *rpl-12*(*sb7750*): *n* = 120, *Ex*[*rpl-12p::rpl-12* WT *cDNA*]: *n* = 146, *Ex*[*rpl-12p::rpl-12* *mut cDNA*]: *n* = 131. **n**, Lifespan analyses of strains. *N*<sub>2</sub>: *n* = 125, *atg-3*(*bp412*): *n* = 106, *rpl-12*(*sb7750*): *n* = 128, *daf-2*(*e1370*): *n* = 113, *rpl-12*(*sb7750*): *daf-2*(*e1370*): *n* = 130. Data in **a–c** and **e** are representative of three independent experiments. Statistical significance: \*\*\**P* < 0.001, \*\**P* < 0.01 and \**P* < 0.05. *P* values were calculated by two-tailed Student's *t*-tests (**d**, **f**, **i**, **k** and **l**) or log-rank (Mantel–Cox) test (**j**, **m** and **n**). The data in **d**, **f**, **i**, **k** and **l** are presented as mean ± s.d. (*n* = 3 biological replicates). Exact *P* values, source numerical data and unprocessed blots or gels are provided.



To further test the binding between the endogenous RPL-12 and LGG-1, we generated an anti-RPL-12 antibody and introduced P3N-E21L mutations in the endogenous *rpl-12* gene (*syb7750[P3N-E21L]*) in *C. elegans*. Co-IP results showed that both the P3 and E21 residues within RPL-12 are crucial for interaction with LGG-1 in *C. elegans* (Fig. 5b).

We then explored whether the binding of RPL-12 with LGG-1 is required for ribophagy in *C. elegans*. Specific antibodies targeting *C. elegans* ribosomal proteins revealed significant degradation of ribosomal proteins in WT worms under starvation conditions. By contrast, both the *atg-3(bp412)* and *rpl-12(syb7750[P3N-E21L])* mutants displayed notable inhibition of ribosomal protein degradation<sup>24</sup> (Fig. 5c,d). Similarly, inhibition in rRNA degradation was observed in both mutants compared with WT animals under starvation conditions (Fig. 5e,f). Moreover, this degradation of ribosomal proteins dependent on lysosomal activity<sup>25</sup> (Extended Data Fig. 6c,d). Collectively, these findings indicate the conservation of RPL-12 as a ribophagy receptor in *C. elegans*.

Subsequently, we investigated the physiological functions of ribophagy in *C. elegans*. Earlier studies have highlighted the critical role of autophagy in maintaining the survival of *C. elegans* during starvation<sup>24</sup>. As shown in Fig. 5g–i, the number of days required for complete mortality under starvation conditions was 24 days for WT, 5 days for *atg-3(bp412)* and 9 days for *rpl-12(syb7750[P3N-E21L])* mutants, indicating a significant contribution of ribophagy to worm mortality induced by autophagy defects during starvation. In addition, ribophagy played a protective role against external pathogenic bacterial infections, as *rpl-12(syb7750[P3N-E21L])* mutants displayed decreased survival during infection with pathogenic *Pseudomonas aeruginosa* (PA14)<sup>26</sup>. Conversely, overexpression of WT RPL-12, but not the P3N-E21L mutant variant, enhanced survival during PA14 infection (Fig. 5j and Extended Data Fig. 6e), suggesting a positive role of ribophagy in infection and immune responses. Further investigation into the impact of ribophagy on growth, development and reproduction revealed its involvement in various crucial physiological functions. The *rpl-12(syb7750[P3N-E21L])* mutant displayed phenotypes similar to *atg-3(bp412)* mutant, including shorter body length, reduced brood size and retarded larval development (Fig. 5k,l and Extended Data Fig. 6f). Nevertheless, unlike the *atg-3(bp412)* mutant, the *rpl-12(syb7750[P3N-E21L])* mutant did not show a significant difference in the percentage of embryos hatching into larvae (Extended Data Fig. 6g), suggesting that other forms of autophagy, rather than ribophagy, contribute to this process.

Next, we investigated the impact of ribophagy on lifespan. Lifespan measurements revealed that *C. elegans* treated with *rpl-12* RNA interference (RNAi) had a shortened lifespan, while *rpl-26* RNAi worms showed no lifespan difference compared with WT worms (Extended Data Fig. 6h,i). Furthermore, we examined the effects of the *rpl-12(syb7750[P3N-E21L])* mutant and RPL-12 overexpression on lifespan. Our results showed that, similar to *rpl-12* RNAi worms, *rpl-12(syb7750[P3N-E21L])* mutant exhibited a shortened lifespan, whereas overexpression of WT RPL-12 extended

lifespan (Fig. 5m). In addition, when we introduced the P3N-E21L mutation in RPL-12 into the *daf-2* mutant background, known for its significantly extended lifespan<sup>27</sup>, we observed a substantial reduction in the lifespan of long-lived *daf-2* mutant animals with the *rpl-12* mutation (Fig. 5n). Collectively, these results demonstrate the involvement of RPL-12 as a ribophagy receptor in various crucial physiological functions in *C. elegans*.

### RpL12 is a conserved receptor for ribophagy in *Drosophila*

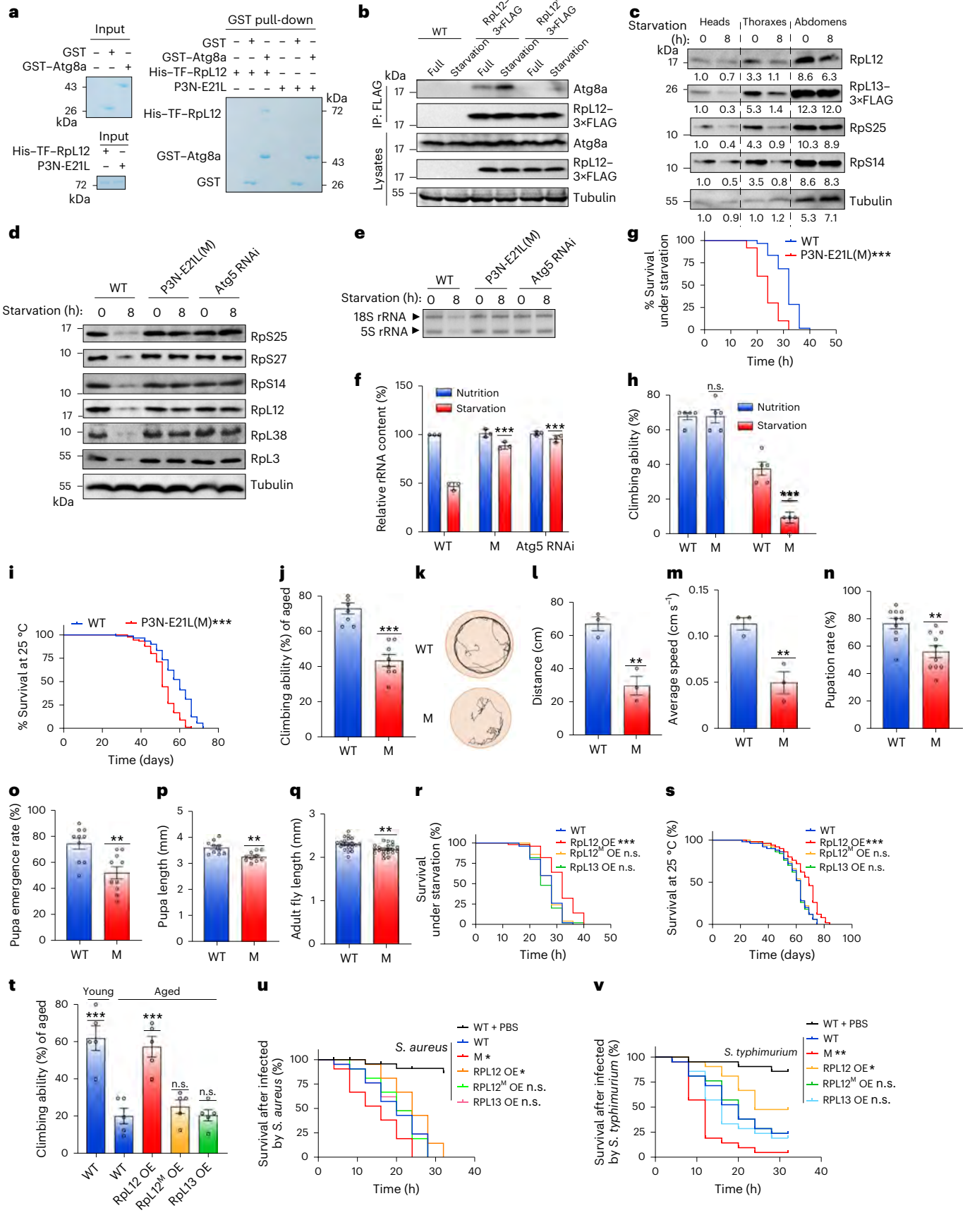
Considering the conserved Atg8/LC3 docking sites, P3 and E21, within RpL12 protein and the presence of a mammalian NUFIP1 homologue in *Drosophila*, we examined RpL12 whether functions as a ribophagy receptor in *Drosophila*. Both in vitro pull-down and co-IP assays consistently showed that WT RpL12, but not the RpL12 P3N-E21L mutant, interacted with Atg8a (the *Drosophila* homologue of Atg8)<sup>28</sup> (Fig. 6a,b). Next, we investigated which part of the flies displayed the most notable ribophagy during starvation and found that ribophagy was dramatically induced in the thoraxes of starved flies (Fig. 6c), suggesting a close association between ribophagy and muscle-related functions.

To investigate the functional conservation of RpL12 in fly ribophagy, we used a Cas9-mediated knock-in strategy to generate the RpL12 P3N-E21L mutant. Under starvation conditions, both the expression level of ribosome proteins and rRNA indicated that flies harbouring the RpL12 P3N-E21L mutant or undergoing RNA interference targeting Atg5 exhibited resistance to starvation-induced ribophagy (Fig. 6d–f and Extended Data Fig. 7a). Concurrently, this degradation of ribosomal proteins is dependent on lysosomal activity (Extended Data Fig. 7b,c). Immunofluorescence assays further revealed that co-localization of RpL12 with Atg8a was significantly suppressed in the RpL12 P3N-E21L mutant (Extended Data Fig. 7d,e). A ribosome profiling assay confirmed that the P3N-E21L substitution did not impair ribosome functionality (Extended Data Fig. 7f). These findings suggest that RpL12 serves as a conserved ribophagy receptor in *Drosophila*.

Next, we investigated the physiological functions of RpL12-mediated ribophagy. Consistent with findings in yeast and *C. elegans*, flies with RpL12 P3N-E21L mutation exhibited high sensitivity to starvation, with their median survival time reduced from ~32 h to ~24 h (Fig. 6g). The P3N-E21L mutation also worsened starvation-induced impairments in climbing ability, suggesting that ribophagy defects contribute to heightened starvation susceptibility (Fig. 6h). In addition, the lifespans of RpL12 P3N-E21L mutant flies were significantly shortened, with the median lifespan reduced from ~60 days to ~51 days (Fig. 6i). Climbing ability also declined with age in these mutant flies (Fig. 6j). Locomotion assays revealed that the RpL12 P3N-E21L mutant significantly reduced both the distance moved and average speed in aged flies (Fig. 6k–m), indicating the pivotal role of ribophagy in regulating fly ageing. Given that ribophagy occurs most notably in the thoraxes of flies, we examined their muscles using paraffin sections and haematoxylin and eosin (H&E) staining<sup>29</sup>. The P3N-E21L mutation

**Fig. 6 | RPL12 is a conserved ribophagy receptor in *Drosophila*.** **a**, GST pull-downs were performed using His-tagged TF-RPL12 or RPL12<sup>P3N-E21L</sup> with GST-Atg8a from *E. coli*. The experiments were repeated independently three times with similar results. **b**, Co-IP was used to analyse the interaction of RpL12–3×FLAG, RpL12<sup>P3N-E21L</sup>(M)–3×FLAG and ATG8a. Flies were starved for 1 h ( $n = 3$  biological replicates). **c**, The levels of ribosomal proteins in various tissues after starvation treatment. The results were quantified ( $n = 3$  biological replicates). **d,e**, Both images show ribosome degradation, displaying ribosomal proteins (**d**) and illustrating rRNA degradation (**e**). The levels of ribosomal proteins and RNAs in WT, RPL12<sup>P3N-E21L</sup>(M) and Atg5 RNAi flies after 8 h of starvation. The experiments were repeated independently three times with similar results. **f**, The quantitation of **e**. Three groups,  $n = 15$  each. **g**, Starvation resistance of WT and RPL12<sup>P3N-E21L</sup>(M) flies.  $n = 60$ . **h**, The climbing ability of WT and RPL12<sup>P3N-E21L</sup>(M) flies after starvation treatment. Five groups,  $n = 10$  each. **i**, The longevity of WT and RPL12<sup>P3N-E21L</sup>(M) flies at 25 °C.  $n = 90$ . **j–m**, The climbing ability (**j**, 8 groups,

$n = 10$  each) and locomotion (visualized motion trajectories (**k**) and quantified motion (distance (**l**) and speed (**m**)),  $n = 3$ ) of the aged WT and RPL12<sup>P3N-E21L</sup>(M) flies. Panels **l** and **m** are quantitated from **k**. **n–q**, The pupation rate (**n**) and pupa emergence rate (**o**) and the length of pupa (**p**) and adult flies (**q**) were quantified; 10 groups,  $n = 20$  each (**n** and **o**);  $n = 10$  (**p**);  $n = 20$  (**q**). **r**, The starvation resistance of WT, RpL12 overexpression (OE) and RPL12<sup>P3N-E21L</sup>(M) OE flies.  $n = 50$ . **s**, Lifespans of the indicated flies were recorded at 25 °C.  $n = 50$ . **t**, The climbing ability of the indicated aged flies; 5 groups,  $n = 10$  each. **u,v**, Survival rates of indicated flies exposed to *S. aureus* (**u**) and *S. typhimurium* (**v**).  $n = 21$ . MHC-Gal4 was used to drive the expression and KD of genes in **b** and **r–t**; Da-Gal4 was used in **c**. Statistical significance: \*\*\* $P < 0.001$ , \*\* $P < 0.01$  and \* $P < 0.05$ . The log-rank (Mantel–Cox) test was used to analyse survival rate differences (**g**, **i**, **r**, **s** and **v**), two-tailed Student's *t*-test was used for comparing differences between two groups (**f**, **h**, **j**, **l–q** and **t**) and the data represent mean  $\pm$  s.d. Exact *P* values, source numerical data and unprocessed blots or gels are provided.



substantially exacerbated age-related muscle degeneration (Extended Data Fig. 7g). Phalloidin staining further showed an expansion of Z-lines in mutant flies, providing additional support for the aggravating effect of ribophagy defect on muscle integrity (Extended Data Fig. 7h,i). Subsequently, the impact of ribophagy on fly development was explored, showing that the Rpl12 P3N-E21L mutant led to a decrease in both the pupation and pupa emergence rates, along with smaller pupa length and adult fly sizes (Fig. 6n–q). These results collectively indicate the involvement of ribophagy in the regulation of fly ageing, growth and development.

To confirm the specific role of Rpl12 in ribophagy, Rpl12 was specifically knocked down in the indirect flight muscle tissue of flies. As controls, Atg5, another ribosomal large subunit protein Rpl11, and Nufip (CG4076) (the mammalian NUFIP1 homologue in *Drosophila*)<sup>30</sup>, were also knocked down (Extended Data Fig. 7j). Upon treatment with starvation, significant degradation of ribosomal proteins and rRNAs was observed in WT, Rpl11 RNAi and Nufip RNAi flies. By contrast, KD of Rpl12 or Atg5 prevented the reduction of ribosomal proteins and rRNAs (Extended Data Fig. 7k–o). Similar to the Rpl12 P3N-E21L mutant, Rpl12 RNAi flies were more sensitive to starvation (Extended Data Fig. 7p), with the decline in climbing ability induced by starvation further exacerbated (Extended Data Fig. 7q). In addition, Rpl12 RNAi flies exhibited reduced lifespan and worsened age-related declines in climbing ability (Extended Data Figs. 7r and 8a). Furthermore, the downregulation of Rpl12 also impaired fly development. However, these effects were not observed in Rpl11 or Nufip RNAi flies (Extended Data Fig. 8b–e), highlighting the unique role of Rpl12 as a ribophagy receptor in *Drosophila*.

Furthermore, overexpression of WT Rpl12, rather than Rpl12 P3N-E21L or Rpl13, markedly enhanced the resistance of *Drosophila* to starvation and ageing, with the median survival time increasing from ~28 h to ~32 h, and the median lifespan increased from ~63 days to ~69 days (Fig. 6r,s). Notably, ageing, starvation or A $\beta$  accumulation-induced impairment in climbing ability was also significantly alleviated by the overexpression of WT Rpl12 (Fig. 6t and Extended Data Fig. 8f–h). Subsequently, the investigation extended to explore whether ribophagy plays a crucial role in the defence against pathogenic bacteria. The Rpl12 P3N-E21L mutant flies significantly exacerbated the susceptibility to *Staphylococcus aureus* and *Salmonella* spp., resulting in a decrease in median survival time from ~20 h to ~16 h and from ~20 h to ~12 h, respectively. By contrast, WT Rpl12 overexpression significantly enhanced resistance to pathogenic bacteria, whereas overexpression of Rpl12 P3N-E21L or Rpl13 had no effect (Fig. 6u,v). Collectively, these findings suggest that Rpl12, as a

ribophagy receptor, plays a critical role in the defence against pathogen infection.

We then investigated whether overexpression of Rpl12 could promote ribophagy. After 4 h of starvation, flies overexpressing Rpl12 showed significantly higher levels of ribosomal protein degradation compared with WT flies (Extended Data Fig. 8i,j). Co-IP experiments revealed that the overexpressed Rpl12–3 $\times$ FLAG protein interacted with multiple ribosomal proteins (Extended Data Fig. 8k). Furthermore, polysome profiling of both WT and Rpl12–3 $\times$ FLAG-overexpressing flies showed a slight increase in polysomes in the latter (Extended Data Fig. 8l). Western blot analysis confirmed that both endogenous Rpl12 and Rpl12–3 $\times$ FLAG were present in the 60S, 80S and polysome fractions, with a higher abundance in polysomes (Extended Data Fig. 8m,n). These findings collectively suggest that Rpl12–3 $\times$ FLAG overexpression in flies promotes ribophagy during starvation, and the overexpressed Rpl12–3 $\times$ FLAG is effectively incorporated into ribosomes.

### RPL12 is a conserved ribophagy receptor in mammals

Next, we investigated whether RPL12 functions as a ribophagy receptor in mammalian cells. Given that human cells contain six Atg8 paralogues<sup>31</sup>, we sought to identify which of these paralogues interacts with RPL12. Co-IP assays revealed that LC3C, GABARAP and GABARAPL1 interact with RPL12 (Fig. 7a). Moreover, the binding of human RPL12 (hRPL12) to these paralogues depends on the P3 and E21 residues of Rpl12 (Fig. 7b and Extended Data Fig. 9a). GST pull-down experiments further showed that only LC3C and GABARAP directly interact with hRPL12, while GABARAPL1 does not bind directly to RPL12, suggesting that GABARAPL1's interaction may be indirect or context dependent within cells (Extended Data Fig. 9b). In addition, in vitro pull-down assays confirmed that WT RPL12, but not the RPL12 P3N-E21L mutant, can directly interact with LC3C and GABARAP (Extended Data Fig. 9c). Subsequently, we investigated whether RPL12 is required for ribophagy in mammals. First, we confirmed the pivotal role of autophagy in ribosome turnover during starvation<sup>5</sup> (Extended Data Fig. 9d,e). We then generated stable RPL12 KD in the HEK293T cell line. Under Earle's balanced salt solution (EBSS) starvation conditions, the expression levels of endogenous ribosomal proteins, other organelle proteins (mitochondria, TIM23; ER, RTN4) and rRNAs indicated a specific involvement of RPL12 in ribophagy (Extended Data Fig. 9f–i). Furthermore, the RPL12 P3N-E21L mutation, which disrupts RPL12's binding to LC3s, also impaired starvation-induced ribophagy (Fig. 7c–f). This degradation of ribosomal proteins was dependent on lysosomal activity (Extended Data Fig. 9j). TEM analysis further confirmed that the interaction between RPL12 and Atg8s is crucial for mammalian ribophagy

### Fig. 7 | RPL12 is a conserved ribophagy receptor in mammalian cells.

**a**, HEK293T cells co-transfected with HA–LC3A, HA–LC3B, HA–LC3C, HA–GABARAP, HA–GABARAPL1 or HA–GABARAPL2 along with RPL12–3 $\times$ FLAG plasmids were starved in EBSS for 1 h. Cell lysates were immunoprecipitated using anti-HA agarose beads and analysed by western blot with an anti-FLAG antibody. **b**, HEK293T cells co-transfected with HA–LC3C and either RPL12–3 $\times$ FLAG or RPL12<sup>P3N-E21L</sup>–3 $\times$ FLAG plasmids were starved in EBSS for 1 h. Cell lysates were immunoprecipitated using anti-HA agarose beads and analysed by western blot with an anti-FLAG antibody. **c**, RPL12 KD HEK293T cells co-transfected with the indicated plasmids were starved for the indicated times, and ribophagy activity was assessed by western blot for the degradation of ribosomal proteins, with tubulin serving as a loading control. **d**, Quantification of protein degradation ratios from **c**. **e**, Total RNA extracted from cells starved for 0 h or 10 h was analysed on formaldehyde agarose gels. **f**, rRNAs from **e** were quantified. **g,h**, The effects of RPL12 KD cells (**g**) and the impact of supplementing different plasmids in the context of RPL12 KD cells (**h**). Panels **g** and **h** have different cell backgrounds and exhibit a progressive logical relationship. The indicated cells treated with Torin1 and concanamycin A for 4 h were analysed using electron microscopy. Ribosomes in the cytoplasm are indicated by blue arrowheads and those within autophagosomes by red arrowheads. Scale bar, 500 nm. **i**,

Immunofluorescence was performed on U2OS cells expressing RPL12–3 $\times$ FLAG or Rpl12<sup>P3N-E21L</sup>–3 $\times$ FLAG treated with EBSS starvation for 0 h or 1 h using anti-FLAG and anti-LC3 antibodies. Scale bars, 10  $\mu$ m (overview) and 2  $\mu$ m (insets: magnified views). **j**, Co-localization of LC3 with RPL12–3 $\times$ FLAG or Rpl12<sup>P3N-E21L</sup>–3 $\times$ FLAG was quantified from **i** ( $n = 30$  cells). **k**, Ribosome profiling of the indicated cell lines under nutrient-rich and starvation conditions. **l,m**, Cells cultured in HBSS medium for 0 h or 48 h were stained with Giemsa solution and imaged (**l**), and cell survival was quantified (**m**). **n,o**, The indicated cells infected with RFP-labelled *S. typhimurium* for 4 h or 8 h were analysed for bacterial replication via immunostaining (**n**) and colony-forming unit assays (**o**). After 1 h of infection with *S. typhimurium*, the cells were cultured in fresh DMEM containing gentamicin for continued incubation. Samples were collected at 0 h, 4 h and 8 h of culture. Counterstaining was conducted using an anti-tubulin antibody (green). Scale bar, 10  $\mu$ m (Methods). **p**, A model illustrating RPL12 as a ribophagy receptor mediating ribosome turnover. Data in **a–e**, **g–i**, **k**, **l** and **n** are representatives of three independent experiments. Statistical significance: \*\*\* $P < 0.001$  and \*\* $P < 0.01$ .  $P$  values in **d**, **f**, **j**, **m** and **o** were calculated using two-tailed Student's  $t$ -tests and are presented as mean  $\pm$  s.d. ( $n = 3$  biological replicates). Exact  $P$  values, source numerical data and unprocessed blots or gels are provided.

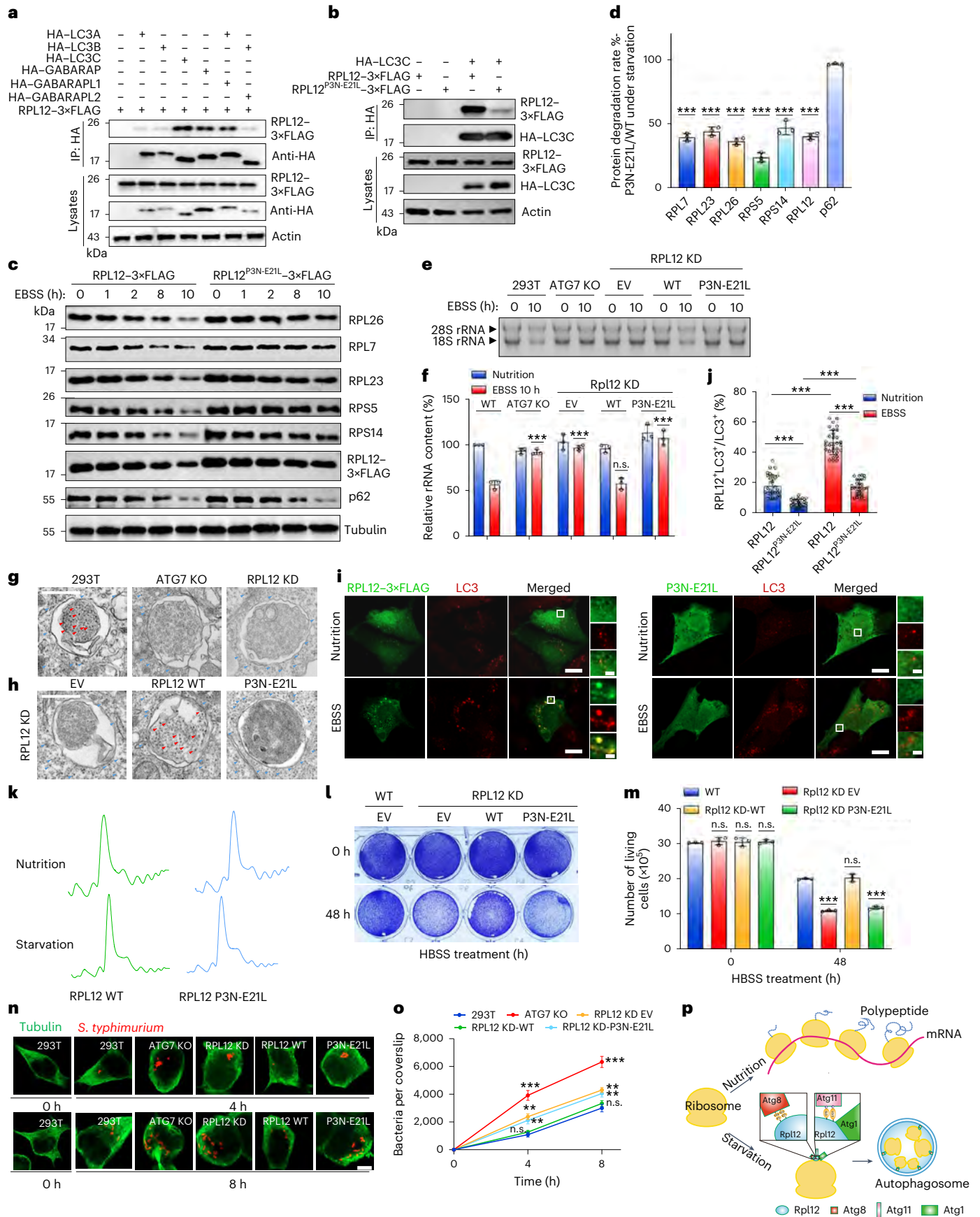


(Fig. 7g,h). We next examined the co-localization of RPL12 and LC3 in mammalian cells. Immunofluorescence assays indicated substantial co-localization between RPL12 and LC3 under EBSS starvation conditions, while the RPL12 P3N-E21L mutation showed a marked decrease in co-localization with LC3 (Fig. 7i,j). Early markers of autophagosome formation, such as ATG14 and ATG16, also displayed significant co-localization with RPL12 under starvation conditions<sup>32,33</sup> (Extended Data Fig. 9k–n). In addition, both WT RPL12 and the RPL12 P3N-E21L mutant exhibited similar polysome profiles under nutrient-rich and EBSS starvation conditions (Fig. 7k), indicating that the P3N-E21L mutation does not impair ribosome function. Taken together, these data show that Rpl12 serves as a bona fide ribophagy receptor in mammalian cells.

We then investigated whether RPL12 is required for cellular survival during starvation. Results from clonogenic survival assays and direct cell counting revealed that RPL12 KD or loss of its Atg8s-binding ability reduced cell survival under nutrient deprivation (Fig. 7l,m). Subsequently, we investigated the physiological function of RPL12 as a ribophagy receptor by conducting a bacterial infection assay<sup>34</sup>. Various cell lines, including WT HEK293T, Atg7 KO, RPL12 KD, RPL12 KD + WT RPL12 and RPL12 KD + RPL12 P3N-E21L, were infected with red fluorescent protein (RFP)-marked *Salmonella*. ATG7 KO, RPL12 KD and RPL12 KD + RPL12 P3N-E21L cells showed increased permissiveness to *Salmonella* replication compared with WT HEK293T and RPL12 KD + WT RPL12 cells, as indicated by higher numbers of red fluorescent bacteria in the cytosol (Fig. 7n). A quantitative assay measuring in vivo bacterial growth also showed significantly increased *Salmonella* replication in RPL12 KD and RPL12 KD + RPL12 P3N-E21L cells compared with WT HEK293T and RPL12 KD + WT RPL12 cells<sup>34</sup> (Fig. 7o). Cumulatively, these results align with findings from *C. elegans* and *Drosophila*, demonstrating that ribophagy contributes to the autophagy-mediated suppression of bacterial replication in vivo.

We next explored which Atg8 homologues in mice directly bind to mouse RPL12 (mRPL12). Mice possess five Atg8 paralogues<sup>35</sup>, and co-IP experiments revealed that mRPL12 interacts with mLC3A, mLC3B and mGABARAP (Extended Data Fig. 10a), with the P3 and E21 sites of mRPL12 being crucial for these interactions (Extended Data Fig. 10b). In vitro GST pull-down assays further confirmed direct interactions between mRPL12 and mLC3A, mLC3B and mGABARAP (Extended Data Fig. 10c), which also depend on the P3 and E21 sites of mRPL12 (Extended Data Fig. 10d). These findings suggest that P3 and E21 sites of mRPL12 are important for its binding to Atg8 homologues in mice. To examine whether mRPL12 regulates liver ribophagy in mice, fed mice were intraperitoneally injected with recombinant adeno-associated virus (rAAV) expressing liver-specific WT RPL12 (rAAV-RPL12) or RPL12-P3N-E21L (rAAV-RPL12-P3N-E21L)<sup>36</sup>. After 4 weeks of viral infection, no notable differences in body weight were observed among the groups. In the livers of treated mice, the RPL12-P3N-E21L mutant impaired ribosome protein and rRNA degradation in response to starvation, compared with WT RPL12 (Extended Data Fig. 10e–h). Analysis of liver metabolic flux revealed that RPL12-mediated ribophagy regulates amino acid, carbohydrate, lipid and nucleotide metabolism (Extended Data Fig. 10i,j and Supplementary Table 4). Remarkably, the glucose level notably decreased in the livers of mice overexpressing RPL12-P3N-E21L (Extended Data Fig. 10j). Furthermore, under fasting conditions, these mice exhibited lower blood glucose levels (Extended Data Fig. 10k). Previous reports have highlighted the crucial role of autophagy in maintaining serum glucose homeostasis during starvation<sup>37</sup>. These data suggest that RPL12-mediated ribophagy plays a key role in maintaining serum glucose homeostasis under starvation conditions. Further analysis revealed that hepatic glycogen accumulates in mice with the overexpression of RPL12-P3N-E21L under starvation (Extended Data Fig. 10l). Collectively, these results confirm the physiological role of RPL12 as a ribophagy receptor in regulating ribosome turnover

and maintaining cellular homeostasis in the liver under starvation conditions.

## Discussion

In this study, we identified a highly conserved ribophagy receptor, Rpl12, from yeast to mammalian cells. It fulfils the characteristics of being a ribophagy receptor: (1) it is required for ribosome degradation under starvation conditions; (2) it is located on the inner surface of the ribosome and directly interacts with Atg8s; (3) deficiency of its interaction with Atg8s inhibits ribosome degradation during starvation. In addition, we defined the trigger signal for ribophagy under starvation conditions. Under nitrogen starvation, Atg1 activation leads to RPL12 phosphorylation, which enhances its binding to Atg11 and directs ribosomes to the autophagosome for degradation (Fig. 7p).

Ribosomal turnover is essential for maintaining cellular homeostasis. Current research indicates that ribosomes degrade not only through ribophagy but also via bulk autophagy and the ubiquitin–proteasome pathway<sup>4,5,38,39</sup>. Therefore, identifying the dominant pathway for ribosome turnover remains a persistent question within this field. Previous studies revealed that NUFIP1 is not required for ribophagic flux during amino acid withdrawal in HEK293T cells<sup>40</sup>, and while it is crucial for rRNA degradation in mCAF cells under glutamine starvation, it does not affect ribosomal protein degradation<sup>6</sup>. Therefore, understanding the physiological functions of ribophagy is vital for comprehending its significance in ribosome turnover. In this study, we found that the loss of RPL12-mediated ribophagy impairs the survival of *S. cerevisiae*, *C. elegans*, *Drosophila* and mammalian cells under starvation conditions, indicating that ribophagy emerges as a crucial mechanism for nutrient sourcing and an important contributor to bulk autophagy in promoting cell survival upon starvation. Furthermore, our findings demonstrate that impairing RPL12-mediated ribophagy significantly impedes the growth, development and lifespan in both *C. elegans* and *Drosophila*, underscoring its pivotal role in fundamental physiological processes. Notably, we found a notable ribophagy induction in the thoraxes of flies under starvation conditions, and the loss of RPL12-mediated ribophagy in flies manifested as a motor deficit, showing a close association between ribophagy and muscle-related functions. Lastly, we have uncovered that RPL12-mediated ribophagy plays a crucial role in the infection and immune response processes across multiple organisms.

Interestingly, we found that overexpressing WT RPL12, rather than the RPL12 E3N-P21L or other ribosomal proteins, significantly extends the lifespan in both nematodes and flies. We also showed that overexpression of RPL12 in flies can partially rescue the impairment of climbing ability under starvation, ageing or A $\beta$  accumulation conditions. Furthermore, we uncovered in both *C. elegans* and flies that overexpression of RPL12 can significantly increase their resistance to pathogen infection. These results suggest that enhancing RPL12 expression could prolong lifespan, improve motor function in aged organisms and increase organism resistance to pathogen infection. Further investigation revealed that RPL12 overexpression promotes starvation-induced ribophagy, aligning with evidence that upregulating specific receptors involved in selective autophagy can accelerate substrate degradation<sup>41–43</sup>. Consequently, RPL12 emerges as a potential target for enhancing ribophagy, with implications for lifespan extension, improved motor function and increased pathogen resistance. This aspect will be a primary focus of our future research.

## Online content

Any methods, additional references, Nature Portfolio reporting summaries, source data, extended data, supplementary information, acknowledgements, peer review information; details of author contributions and competing interests; and statements of data and code availability are available at <https://doi.org/10.1038/s41556-024-01598-2>.

## References

1. Panse, V. G. & Johnson, A. W. Maturation of eukaryotic ribosomes: acquisition of functionality. *Trends Biochem. Sci.* **35**, 260–266 (2010).
2. López, A. R. et al. Autophagy-mediated control of ribosome homeostasis in oncogene-induced senescence. *Cell Rep.* **42**, 113381 (2023).
3. Kazibwe, Z., Liu, A. Y., MacIntosh, G. C. & Bassham, D. C. The ins and outs of autophagic ribosome turnover. *Cells* **8**, 1603 (2019).
4. Kraft, C., Deplazes, A., Sohrmann, M. & Peter, M. Mature ribosomes are selectively degraded upon starvation by an autophagy pathway requiring the Ubp3p/Bre5p ubiquitin protease. *Nat. Cell Biol.* **10**, 602–610 (2008).
5. Wyant, G. A. et al. NUFIP1 is a ribosome receptor for starvation-induced ribophagy. *Science* **360**, 751–758 (2018).
6. Yuan, M. et al. Cancer-associated fibroblasts employ NUFIP1-dependent autophagy to secrete nucleosides and support pancreatic tumor growth. *Nat. Cancer* **3**, 945–960 (2022).
7. Mi, H. Y. et al. PANTHER version 16: a revised family classification, tree-based classification tool, enhancer regions and extensive API. *Nucleic Acids Res.* **49**, D394–D403 (2021).
8. Wilfling, F. et al. A selective autophagy pathway for phase-separated endocytic protein deposits. *Mol. Cell* **80**, 764–778 e767 (2020).
9. Tu, W. Y., Huang, Y. C., Liu, L. F., Chang, L. H. & Tam, M. F. Rpl12p affects the transcription of the PHO pathway high-affinity inorganic phosphate transporters and repressible phosphatases. *Yeast* **28**, 481–493 (2011).
10. Yorimitsu, T. & Klionsky, D. J. Atg11 links cargo to the vesicle-forming machinery in the cytoplasm to vacuole targeting pathway. *Mol. Biol. Cell* **16**, 1593–1605 (2005).
11. Johansen, T. & Lamark, T. Selective autophagy: ATG8 family proteins, LIR motifs and cargo receptors. *J. Mol. Biol.* **432**, 80–103 (2020).
12. Jacomin, A. C., Samavedam, S., Promponas, V. & Nezis, I. P. iLIR database: a web resource for LIR motif-containing proteins in eukaryotes. *Autophagy* **12**, 1945–1953 (2016).
13. Nishimura, K., Fukagawa, T., Takisawa, H., Kakimoto, T. & Kanemaki, M. An auxin-based degron system for the rapid depletion of proteins in nonplant cells. *Nat. Methods* **6**, 917–922 (2009).
14. Mochida, K. et al. Receptor-mediated selective autophagy degrades the endoplasmic reticulum and the nucleus. *Nature* **522**, 359–362 (2015).
15. Huang, H. et al. Bulk RNA degradation by nitrogen starvation-induced autophagy in yeast. *EMBO J.* **34**, 154–168 (2015).
16. Noda, T. & Ohsumi, Y. Tor, a phosphatidylinositol kinase homologue, controls autophagy in yeast. *J. Biol. Chem.* **273**, 3963–3966 (1998).
17. Yi, C. et al. Formation of a Snf1–Mec1–Atg1 Module on Mitochondria Governs Energy Deprivation-Induced Autophagy by Regulating Mitochondrial Respiration. *Dev. Cell* **41**, 59–71.e54 (2017).
18. Matsuura, A., Tsukada, M., Wada, Y. & Ohsumi, Y. Apg1p, a novel protein kinase required for the autophagic process in *Saccharomyces cerevisiae*. *Gene* **192**, 245–250 (1997).
19. Allen, J. J. et al. A semisynthetic epitope for kinase substrates. *Nat. Methods* **4**, 511–516 (2007).
20. Chasse, H., Boulben, S., Costache, V., Cormier, P. & Morales, J. Analysis of translation using polysome profiling. *Nucleic Acids Res.* **45**, e15 (2017).
21. Li, H., He, C. W., Zhu, J. & Xie, Z. A validated set of ascorbate peroxidase-based organelle markers for electron microscopy of *Saccharomyces cerevisiae*. *mSphere* **7**, e0010722 (2022).
22. Tsukada, M. & Ohsumi, Y. Isolation and characterization of autophagy-defective mutants of *Saccharomyces cerevisiae*. *FEBS Lett.* **333**, 169–174 (1993).
23. Palmisano, N. J. & Melendez, A. Autophagy in *C. elegans* development. *Dev. Biol.* **447**, 103–125 (2019).
24. Lin, L. et al. The scaffold protein EPG-7 links cargo receptor complexes with the autophagic assembly machinery. *J. Cell Biol.* **201**, 113–129 (2013).
25. Sun, T., Wang, X., Lu, Q., Ren, H. & Zhang, H. CUP-5, the *C. elegans* ortholog of the mammalian lysosomal channel protein MLN1/TRPML1, is required for proteolytic degradation in autolysosomes. *Autophagy* **7**, 1308–1315 (2011).
26. Zheng, Z. et al. GABAergic synapses suppress intestinal innate immunity via insulin signaling in *Caenorhabditis elegans*. *PNAS* **118**, e2021063118 (2021).
27. Kenyon, C., Chang, J., Gensch, E., Rudner, A. & Tabtiang, R. A *C. elegans* mutant that lives twice as long as wild-type. *Nature* **366**, 461–464 (1993).
28. Jipa, A. et al. Analysis of *Drosophila* Atg8 proteins reveals multiple lipidation-independent roles. *Autophagy* **17**, 2565–2575 (2021).
29. Bar, S., Prasad, M. & Datta, R. Neuromuscular degeneration and locomotor deficit in a *Drosophila* model of mucopolysaccharidosis VII is attenuated by treatment with resveratrol. *Dis. Model Mech.* **11**, dmm036954 (2018).
30. Tan, W., Schauder, C., Naryshkina, T., Minakhina, S. & Steward, R. Zfrp8 forms a complex with fragile-X mental retardation protein and regulates its localization and function. *Dev. Biol.* **410**, 202–212 (2016).
31. Martens, S. & Fracchiolla, D. Activation and targeting of ATG8 protein lipidation. *Cell Discov.* **6**, 23 (2020).
32. Hamasaki, M. et al. Autophagosomes form at ER-mitochondria contact sites. *Nature* **495**, 389–393 (2013).
33. Fan, W., Nassiri, A. & Zhong, Q. Autophagosome targeting and membrane curvature sensing by Barkor/Atg14(L). *Proc. Natl Acad. Sci. USA* **108**, 7769–7774 (2011).
34. Cheng, X. et al. Pacer Mediates the Function of Class III PI3K and HOPS Complexes in Autophagosome Maturation by Engaging Stx17. *Mol. Cell* **65**, 1029–1043.e5 (2017).
35. Sasai, M. et al. Essential role for GABARAP autophagy proteins in interferon-inducible GTPase-mediated host defense. *Nat. Immunol.* **18**, 899–910 (2017).
36. Wan, W. et al. mTORC1-Regulated and HUWE1-Mediated WIP2 Degradation Controls Autophagy Flux. *Mol. Cell* **72**, 303–315.e6 (2018).
37. Karsli-Uzunbas, G. et al. Autophagy is required for glucose homeostasis and lung tumor maintenance. *Cancer Discov.* **4**, 914–927 (2014).
38. An, H. & Harper, J. W. Ribosome abundance control via the ubiquitin–proteasome system and autophagy. *J. Mol. Biol.* **432**, 170–184 (2020).
39. An, H. & Harper, J. W. Systematic analysis of ribophagy in human cells reveals bystander flux during selective autophagy. *Nat. Cell Biol.* **20**, 135–143 (2018).
40. An, H., Ordureau, A., Korner, M., Paulo, J. A. & Harper, J. W. Systematic quantitative analysis of ribosome inventory during nutrient stress. *Nature* **583**, 303–309 (2020).
41. Lu, K., Psakhye, I. & Jentsch, S. Autophagic clearance of polyQ proteins mediated by ubiquitin–Atg8 adaptors of the conserved CUET protein family. *Cell* **158**, 549–563 (2014).
42. Khaminets, A. et al. Regulation of endoplasmic reticulum turnover by selective autophagy. *Nature* **522**, 354–358 (2015).
43. Liu, R. et al. FUNDC1-mediated mitophagy and HIF1 $\alpha$  activation drives pulmonary hypertension during hypoxia. *Cell Death Dis.* **13**, 634 (2022).

**Publisher's note** Springer Nature remains neutral with regard to jurisdictional claims in published maps and institutional affiliations.

the author(s) or other rightsholder(s); author self-archiving of the accepted manuscript version of this article is solely governed by the terms of such publishing agreement and applicable law.

Springer Nature or its licensor (e.g. a society or other partner) holds exclusive rights to this article under a publishing agreement with

© The Author(s), under exclusive licence to Springer Nature Limited 2025

<sup>1</sup>Department of Biochemistry and Department of Hepatobiliary and Pancreatic Surgery of the First Affiliated Hospital, Zhejiang University School of Medicine, Hangzhou, China. <sup>2</sup>State Key Laboratory of Respiratory Disease, Guangzhou Municipal and Guangdong Provincial Key Laboratory of Protein Modification and Degradation, School of Basic Medical Sciences, Guangzhou Medical University, Guangzhou, China. <sup>3</sup>Key Laboratory of Systems Health Science of Zhejiang Province, School of Life Science, Hangzhou Institute for Advanced Study, University of Chinese Academy of Sciences, Hangzhou, China. <sup>4</sup>The Fourth Affiliated Hospital, Zhejiang University School of Medicine, Yiwu, China. <sup>5</sup>Institute of Translational Medicine, Zhejiang University, Hangzhou, China. <sup>6</sup>Department of Cell Biology and Bone Marrow Transplantation Center of the First Affiliated Hospital, Zhejiang University School of Medicine, Hangzhou, China. <sup>7</sup>Department of Anesthesiology, The Second Affiliated Hospital of Guangzhou Medical University, Guangzhou, China. <sup>8</sup>Key Laboratory of Vector Biology and Pathogen Control of Zhejiang Province, School of Life Sciences, Huzhou University, Huzhou, China. <sup>9</sup>School of Pharmaceutical Science and Technology, Tianjin University, Tianjin, China. <sup>10</sup>School of Public Health, Zhejiang University School of Medicine, Hangzhou, China. <sup>11</sup>Assisted Reproduction Unit, Department of Obstetrics and Gynecology, Sir Run Run Shaw Hospital, Zhejiang University School of Medicine, Hangzhou, China. <sup>12</sup>Key Laboratory of Reproductive Dysfunction Management of Zhejiang Province, Sir Run Run Shaw Hospital, Zhejiang University School of Medicine, Hangzhou, China. <sup>13</sup>Department of Pathology of Sir Run Run Shaw Hospital, and Department of Human Anatomy, Histology and Embryology, System Medicine Research Center, NHC and CAMS Key Laboratory of Medical Neurobiology, Zhejiang University School of Medicine, Hangzhou, China. <sup>14</sup>Department of Neurobiology and Department of Anesthesiology of First Affiliated Hospital, Zhejiang University School of Medicine, Hangzhou, China. <sup>15</sup>NHC and CAMS Key Laboratory of Medical Neurobiology, MOE Frontier Science Center for Brain Research and Brain-Machine Integration, School of Brain Science and Brain Medicine, Zhejiang University, Hangzhou, China. <sup>16</sup>Mass Spectrometry and Metabolomics Core Facility, Key Laboratory of Structural Biology of Zhejiang Province, Westlake University, Hangzhou, China. <sup>17</sup>Department of Neurology, the Second Affiliated Hospital of Zhejiang University School of Medicine, Zhejiang University, Hangzhou, China. <sup>18</sup>Centre for Cellular Biology and Signaling, Zhejiang University-University of Edinburgh Institute, Haining, China. <sup>19</sup>School of Life Sciences, Tsinghua University, Beijing, China. <sup>20</sup>Zhejiang Provincial Key Laboratory for Cancer Molecular Cell Biology, Life Sciences Institute, Zhejiang University, Hangzhou, China. <sup>21</sup>These authors contributed equally: Yuting Chen, Jiaxin Hu, Pengwei Zhao, Jie Fang. ✉ e-mail: [kmei@tju.edu.cn](mailto:kmei@tju.edu.cn); [zouwei@zju.edu.cn](mailto:zouwei@zju.edu.cn); [huangyp@ucas.ac.cn](mailto:huangyp@ucas.ac.cn); [Fenglab@gzhmu.edu.cn](mailto:Fenglab@gzhmu.edu.cn); [yiconglab@zju.edu.cn](mailto:yiconglab@zju.edu.cn)

## Methods

Our research complied with all of the relevant ethical regulations. All of the animal procedures were conducted according to the protocols approved by the Animal Care and Use Committee of the animal facility at Zhejiang University.

### Yeast strains, constructs and growth conditions

All yeast strains used in this study are listed in Supplementary Table 5. The WT strain (BY4741) and the gene deletion library were purchased from Invitrogen (95401.H2). Related strains were constructed as described previously<sup>44</sup> and confirmed through western blot analysis or polymerase chain reaction (P505-d1, Vazyme). All mutant plasmids and related strains underwent sequencing (Tsingke Biotechnology). Yeast cells were cultured at 30 °C in synthetic medium (SD), which contained 0.17% yeast nitrogen base without amino acids and ammonium sulfate, 0.5% ammonium sulfate, 2% glucose and the requisite auxotrophic amino acids and vitamins. To induce autophagy, cells were grown to the early-log phase and treated with nitrogen starvation (SD-N), comprising 0.17% yeast nitrogen base without amino acids and ammonium sulfate, along with 2% glucose.

### C. elegans strains and genetics

The Bristol *N*<sub>2</sub> strain was used as the WT, with all strains cultured on nematode growth medium (NGM) plates seeded with *E. coli* OP50 at 20 °C. The following strains were used: *N*<sub>2</sub>, *atg-3(bp412)*, *rpl-12(syb7750[P3N-E21L])* (PHX7750, SunyBiotech), *daf-2(e1370)*, *rpl-12(syb7750[P3N-E21L])*; *daf-2(e1370)*, *zacEx2240 [rpl-12p::rpl-12 WT cDNA]* and *zacEx2238[rpl-12p::rpl-12 P3N-E21L cDNA]*. Transgenic lines *zacEx2240* and *zacEx2238* were generated using standard microinjection methods<sup>45</sup>. *syb7750(rpl-12 P3N-E21L)* mutant strain was generated using CRISPR–Cas9-mediated homologous recombination at the genomic locus of *rpl-12*(JC8.3) in the WT genetic background, which was designed and generated by SunyBiotech. The point mutations were confirmed by Sanger sequencing.

### Drosophila stocks and genetics

The Elav-Gal4, MHC-Gal4 and Da-Gal4 flies were obtained from the Bloomington *Drosophila* Stock Center (Indiana University, Bloomington, USA). UAS-Atg5 RNAi flies and UAS-Nufip RNAi were acquired from the Tsinghua Fly Centre (Beijing, China), while UAS-RPL11 RNAi and UAS-RPL12 RNAi flies were obtained from the Vienna *Drosophila* Resource Center (VDRC, Austria). To generate the UAS-RPL12–3×FLAG and UAS-RPL12 P3N-E21L–3×FLAG flies, RPL12–3×FLAG and RPL12 P3N-E21L–3×FLAG sequences were synthesized and cloned into the pUAST plasmid by TSINGKE, then injected into WT (*w<sup>1118</sup>*) flies to obtain the transgenes. The UAS-RPL13A–3×FLAG flies were generously provided by Dr Feng He from Zhejiang University.

The RPL12(P3N-E21L) mutant flies were generated using CRISPR–Cas9 technology at the genomic locus of RPL12(CG3195) in WT (*w<sup>1118</sup>*) flies, which was designed and produced by Fungene Biotech. The mutational status of the flies was confirmed by sequencing. In experiments involving RPL12(P3N-E21L) flies, WT (*w<sup>1118</sup>*) flies served as the control group. Fly starvation induction followed a slightly modified version of previously described methods<sup>46</sup>. In brief, newly eclosed flies were subjected to an 8 h starvation period in empty vials containing only dH<sub>2</sub>O-soaked filter paper.

### Cell culture and authentication

The cells were cultured in Dulbecco's modified Eagle medium (DMEM) containing 10% foetal bovine serum and incubated at 37 °C with 5% CO<sub>2</sub> in a tissue culture chamber. U2OS, HEK293T and ATG7 KO HEK293T cells were donated by Prof. Sun Qiming from Zhejiang University. RPL12 KD HEK293T cells were constructed in our laboratory. The U2OS and HEK293T cell lines were authenticated by Procell Life Science & Technology (short tandem repeat profiling). ATG7 KO HEK293T cells and RPL12 KD HEK293T cells were authenticated by western blot.

### Construction of stable RPL12 KD cell lines

A pLV3-RPL12-Puro vector containing the designed shRNA sequence (5'-CATTAACACAGTGGGAATAT-3') was cloned. HEK293T cell lines stably expressing RPL12 shRNA or control shRNA were obtained through lentivirus infection and subsequently selected with 1 μg ml<sup>-1</sup> of puromycin. Recombinant lentiviruses were generated following the lentiviral packaging protocol. The efficiency of RPL12 KD was assessed using western blotting with an anti-RPL12 antibody (Proteintech, 14536-1-AP).

### Antibodies

The antibodies used in this study were as follows: anti-Pgk1 (Nordic Immunology, NEI30/7S; 1:10,000), anti-FLAG (Sigma, F1804; 1:2,500) for western blot, anti-FLAG (TRAN, R10427; 1:600) for immunostaining, anti-HA (Abmart, M20003L; 1:3,000), anti-thiophosphate ester (Abcam, ab133473; 1:10,000), anti-GFP (Roche, 11814460001; 1:2,500), anti-His (Proteintech, Hrp-66005, 1:2,000), anti-RPL12 (Proteintech, 14536-1-AP P, 1:2,000), anti-RPL23 (Proteintech, 16086-1-AP, 1:2,000), anti-RPL7 (Proteintech, 14583-1-AP, 1:2,000), anti-RPS5 (Proteintech, 16964-1-AP, 1:2,000), anti-RPL26 (Proteintech, 17619-1-AP, 1:2,000), anti-RPS14 (Proteintech, 16683-1-AP, 1:2,000), anti-Atg7 (Proteintech, 10082-2-AP, 1:5,000), anti-tubulin (Proteintech, 11224-1-AP, 1:10,000), anti-TIM23 (Proteintech, 11123-1-AP, 1:3,000), anti-RTN4 (Proteintech, 10950-1-AP, 1:3,000), anti-p62/SQSTM1 (Proteintech, 18420-1-AP, 1:5,000), anti-LC3 (MBL, PM036, 1:1,000), anti-Cherry (Biodragon, B1026, 1:2,000), anti-ATG14 (Proteintech, 19491-1-AP, 1:100 for immunostaining), anti-ATG16L (Proteintech, 29445-1-AP, 1:100 for immunostaining), anti-Atg8a (Millipore, ABC974; 1:2,000 for western blot; 1:600 for immunostaining), anti-Ape1 antibody was obtained from Dr Zhiping Xie Lab (Shanghai Jiaotong University, China); 1:5,000 for western blot, anti-RPS-0, anti-RPL-5 and anti RPL-25.2 antibodies were obtained from Dr Xiaochen Wang (IBP, Chinese Academy of Sciences, China); 1:1,000 for western blot, goat anti-mouse IgG1, human ads-HRP (SouthernBiotech, 1070-05; 1:10,000); goat anti-rabbit, human ads-HRP (SouthernBiotech, 4010-05; 1:10,000) goat anti-mouse IgG H&L Alexa Fluor 488 (Abcam, cab150113; 1:1,000); goat anti-rabbit IgG H&L Alexa Fluor 594 (Abcam, ab150080; 1:1,000). Anti-Rps2, anti-Rps5, anti-Rpl12, anti-Rpl25 and anti-Rpl38 antibodies for *S. cerevisiae* (1:1,000 for western blot); anti-RPS-2, anti-RPS-5, anti-RPS-13, anti-RPL-12, anti-RPL-26 and anti-RPL-27 antibodies for *C. elegans* (1:1,000 for western blot); and anti-RpS14, anti-RpS25, anti-RpS27, anti-RpL3, anti-RpL12 and anti-RpL38 for *D. melanogaster* (1:1,000 for western blot) were produced by Biodragon Company.

### Imaging, auxin treatment, Y2H assay, western blotting and immunoprecipitation

For imaging, yeast strains tagged with fluorescent markers were cultured in nutrient-rich medium until reaching an optical density (OD) of 1.0–1.2, followed by a 6 h nitrogen starvation period (SD-N). Cells were then observed using inverted fluorescence microscopy (IX83; Olympus). Image processing was performed using Fiji ImageJ software and its plugins. The proportion of cells with GFP-tagged ribosomal protein entering the vacuole was determined by counting these cells among 300 yeast cells across three independent experiments. Vph1–mCherry is used to label the yeast vacuolar membrane. Y2H, auxin treatment, western blotting and immunoprecipitation assays were described previously<sup>47</sup>.

### In vitro phosphorylation assay

*atg1Δ* yeast strain expressing either Atg1–3×FLAG or the kinase-dead mutant Atg1 D211A–3×FLAG was subjected to nitrogen starvation for 1 h. A total of 50 OD<sub>600</sub> (optical density measured at a wavelength of 600 nm) yeast cells were collected, and lysates were subjected to immunoprecipitation using anti-FLAG agarose beads (GenScript, L00432). The purified Atg1–3×FLAG or Atg1 D211A–3×FLAG was incubated with 5 μg of purified His–TF–Rpl12a from *E. coli* and 1.5 μl of 10 mM ATP-γ-S (Sigma, A1388) in Atg1 kinase buffer (50 mM HEPES-KOH pH 7.4, 5 mM

NaF, 10 mM MgCl<sub>2</sub> and 1 mM dithiothreitol (DTT)) at 30 °C for 30 min. Subsequently, 2 µl of 50 mM *p*-nitrobenzyl mesylate (Abcam, ab138910) was added, and the reaction continued for another hour at 30 °C. The reaction was terminated by boiling the sample in protein loading buffer for 5 min. The phosphorylation level of His-TF-Rpl12a was assessed using an anti-thiophosphate ester antibody (Abcam, ab92570).

### Semi-in vitro binding assay

GST beads were incubated with purified GST, GST-Atg8 or GST-Atg8<sup>Y49A-L50A</sup> proteins from *E. coli* in binding buffer (50 mM Tris-HCl pH 7.5, 500 mM NaCl, 0.1% Triton X-100, 0.1 mM phenylmethylsulfonyl fluoride and 1 mM DTT) for 2 h at 4 °C. Meanwhile, yeast cells subjected to nitrogen starvation were collected, and their lysates were combined with the GST bead-enriched proteins for 3 h. After washing three times with washing buffer, the protein samples were boiled in 2× protein loading buffer for 5 min at 95 °C.

### Yeast total RNA extraction

To extract total RNA from yeast, cells were cultured to the logarithmic growth phase. A portion of the cells was directly collected, while the remaining cells were transferred to SD-N medium and starved for 6 h before collection. To each sample (one OD<sub>600</sub> yeast cell), 40 µl of a buffer containing 98% formamide and 10 mM EDTA was added. The samples were heated at 70 °C for 10 min to facilitate RNA extraction, then vortexed briefly and centrifuged at 14,000g for 2 min. The supernatant containing RNA was transferred to a new tube. Equal volumes of the supernatant and nucleic acid buffer were mixed and then analysed using gel electrophoresis and a nucleic acid imaging system<sup>48</sup>.

### Yeast polysome profile

Yeast strains were cultured in 100 ml of medium to an OD<sub>600</sub> of 0.6–1.0. CHX was added at a final concentration of 100 µg ml<sup>-1</sup> immediately before collection, and the cultures were promptly chilled in ice water. The cells were collected, washed twice with ice-cold lysis buffer (20 mM HEPES-KOH pH 7.6, 100 mM KCl, 12 mM MgCl<sub>2</sub>, 100 mM sucrose, 100 µg ml<sup>-1</sup> CHX, 200 µg ml<sup>-1</sup> heparin and 1 mM DTT) and centrifuged at 2,400g for 5 min. The cell pellets were then resuspended in 800 µl lysis buffer, and glass beads were added to about one-fourth of the total volume. The mixture was vortexed for 15 s, followed by 45 s intervals on ice, repeated 15 times. After centrifugation at 21,000g for 1 h, the supernatant was then placed on a 10–50% sucrose gradient and centrifuged at 260,800g for 2.5 h at 4 °C. Gradients were scanned at absorbance at 260 (A260) nm and fractionated using an Instrument Specialties Company (ISCO) gradient collector<sup>49</sup>. The ultraviolet absorption peak graph is displayed by the Flow Cell software (version 1.56A).

### Yeast cell viability assay

Yeast cells in mid-logarithmic phase were shifted to SD-N medium for the indicated timepoints. Cell viability was evaluated by staining with Phloxine B (Sigma, P4030) at a final concentration of 2.5 µg ml<sup>-1</sup>. The cultures were then observed using fluorescence microscopy with a blue filter, and cells displaying bright fluorescence were identified as deceased<sup>14</sup>.

### Yeast TEM

Yeast strains expressing Rpl10-APEX2 or Rps27a-APEX2 were cultured to log phase. Samples equivalent to 10 OD<sub>600</sub> units were collected after 6 h of SD-N treatment, washed with ice-cold phosphate-buffered saline (PBS) and fixed in 1 ml of 2% paraformaldehyde (Sangon Biotech, A500684) and 2.5% glutaraldehyde (Hushi, 30092436) in PBS. The cells were incubated at 30 °C with shaking at 200 rpm for 30 min, then left at 4 °C overnight. The next day, the cells were washed three times with 0.1 M PBS, stained with 1 ml 3,3'-diaminobenzidine (DAB) staining solution (Solarbio, DA1010) for 15 min at room temperature, and then washed with PBS. Cells were treated with 2% potassium permanganate (Hushi,

7722-64-7) for 2 h, followed by extensive washing with double-distilled water until the cells appeared black. Cells were then dehydrated with ethanol (30–100%) and acetone (100%) before embedding in Epon 812 (Sigma, 45359) and incubating at 37 °C for 12 h, followed by 65 °C for 48 h. Sections were stained and observed via TEM<sup>21</sup>.

### In vitro cross-linking

His<sub>6</sub>-SUMO-Rpl12a and His<sub>6</sub>-Atg8 (at a final concentration of 1 µg µl<sup>-1</sup>) were incubated with disuccinimidyl suberate (DSS) cross-linkers (0.5 mM final concentration), freshly dissolved in 1% (v/v) DMSO/reaction buffer (50 mM HEPES, pH 7.5, and 150 mM NaCl). The cross-linking reaction was carried out at room temperature for 1 h. To terminate the reaction, 50 mM ammonium bicarbonate was added. A 30 µl reaction mixture containing His<sub>6</sub>-SUMO-Rpl12a (400 µg ml<sup>-1</sup>), or its mutant His<sub>6</sub>-SUMO-Rpl12a K4FSY (400 µg ml<sup>-1</sup>), and His<sub>6</sub>-Atg8 (400 µg ml<sup>-1</sup>) in HEPES buffer (pH 7.5) was incubated at 37 °C for 12 h. A portion of the reaction mixture (10 µl) was prepared either for MS analysis via in-solution digestion or for analysis by western blot using an anti-His antibody.

### Analysis by LC-MS/MS for cross-linking

The reaction mixture was resuspended in 0.1% formic acid (FA) for liquid chromatography (LC)-MS/MS analysis. Peptide separation was performed using an EASY-nLC1200 system coupled to a ThermoFisher Orbitrap Exploris 480 mass spectrometer. Samples were directly loaded onto a custom-made capillary column (75 µm × 20 cm, 1.9 µm C18, 5 µm tip). The mobile phases were phase A, containing 0.1% FA, 2% acetonitrile (ACN), and 98% water (H<sub>2</sub>O), and phase B, consisting of 0.1% FA, 20% H<sub>2</sub>O and 80% ACN. The gradient ran for 60 min, starting at 4% phase B (0 min), increasing to 5% (1 min), 25% (41 min), 37% (54 min), 90% (57 min) and held at 90% until 60 min. The flow rate was set to 450 nl min<sup>-1</sup>. Data acquisition was done in data-dependent mode (top30). For MS1 scans, the range was 350–1,500 *m/z*, with a resolution of 60,000, an automatic gain control (AGC) target of 1 × 10<sup>6</sup> and a maximum injection time of 20 ms. For MS2 scans, the resolution was 15,000 with a fixed first mass of 125 *m/z*. The AGC target was 1 × 10<sup>5</sup>, and the maximum injection time was 22 ms. Dynamic exclusion was set to 30 s, with a mass tolerance of 10 ppm around the precursor. Ions with charge states of 1, 6–8 and greater than 8 were excluded.

### Data analysis for cross-linking

Cross-linked peptides were identified using pLink2 (version 2.3.11). The search parameters for pLink were as follows: precursor mass tolerance 20 ppm; fragment mass tolerance 20 ppm; filter tolerance 10 ppm; false discovery rate ≤5 at peptide spectrum match level; peptide length minimum 6 amino acids and maximum 60 amino acids per chain; peptide mass minimum 600 and maximum 6,000 Da per chain, three missed cleavage sites per chain. Protein sequences were downloaded from UniProt.

### Western blotting analysis of *C. elegans* proteins

Synchronized L4-stage worms were grown in 30 6-cm NGM plates for each strain and starved for 0 h and 24 h. Then, the worms were collected from the plates by washing with M9 solution for three times, and the supernatant was removed. Next, the worms were frozen in the liquid nitrogen before transferring to ice for dissolution. A total of 150 µl protein lysate was added into each 2 ml Eppendorf (EP) tube (with a Tris-acetate-phosphate (TAP)/protease inhibitor ratio of 200:1, Bimake). The mixture was ground on ice with a pestle for 5–10 min, then centrifuged at 4 °C and 18,400g for 20 min. The supernatant was transferred to a new 1.5 ml EP tube, and 5× loading buffer was added. The samples were heated in a metal bath at 95 °C for 10 min, then stored at –80 °C. Western blotting was performed by the following standard procedures.

### *C. elegans* RNA interference assay

Worms were transferred onto RNAi plates (freshly prepared NGM containing 1 mg ml<sup>-1</sup> isopropyl-β-D-thiogalactopyranoside and 1 mg ml<sup>-1</sup>

ampicillin) seeded with HT115 *E. coli* stains to express gene-specific double-strand RNAs and cultured at 20 °C. For lifespan experiments, WT ( $N_2$ ) worms at L4 stage were selected and placed on *L4440* (EV as a negative control), *atg-3* RNAi, *rpl-12* RNAi and *rpl-26* RNAi plates to quantify the survival rate. Worms were transferred to a new plate every 2 days.

### Total RNA extraction of *C. elegans*

To assess rRNA content in different strains, L4-stage worms were used. Synchronized worms from ten 6-cm plates were collected into a 1.5 ml centrifuge tube and supplemented with 150  $\mu$ l of TRIzol (Ambion, 15596018). Total RNA was extracted using a cell/tissue total RNA extraction kit (YEASEN, I9221ES50) with an equal mass of worms of  $N_2$ , *atg-3(bp412)* or *rpl-12(syb7750[P3N-E21L])*. RNA samples were separated and examined by agarose gel electrophoresis.

### Quantification of *C. elegans* brood size

Brood size was determined by plating a total of 12–16 individual L4 worms on 6-cm NGM plates in at least three independent experiments at 20 °C. Each P0 worm was allocated a separate plate, starting from day 1 and transferring to a new plate every other day, up to day 9. The number of F1 progenies that hatched and developed into adults was recorded daily, with the count of hatched F1 progenies tallied for each individual worm.

### *C. elegans* embryo hatching assay

Embryo hatching was determined by picking 40 adult worms onto new plates and allowing them to lay embryos for 2 h in at least three independent experiments at 20 °C. Adults were then removed, and the embryos were counted. After 16 h, the number of unhatched embryos was counted to calculate the hatching rate for each strain.

### Quantification of *C. elegans* L1 survival rate under starvation

Six to eight plates of worms for each strain were prepared, and the animals were cultured at 20 °C. *C. elegans* were washed with M9, and embryos were collected with bleach buffer to obtain synchronized L1 (larvae 1) stage worms. L1-stage worms were evenly distributed to 30 1.5-ml centrifuge tubes. Animals in the centrifuge tubes were then transferred to NGM plates with OP50 every day, and the surviving larvae were counted. At least three independent experiments were performed for each strain.

### *C. elegans* lifespan assay

All lifespan measurements in this study were performed at 20 °C, with L4 stage designated as day 0. Animals were recorded as alive, dead or missing every 2 days. Animals that did not respond to the touch of a picker were recorded as dead. Those that died from external factors unrelated to ageing, such as adhering to the wall or vulval rupture, were noted as missing. Kaplan–Meier survival curves were plotted for each lifespan test, and statistical analysis (log-rank (Mantel–Cox) test) was conducted.

### *C. elegans* killing assay by *P. aeruginosa* PA14

The *P. aeruginosa* PA14 killing experiment followed a previously described method with some modifications<sup>26</sup>. Initially, 4 ml of Luria-Bertani broth (LB) medium was added into a 15 ml centrifuge tube, and PA14 monoclonal cultures were obtained, followed by overnight incubation at 200 rpm and 37 °C. Subsequently, 40  $\mu$ l of PA14 was seeded onto 6-cm NGM plates using a triangular stick. The plates were left at room temperature for 20 min before being cultured at 37 °C for 24 h, followed by 25 °C for another 24 h, and then stored at 4 °C. Before use, the plates were equilibrated to room temperature for 2 h. The experiment was performed at 20 °C, starting with 60 animals for each strain. Survival, death and disappearance were recorded every 12 h. Worms that did not respond to touching by a picker were marked

as dead, whereas those that died due to vulva rupture or crawled out of the dish were counted as disappearing. All survival experiments were independently repeated at least three times. Kaplan–Meier survival curves were plotted for each lifespan test, and statistical analysis (log-rank (Mantel–Cox) test) was performed.

### Climbing ability assay, lifespan recording and locomotion assay of flies

For the climbing ability assay, the flies were divided into five groups, each contains ten flies. The flies were aged at 25 °C for 4 weeks before climbing index assay (%), defined as the proportion of flies that can climb 3 cm within 5 s). To investigate starvation sensitivity, the climbing index was determined after undergoing an 8 h starvation period, by calculating the ratio of flies that can climb 6 cm within 2 s.

For lifespan recording, newly eclosed male flies were collected and divided into the indicated groups, with each group containing 10–15 individuals. Flies were maintained at 25 °C, with food exchanged every 2 days. Survival rates (%) were calculated on the basis of the number of deceased individuals recorded every 2 days. To assess locomotion behaviour, individual flies were placed on circular disks with a diameter of 3.5 cm and monitored for 10 min to record their movement trajectories.

### Measuring the pupation and eclosion rates

Pupariation and eclosion rate were assessed following previously established protocols<sup>50</sup>. In brief, fly eggs were collected and plated on low-density fly food. The pupariation rate was determined by dividing the total number of pupae by the number of eggs. Similarly, the eclosion rate was defined as the proportion of adult flies emerging from the pupae.

### Bacterial infection and fly survival rate

Bacterial infection experiments were performed using *S. aureus*, cultured at 37 °C until an OD<sub>600</sub> of ~2.0, and *Salmonella* spp., cultured to an OD<sub>600</sub> of ~3.0. The bacteria were injected into the thoraxes of the flies, and the survival rate was monitored every 4 h by counting the number of deceased flies.

### Paraffin embedding and H&E staining

Paraffin embedding and H&E staining were performed as previously described<sup>51</sup>. Fly thoraxes were collected and fixed with Carnoy fixation solution (ethanol:chloroform:acetic acid = 6:3:1) for 4 h. The samples were then dehydrated in ethanol, immersed in methyl benzoate for 1 h and embedded in molten paraffin. The embedded tissues were sectioned into continuous sections of 8  $\mu$ m thickness using a Leica section apparatus (RM2235). H&E staining (ZSGB-BIO) was used to visualize tissue degeneration.

### Immunostaining

Thoracic muscles of flies were dissected and collected in 1 $\times$  PBS, then fixed with 4% paraformaldehyde, permeabilized with 0.1% Triton X-100 in 1 $\times$  PBS and blocked with 10% goat serum for 2 h. Subsequently, samples were incubated overnight at 4 °C with primary antibodies (anti-fly ATG8a and anti-FLAG antibodies). After rinsing three times with 1 $\times$  PBST, the tissues were incubated at room temperature for 2 h with Alexa594-conjugated anti-rabbit antibody and Alexa488-conjugated anti-mouse antibody. Phalloidin (Solarbio, 626Z011) staining was performed at room temperature for 20 min.

### Fly protein extraction, western blot and RNA extraction

At least 20 thoraxes from flies were collected and homogenized in western/IP buffer (Absin) containing the protease inhibitor. For RNA extraction, the thoraxes of an equal number of fruit flies from different backgrounds were collected and homogenized in TRIzol reagent (Thermo Scientific).

### Fly polysome profile

A specific number of third-instar *Drosophila* larvae was collected under nutrient-rich and starvation conditions. After freezing with liquid nitrogen, the larvae were ground into powder. Lysis buffer (1 ml) was added, composed of 10 mM pH 7.5 Tris-HCl, 5 mM MgCl<sub>2</sub>, 100 mM KCl, 2 mM DTT, 1% Triton X-100 and 50 µg ml<sup>-1</sup> CHX, along with protease and RNase inhibitors. The mixture was reacted on ice for 10 min, then centrifuged at 13,000g for 10 min at 4 °C. A 10–50% sucrose density gradient solution was prepared (10 mM pH 7.5 Tris-HCl, 5 mM MgCl<sub>2</sub>, 100 mM KCl, 2 mM DTT and 5 g or 25 g sucrose). The supernatant was carefully layered on top of the gradient. The sucrose gradient was centrifuged at 222,200g for 3 h in an SW41 rotor at 4 °C. Gradients were scanned at A260 nm and fractionated using an ISCO gradient collector<sup>52</sup>. The ultraviolet absorption peak graph is displayed by the Flow Cell software (version 1.56 A).

### Immunofluorescence of mammalian cells

Cells grown on coverslips were transfected with the indicated plasmids, then fixed in 4% paraformaldehyde in PBS for 20 min at room temperature and permeabilized with 0.1% Triton X-100 in PBS for 20 min. Following permeabilization, cells were treated with block buffer (1% bovine serum albumin, and 0.1% Triton X-100 in PBS) for 1 h at room temperature. Next, cells were incubated with primary antibodies diluted in block buffer overnight at 4 °C. After incubation, cells were washed three times with PBS, each for 10 min, followed by incubation with Alexa Fluor-conjugated secondary antibody for 1 h at room temperature. Finally, slides were examined using a laser scanning confocal microscope (Zeiss LSM 800).

### Immunoprecipitation of mammalian cells

Cell pellets were homogenized in TAP buffer (20 mM Tris-HCl, pH 7.4, 150 mM NaCl, 0.5% NP-40, 1 mM NaF, 1 mM Na<sub>3</sub>VO<sub>4</sub>, 1 mM EDTA, 10 mM MG132, protease cocktail and phosphatase cocktail) and incubated on ice for 30 min. The lysates were cleared by centrifugation at 18,400g for 30 min. The supernatant was then incubated with antibody-conjugated beads, followed by rotation for 4 h at 4 °C. After incubation, the beads were washed three times with TAP buffer.

### Cell survival assays

Mammalian cells were plated in 12-well plates containing DMEM. The next day, when cells reached approximately 50% confluence, they were transfected with various plasmids. Following transfection, the DMEM was replaced with Hank's Balanced Salt Solution (HBSS) and incubated for 48 h. After incubation, cells were fixed in 4% paraformaldehyde in PBS for 20 min at room temperature and stained with Giemsa<sup>5</sup>.

### RNA extraction from mammalian cells

RNA extraction was performed using TRIzol reagent<sup>53</sup> (Vazyme, R401-01), following standard protocols. The number of cells used for RNA extraction was consistent across experiments and determined on the basis of cell counts obtained with a haemocytometer.

### Polysome profile of mammalian cells

When cells reached 80–90% confluence, CHX was added at a final concentration of 50 µg ml<sup>-1</sup> immediately before collection, and the plates were then placed on the ice. Cells were collected using 1× PBS containing 50 µg ml<sup>-1</sup> CHX, and the supernatant was discarded after centrifugation at 400g for 3 min. Next, 1 ml of lysis buffer (10 mM pH 7.5 Tris-HCl, 5 mM MgCl<sub>2</sub>, 100 mM KCl, 2 mM DTT, 1% Triton X-100, 50 µg ml<sup>-1</sup> CHX, protease inhibitors and RNase inhibitors) was added, followed by a 4 min incubation on ice. Samples were then centrifuged at 14,000g for 7 min at 4 °C. The supernatant was layered onto a 10–50% sucrose density gradient (10 mM pH 7.4 Tris-HCl, 5 mM MgCl<sub>2</sub>, 100 mM KCl, 2 mM DTT and 5 g or 25 g of sucrose) and centrifuged at 222,200g for 2 h 30 min in an SW41 rotor at 4 °C. Gradients were analysed at

A260 nm and fractionated using an ISCO gradient collector<sup>52</sup>. The ultraviolet absorption peak graph is displayed by the Flow Cell software (version 1.56A).

### *S. typhimurium* infection assay

For colony-forming unit determination, the indicated mammalian cells were infected with *Salmonella typhimurium* carrying RFP at a multiplicity of infection of 100:1 in triplicate wells of a 24-well plate for 1 h at 37 °C with 5% CO<sub>2</sub> (recorded as 0 h post-infection). After 1 h, cell monolayers were washed with prewarmed PBS, and fresh DMEM supplemented with 20 mg ml<sup>-1</sup> gentamicin was added. At 4 h and 8 h post-infection, cells were extensively washed with PBS and lysed in PBS buffer containing 0.1% Triton X-100. Lysates were vortexed, and appropriate dilutions were plated onto LB agar plates.

For microscopy analysis, mammalian cells were seeded on 60 mm culture dishes with 12-mm-diameter round glass coverslips one day before infection. *S. typhimurium* infection was performed as described above. At 8 h post-infection, cells were fixed with 4% paraformaldehyde in PBS for 20 min and stained with an anti-tubulin antibody, followed by incubation with Alexa Fluor 488-conjugated secondary antibodies. Samples were then analysed using a laser scanning confocal microscope (Zeiss LSM 800). Three independent bacterial infection assays were conducted.

### TEM of mammalian cells

When mammalian cells in a 6 cm dish reached 80–90% confluence, they were treated with Torin1 for 4 h while simultaneously adding 500 nM concanamycin A. Cells were collected, washed with PBS and fixed in 2.5% glutaraldehyde overnight at 4 °C. The following day, cells were washed three times with PBS, incubated with 1% osmium tetroxide for 1 h and washed twice with double-distilled water. The samples were dehydrated with sequential ethanol treatments (50%, 70%, 80%, 90% and 100%) for 15 min each, followed by two treatments with acetone for 20 min each. Samples were then treated with a 1:2 mixture of Epon 812 embedding agent and acetone for 2 h, followed by overnight incubation at room temperature in a 2:1 mixture. On the third day, samples were embedded in 100% embedding agent, incubated at 37 °C for 12 h and then transferred to a 65 °C oven for 48 h. Finally, the samples were sectioned, stained and observed under a TEM.

### Mouse experiments and tissue processing

All animal studies and experimental procedures were approved by the Animal Care and Use Committee at Zhejiang University. Male C57BL/6 mice, aged 7 weeks, were maintained in a controlled environment with a 12 h light/dark cycle and provided with pelleted AIN-76A chow (Research Diets) and water ad libitum. The environmental temperature was maintained at 20–26 °C, with relative humidity controlled at 50–60%. For fasting experiments, the mice were deprived of food for 24 h, while water remained available. Liver tissues for the metabolomics experiment were rapidly frozen in liquid nitrogen upon collection.

To investigate the role of RPL12 in regulating ribophagy in vivo, we generated rAAV vectors carrying WT RPL12 (rAAV-RPL12), RPL12-P3N-E21L and pseudoserotyped AAV9 capsid (Vigene Biosciences) in HEK293T cells. Twelve mice were randomly divided into two groups ( $n = 6$  per group) and injected via the tail vein with the respective viruses. After 4 weeks, the mice were euthanized for analysis. For metabolomics analysis, liver samples were collected from the mice and processed using BrainyVTA<sup>54</sup>. The R package DESeq2 (version 1.34.0) was used to identify components with different abundance in MS with a threshold of  $P < 0.01$  and  $|\log_2 \text{fold change (FC)}| > \log_2(1.2)$ .

### Determination of glycogen in mouse liver

Liver glycogen content was measured using the Glycogen Content Detection Kit (Saint-Bio, BA1376). A 0.1 g liver sample was placed in a 10 ml test tube, and 0.75 ml of extraction solution was added. The

sample was boiled in a water bath for 20 min, with the lid tightly sealed to prevent water evaporation, and the tube was shaken every 5 min for thorough mixing. After tissue dissolution, the tube was allowed to cool, the volume was adjusted to 5 ml with distilled water, mixed and centrifuged at 8,000g at 25 °C for 10 min. The supernatant was collected and measured at 620 nm.

### Extraction of total RNA from liver tissue

Fresh liver tissue was flash-frozen in liquid nitrogen, and identical regions were quickly selected under low temperatures. A 100 mg sample was weighed, and 1 ml of TRIzol reagent (Vazyme, R401-01) along with 1 mm glass beads were added. The sample was homogenized at 4 °C and 60 Hz for 120 s using a homogenizer. Subsequent steps were performed according to the manufacturer's protocol.

### Extraction of liver tissue protein

Fresh liver tissue was treated with liquid nitrogen, and a 50 mg sample was weighed and selected from the same region at low temperature. After adding 1 ml of TAP buffer (20 mM Tris-HCl, pH 7.4, 150 mM NaCl, 0.5% NP-40, 1 mM NaF, 1 mM Na<sub>3</sub>VO<sub>4</sub>, 1 mM EDTA, 10 nM MG132, protease inhibitor cocktail and phosphatase inhibitor cocktail) along with 1 mm glass beads, the sample was homogenized at 4 °C and 60 Hz for 120 s. The homogenate was centrifuged at 21,100g for 15 min at 4 °C, and the supernatant was collected. Protein concentrations were measured using the bicinchoninic acid (BCA) protein assay. Appropriate volumes of the supernatant were mixed with 2× SDS loading buffer to achieve uniform concentrations, then boiled at 95 °C for 5 min.

### Blood glucose measurements

Blood glucose levels were measured by drawing blood from the tail vein. Glucose concentrations were determined using an Accu-Chek glucometer (Roche).

### In vitro pull-down assay

The His<sub>6</sub>-tagged TF-Rpl12 protein was expressed using the pCold-TF DNA vector, while the His<sub>6</sub>-tagged SUMO-Rpl12 protein was expressed using the pET28a-SUMO vector. The GST-Atg8 protein was expressed using the pGEX-4T-1 vector, and GST-Atg8 was cleaved with thrombin to obtain Atg8 protein. For the in vitro pull-down assay, a specific amount of purified protein (ranging from 3 to 5 nM, depending on protein purity) was mixed with 10 µl of either GST beads or Ni-NTA beads in 500 µl of binding buffer A (50 mM Tris-HCl, pH 7.5, 0.5 M NaCl, 1 mM DTT, 1% Triton X-100, 1% phenylmethylsulfonyl fluoride and 20 mM imidazole, if Ni-NTA beads were used). The mixture was incubated on a rotor at 4 °C for 1 h. After incubation, the beads were washed once with binding buffer A and then washed twice with binding buffer B (100 mM NaCl, 1 mM EDTA, 1 mM EGTA and 1% Tween-20 in 1×PBS). The beads associated with the purified protein were mixed with an equal amount of purified target protein from *E. coli*. This mixture was rotated at 4 °C for 3 h. Following three washes with binding buffer B, 50 µl of 2× SDS loading buffer was added, and the samples were boiled at 95 °C for 5 min. The protein samples were then separated by SDS-PAGE and stained with Coomassie brilliant blue dye (G250) for visualization.

### Mass spectrometric analysis

The separation of proteins was accomplished via SDS-PAGE, followed by staining with Coomassie Blue G-250. Gel bands of interest were excised into individual pieces and subjected to trypsin digestion overnight at 37 °C in a 50 mM ammonium bicarbonate solution, after prior reduction and alkylation. The digested products underwent two extractions with a 1% FA solution in a 50% ACN aqueous solution, followed by drying using a speedvac to reduce volume. For LC-MS/MS analysis, peptide separation was carried out over a 65 min gradient elution at a flow rate of 0.300 µl min<sup>-1</sup> within a Thermo EASY-nLC1200 integrated

nano-HPLC system directly linked to a Thermo Q Exactive HF-X mass spectrometer. The analytical column utilized was a custom-made fused silica capillary column (75 µm inner diameter, 150 mm length) packed with C-18 resin (300 Å, 3 µm). The mobile phase A comprised 0.1% FA, while mobile phase B comprised 100% ACN with 0.1% FA. The mass spectrometer operated in data-dependent acquisition mode, with Xcalibur 4.1 software performing a single full-scan mass spectrum in the Orbitrap (ranging from 400 to 1,800 *m/z*, with a resolution of 60,000), followed by 20 data-dependent MS/MS scans using 30% normalized collision energy. Each MS result underwent analysis using Thermo Xcalibur Qual Browser and Proteome Discovery for subsequent database searching.

### Statistics and reproducibility

Two or three biologically independent experiments were performed and yielded consistent results. Sample sizes were not predetermined using statistical methods. Except for MS-based analysis, the investigators were not blinded to allocation during experiments and outcome assessment. Data distribution was assumed to be normal, but this was not formally tested. No data were excluded from the analyses, and all images were randomly collected across all experiments. Data processing and analysis were conducted using GraphPad Prism 8.0. Statistical comparisons between two groups were made using an unpaired two-tailed Student's *t*-test, while the log-rank (Mantel-Cox) test was used to analyse survival rate differences of flies or worms under different physiological conditions. Statistical significance was defined as  $P < 0.05$  (\* $P < 0.05$ , \*\* $P < 0.01$ , \*\*\* $P < 0.001$ ), with exact *P* values provided in the source numerical data. Data are presented as mean ± s.d. Sample sizes are specified in the figure legends. In the worm and fly experiments, age-matched individuals with different genotypes were randomly assigned to experimental groups. For cell culture experiments, cells with different genotypes or treatments were randomly distributed into experimental groups. In the animal experiments, age-matched mice were randomly assigned to different experimental groups. The degradation percentage of GFP-fused proteins was calculated by dividing GFP intensity by the sum of GFP and GFP-fused protein intensities, normalized to WT values.

### Reporting summary

Further information on research design is available in the Nature Portfolio Reporting Summary linked to this article.

### Data availability

The MS proteomics data have been deposited to the ProteomeXchange Consortium (<http://proteomecentral.proteomexchange.org>) via the PRIDE repository<sup>55,56</sup> (<ftp://massive.ucsd.edu/v08/MSV000096540/> and <ftp://massive.ucsd.edu/v08/MSV000096542/>), with the dataset identifier MassIVE MSV000096540 (or PXD058305) and MSV000096542 (or PXD058307). The raw LC-MS-based untargeted metabolomics data files generated in this study are available at the National Genomics Data Center<sup>57</sup> (<https://ngdc.cncb.ac.cn/omix/releaseList>) with the dataset identifier OMIX008012 (<https://ngdc.cncb.ac.cn/omix/release/OMIX008012>) and are publicly available. Source data are provided with this paper. All of the other data supporting the findings of this study are available from the corresponding author upon reasonable request.

### References

- Janke, C. et al. A versatile toolbox for PCR-based tagging of yeast genes: new fluorescent proteins, more markers and promoter substitution cassettes. *Yeast* **21**, 947–962 (2004).
- Mello, C. & Fire, A. DNA transformation. *Methods Cell. Biol.* **48**, 451–482 (1995).
- Eriksson, A. et al. Neuromodulatory circuit effects on *Drosophila* feeding behaviour and metabolism. *Sci. Rep.* **7**, 8839 (2017).

47. Yao, W. et al. Mec1 regulates PAS recruitment of Atg13 via direct binding with Atg13 during glucose starvation-induced autophagy. *Proc. Natl Acad. Sci. USA* **120**, e2215126120 (2023).
  48. Shedlovskiy, D., Shcherbik, N. & Pestov, D. G. One-step hot formamide extraction of RNA from *Saccharomyces cerevisiae*. *RNA Biol.* **14**, 1722–1726 (2017).
  49. Ma, C., Wu, D., Chen, Q. & Gao, N. Structural dynamics of AAA + ATPase Drg1 and mechanism of benzo-diazaborine inhibition. *Nat. Commun.* **13**, 6765 (2022).
  50. Varma, V., Krishna, S., Srivastava, M., Sharma, V. K. & Sheeba, V. Accuracy of fruit-fly eclosion rhythms evolves by strengthening circadian gating rather than developmental fine-tuning. *Biol. Open* **8**, bio042176 (2019).
  51. Huang, Y., Wan, Z., Wang, Z. & Zhou, B. Insulin signaling in *Drosophila melanogaster* mediates A $\beta$  toxicity. *Commun. Biol.* **2**, 13 (2019).
  52. Luo, S. et al. *Drosophila* tsRNAs preferentially suppress general translation machinery via antisense pairing and participate in cellular starvation response. *Nucleic Acids Res.* **46**, 5250–5268 (2018).
  53. Wang, B. et al. PRCC–TFE3 fusion-mediated PRKN/parkin-dependent mitophagy promotes cell survival and proliferation in PRCC–TFE3 translocation renal cell carcinoma. *Autophagy* **17**, 2475–2493 (2021).
  54. Love, M. I., Huber, W. & Anders, S. Moderated estimation of fold change and dispersion for RNA-seq data with DESeq2. *Genome Biol.* **15**, 550 (2014).
  55. Ma, J. et al. iProX: an integrated proteome resource. *Nucleic Acids Res.* **47**, D1211–D1217 (2019).
  56. Chen, T. et al. iProX in 2021: connecting proteomics data sharing with big data. *Nucleic Acids Res.* **50**, D1522–D1527 (2022).
  57. CNCB-NGDC Members and Partners. Database Resources of the National Genomics Data Center, China National Center for Bioinformatics in 2021. *Nucleic Acids Res.* **49**, D18–D28 (2021).
- assay; Z. Wu for his guidance on mouse euthanasia and tissue protein extraction; D. Fang and H. Fan for their analysis and processing of metabolomics data from mouse liver; D. Neculai and S. Yan for providing *Salmonella typhimurium* carrying the RFP marker; and H. Zhang for providing the *C. elegans* cup-5(bp510) mutant. The research was supported by National Natural Science Foundation of China (grant nos. 32122028, 92254307 and 32070739) and Zhejiang Provincial Natural Science Foundation of China under grant no. LR21C070001 to C.Y.; the Research Funds of Hangzhou Institute for Advanced Study, UCAS (grant no. 2022ZZ01011) to Y.H.; National Natural Science Foundation of China (grant no. 32100600) to W.Y.; National Natural Science Foundation of China (grant nos. 32370822 and 31970919) to W.Z.; and the National Key Research and Development Program of China (grant no. 2021YFC2600104) to L.Z.

## Acknowledgements

We are grateful to Y. Ohsumi, H. Nakatogawa and Z. Xie for generously providing the plasmids and yeast strains. We also thank L. Yu, N. Gao, D. Pan, Y. Zhen and all other lab members for their insightful reading and constructive discussions on the paper. A special thanks to the technical support of Y. Zhang from cryo-electron microscopy core facilities, Zhejiang University School of Medicine; J. Zhou, F. He, C. Ma, Y. Wu and M. Xue for their assistance with the polysome profiling

## Author contributions

Y.C., K.M., W.Z., Y.H., D.F. and C.Y. performed experiments, analysed data and wrote the paper. J.H., P.Z., J.F., Y.K., Z.L., S.D., W.Y., Y.D., X.W., Y.P., J.W., J.Y., M.F., K.T., X.L. and Y.Z. performed experiments and analysed data. J.Z., Z.X., H.X., C.W., L.Z., S.F., Z.H., Z.Y., W.L., Q.S. and B.Y. analysed data. All authors approved the final version of the paper.

## Competing interests

The authors declare no competing interests.

## Additional information

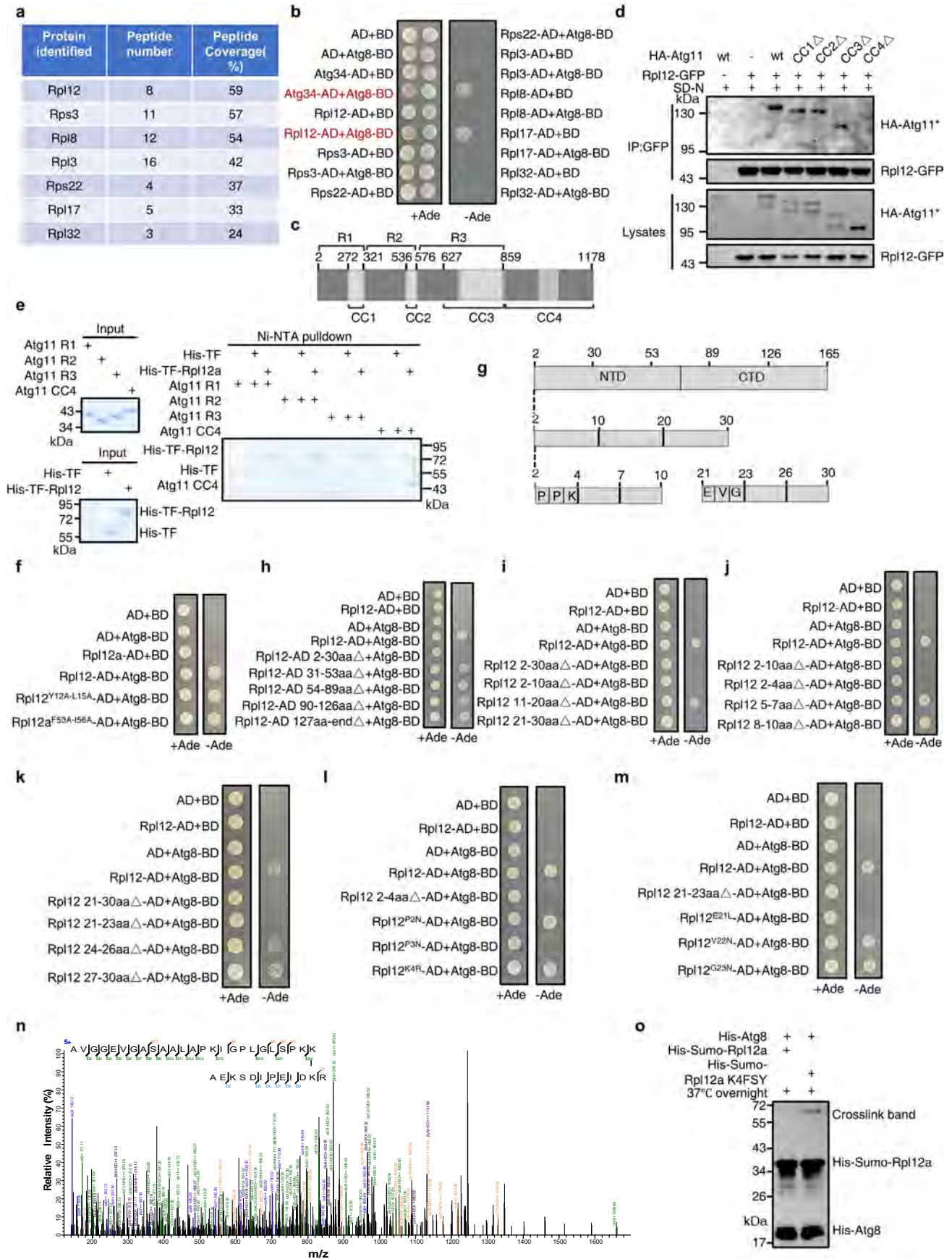
**Extended data** is available for this paper at <https://doi.org/10.1038/s41556-024-01598-2>.

**Supplementary information** The online version contains supplementary material available at <https://doi.org/10.1038/s41556-024-01598-2>.

**Correspondence and requests for materials** should be addressed to Kunrong Mei, Wei Zou, Yunpeng Huang, Du Feng or Cong Yi.

**Peer review information** *Nature Cell Biology* thanks Terje Johansen and the other, anonymous, reviewer(s) for their contribution to the peer review of this work.

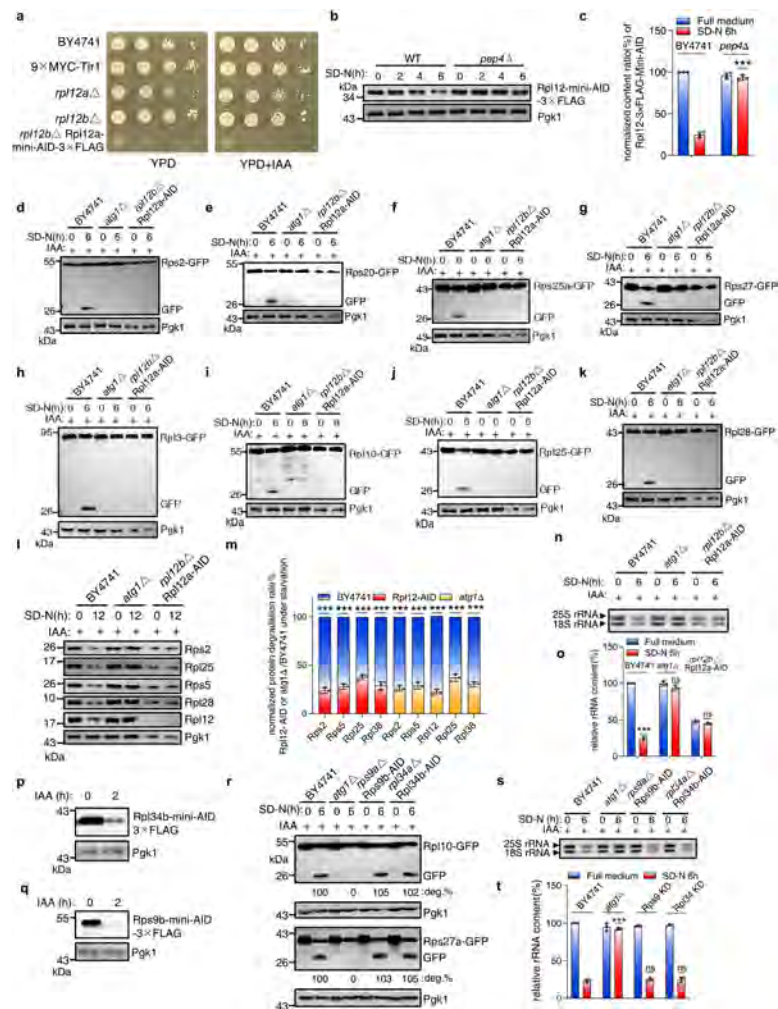
**Reprints and permissions information** is available at [www.nature.com/reprints](http://www.nature.com/reprints).



Extended Data Fig. 1 | See next page for caption.

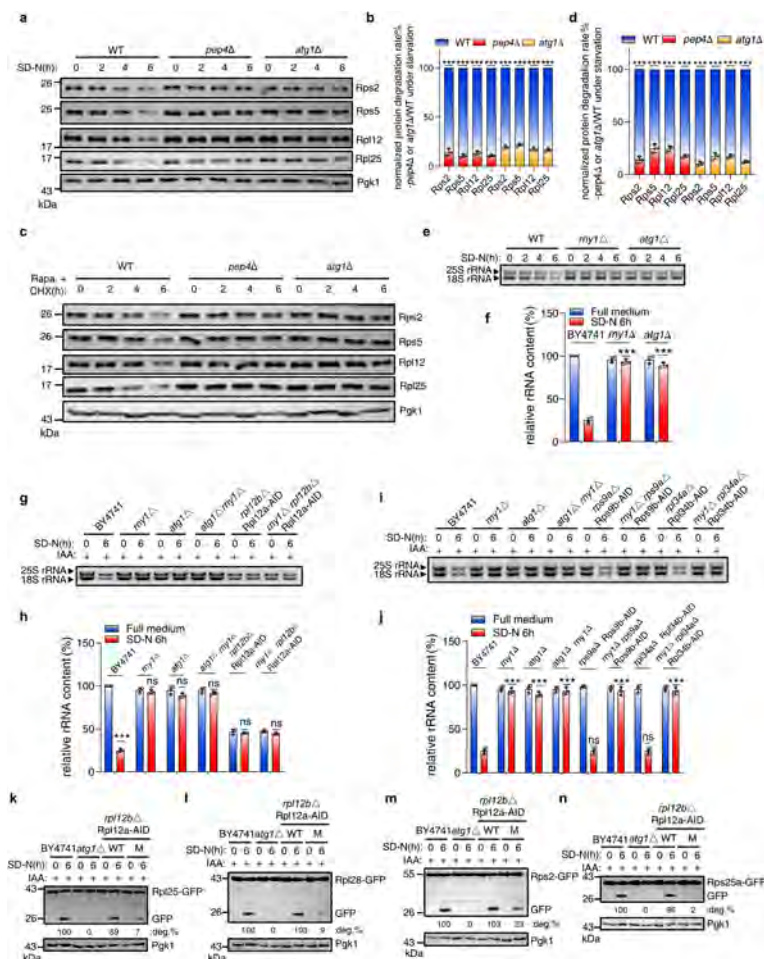
**Extended Data Fig. 1 | Identifying the binding region(s) on Rpl12 associated with Atg8 and Atg11 in yeast.** **a**, Protein samples from Fig. 1b were separated by SDS-PAGE and analyzed by mass spectrometry (MS). The indicated ribosomal proteins binds to Atg8 but does not bind to the Atg8<sup>Y49A-L50A</sup> mutant. **b**, The AH109 strain was transformed with the indicated proteins fused with Atg8-BD, then grown on the indicated agar plates at 30 °C for 3 d. **c**, Schematic representation of the Atg11 domains. **d**, *atg11Δ* yeast cells co-expressing either WT HA-Atg11 or HA-Atg11 variants with Rpl12-GFP were subjected to SD-N for 1 h. Cell lysates were immunoprecipitated using anti-GFP agarose beads and analyzed by western blot with anti-HA antibody. **e**, Ni-NTA pulldowns were performed using purified His-TF-Rpl12 protein with GST-Atg11 R1, R2, R3, or CC4 proteins from *E. Coli*. **f**, The AH109 strain was transformed with either Rpl12 or the indicated

Rpl12 variants fused with AD and Atg8-BD, then grown on the indicated agar plates at 30 °C for 3 d. **g**, Schematic representation of the Rpl12 domains and mutations, including N-terminal domain (NTD) and C-terminal domain (CTD). **h-m**, The AH109 strain was transformed with either Rpl12 or the indicated Rpl12 variants fused with AD and Atg8-BD, and subsequently grown on the indicated agar plates at 30 °C for 3 d. **n**, Tandem mass spectra of cross-linked peptide (AVGGVEGASAALAPKIGPLGLSPK-AEKSDIPEIDKR) demonstrate a direct interaction between Rpl12 and Atg8, with the Rpl12 E21 site is close to Atg8<sup>Y49-L50</sup> sites. **o**, Western blot analysis shows that Rpl12 K4FSY cross-linked with Atg8 *in vitro*. Blots, gels, and Y2H assays are representatives of three independent experiments. Unprocessed blots/gels are available in Source data.



**Extended Data Fig. 2 | Rpl12 is required for starvation-induced ribophagy in yeast.** **a**, The indicated cells were grown on YPD with or without IAA agar plate at 30 °C for 2 days. **b**, *rpl12b* $\Delta$  or *rpl12b pep4* $\Delta$  yeast cells expressing Rpl12a-mini-AID-3 $\times$ FLAG were subjected to SD-N for the indicated times. Protein levels were analyzed by Western blot using anti-FLAG antibody. **c**, The ratio of Rpl12a-mini-AID-3 $\times$ FLAG degradation was quantified from **(b)**. **d–k**, The indicated yeast cells expressing GFP-tagged ribosomal proteins were treated with IAA for 2 h and subjected to SD-N for 0 or 6 h. Ribophagic activity were analyzed by western blot for the cleavage of GFP fusion protein. **l**, The indicated yeast cells were treated with IAA for 2 h and subjected to SD-N for 0 or 12 h. Ribosomal protein levels were analyzed by Western blot. **m**, Degradation ratios of proteins in **(l)** were quantified. **n**, Total RNA was extracted from the indicated yeast cells treated with IAA and subjected to SD-N for 0 or 6 h to assess rRNA levels. **o**, Yeast rRNA from **(n)** were quantified. **p, q**, *rpl34a* $\Delta$  or *rps9a* $\Delta$  cells expressing Rpl34b-mini-AID-3 $\times$ FLAG

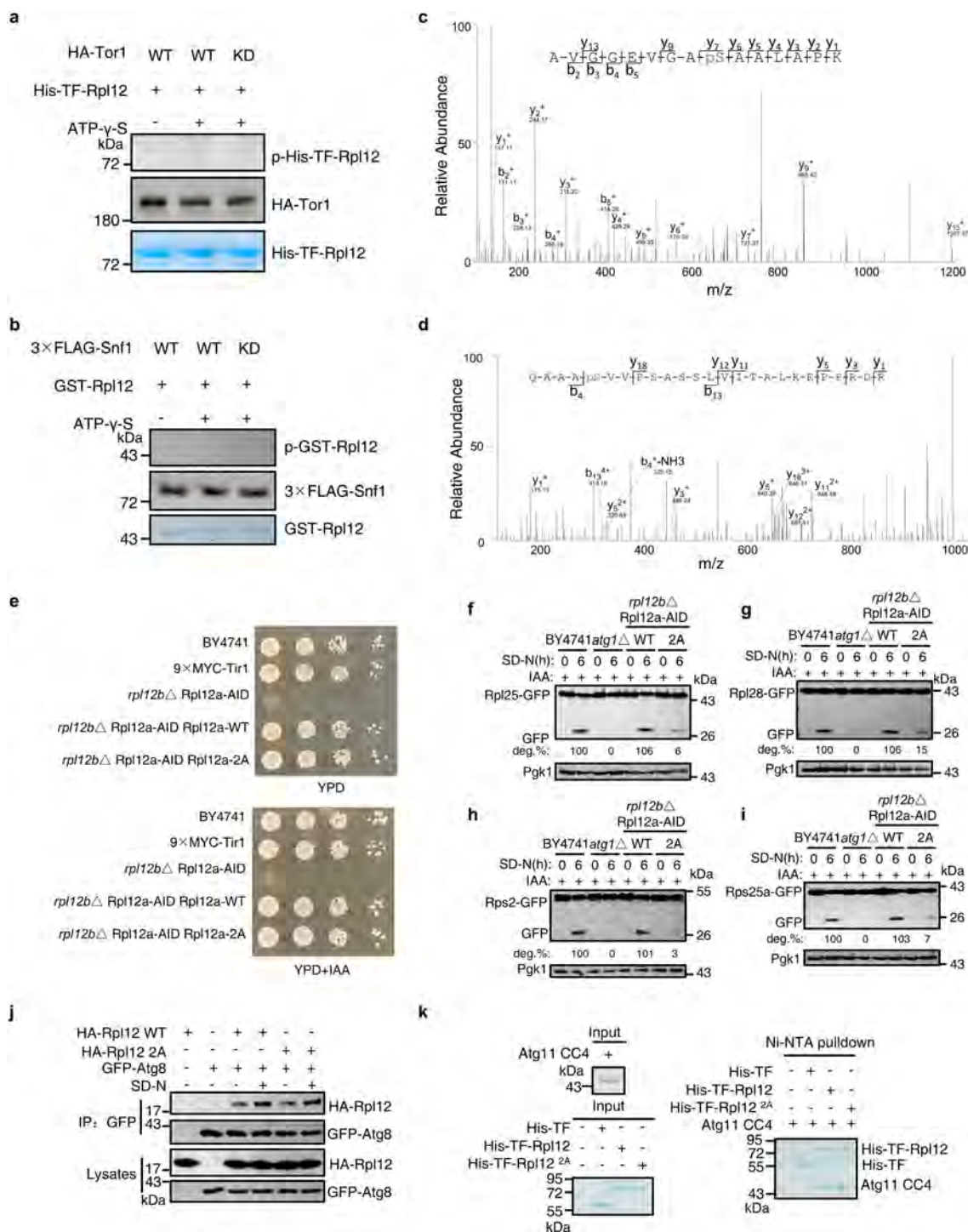
(Rpl34b-AID) or Rps9b-mini-AID-3 $\times$ FLAG (Rps9b-AID) were subjected to 0.5 mM IAA treatment for 0 or 2 h, Rps9a/Rpl34b-AID expression was detected by anti-FLAG antibody. The data are representatives of two independent experiments. **r**, The indicated yeast cells expressing GFP-tagged ribosomal proteins were treated with IAA for 2 h, and then subjected to SD-N for 0 or 6 h. Ribophagic activity were analyzed by western blot for the cleavage of GFP fusion protein. The results were quantified (see Methods). **s**, Total RNA of the indicated yeast cells was extracted to assess rRNA levels. **t**, Yeast rRNAs from **(s)** were quantified. Pgl1 served as a loading control. Blots, gels, and Y2H assays are representatives of three independent experiments unless specified in the legends. \*\*\* $P < 0.001$ , ns, no significance.  $P$  values were calculated by two-tailed Student's  $t$  tests (**c, m, o, t**) and data are presented as mean  $\pm$  s.d. ( $n = 3$  biological replicates). Exact  $P$  values, source numerical data and unprocessed blots/gels are available in Source data.



### Extended Data Fig. 3 | Vacuole is required for the degradation of ribosomal proteins and rRNAs under starvation conditions.

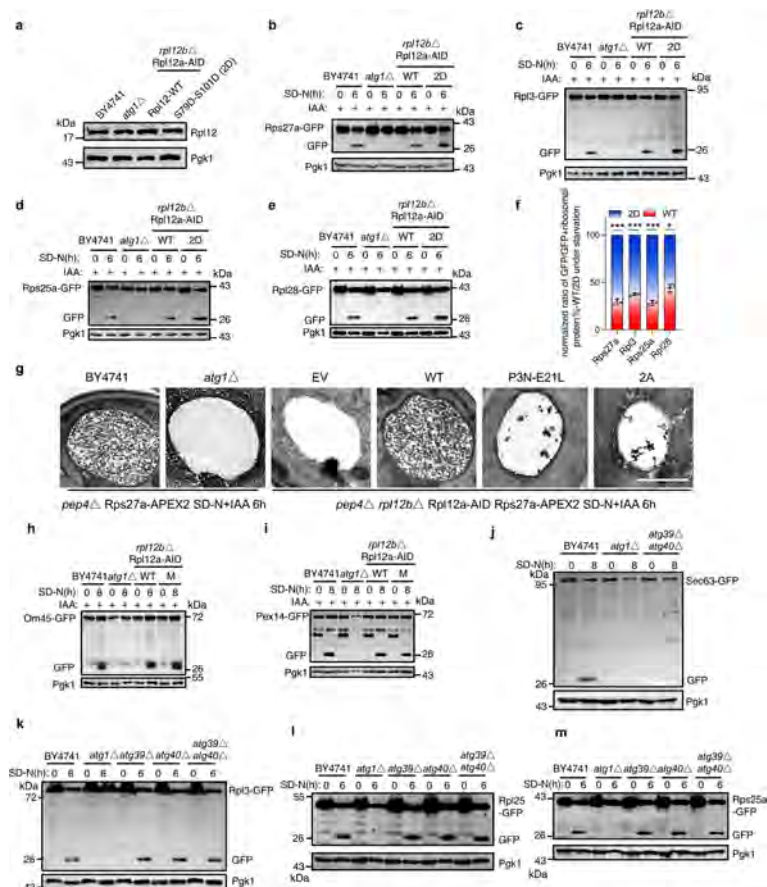
**a**, The indicated yeast cells were subjected to SD-N for the indicated times and protein levels were analyzed by western blot. **b**, Degradation ratios of proteins in (a) were quantified. **c**, WT, *pep4Δ*, or *atg1Δ* yeast cells were grown to mid-log phase, pretreated with 100  $\mu$ g/ml cycloheximide (CHX) for 1 h, and subsequently treated with 0.2  $\mu$ g/ml rapamycin for 0, 2, 4, and 6 h. Ribosomal proteins were analyzed by Western blot. **d**, Degradation ratios of proteins in (c) were quantified. **e**, BY4741, *my1Δ*, or *atg1Δ* yeast cells were subjected to SD-N for 0, 2, 4, or 6 h. Total RNA was extracted from SOD yeast cells to assess rRNA levels. **f**, Yeast rRNA from (e) was quantified. **g**, The indicated yeast cells were treated with IAA for 2 h and then subjected to SD-N for 0 or 6 h. Total RNA was extracted from SOD yeast cells to assess rRNA levels. **h**, The rRNA levels from (g) were quantified. **i**, The indicated yeast cells were

treated with IAA for 2 h and then subjected to SD-N for 0 or 6 h. A total of 5 OD<sub>600</sub> yeast cells were harvested, and total RNA was extracted to assess yeast rRNA levels. **j**, The rRNA levels from panels (i) were quantified. **k-n**, The indicated yeast cells expressing the indicated ribosomal proteins fused with GFP tags were treated with IAA for 2 h, and then subjected to SD-N for 0 or 6 h. Ribophagic activity were analyzed by western blot to detect cleavage of GFP-fusion protein. Pgk1 served as a loading control. Blots and gels are representatives of three independent experiments. Statistical significance: \*\*\* $P < 0.001$ , ns, no significance.  $P$  values were calculated by two-tailed Student's  $t$  tests (**b**, **d**, **f**, **h**, **j**) and the data are presented as mean  $\pm$  SD ( $n = 3$  biological replicates). Exact  $P$  values, source numerical data and unprocessed blots/gels are provided in Source data.



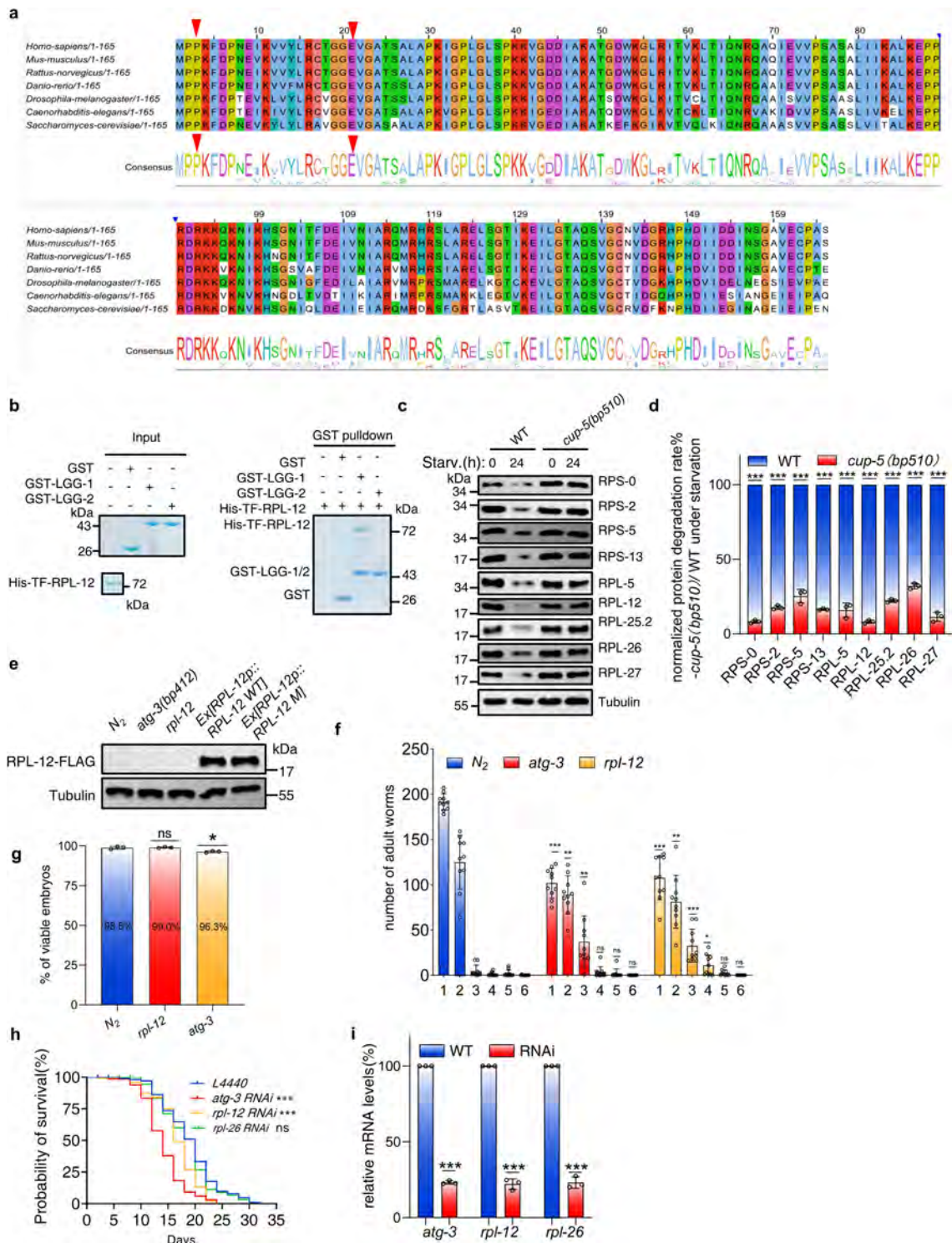
**Extended Data Fig. 4 | Rpl12 is a substrate for Atg1 and the identification of phosphorylation sites on Rpl12 by Atg1.** **a**, *In vitro* kinase assays were performed using purified His-TF-Rpl12 from *E. coli* as substrates, with purified HA-Tor1 or HA-Tor1 KD (kinase dead) from yeast cells serving as protein kinase. The phosphorylation level of His-TF-Rpl12 was detected using an anti-thioP antibody. **b**, *In vitro* kinase assays were performed using purified GST-Rpl12 from *E. coli* as substrates, with purified glucose-starved 3× FLAG-Snf1 or 3× FLAG-Snf1 KD (kinase dead) from yeast cells as protein kinase. The phosphorylation level of GST-Rpl12 was detected using an anti-thioP antibody. **c, d**, Mass spectrometry identified that residues S79 and S174 of Rpl12 are phosphorylated by Atg1. **e**, BY4741, 9× MYC-TIR1 cells, *rpl12b*Δ Rpl12a-AID cells, *rpl12b*Δ Rpl12a-AID + WT Rpl12a cells, and *rpl12b*Δ Rpl12a-AID + Rpl12a-2A cells were grown on YPD or

YPD supplemented with 0.5 mM IAA agar plate for 2 d at 30 °C. **f-i**, The indicated yeast cells were treated with IAA for 2 h, and then subjected to SD-N for 0 or 6 h. Ribophagic activity were analyzed by western blot to detect cleavage of GFP-fusion proteins. The results were quantified (see Methods). **j**, Yeast cells co-expressing either HA-Rpl12 or HA-Rpl12 2A with GFP-Atg8 were subjected to SD-N for 0 or 1 h. Cell lysates were immunoprecipitated using anti-GFP agarose beads and analyzed by western blot using an anti-HA antibody. **k**, Ni-NTA pull-down assays were performed using His-TF-Rpl12 or His-TF-Rpl12 2A with Atg11 CC4 protein from *E. coli*. Pgk1 served as a loading control. Blots, gels, and Y2H assays are representatives of three independent experiments. Unprocessed blots/gels are provided in Source data.



**Extended Data Fig. 5 | Rpl12 is specifically required in yeast ribophagy under starvation conditions.** **a**, BY4741, *atg1* $\Delta$ , or *rpl12b* $\Delta$  Rpl12a-AID cells expressing either wild-type (WT) Rpl12 or Rpl12<sup>S79D-S101D</sup> (2D) were grown to the log phase, harvested, and analyzed using an anti-Rpl12 antibody. The data are representative of two independent experiments. **b–e**, The indicated yeast cells were treated with IAA for 2 h, followed by incubation in SD-N for 0 or 6 h. Ribophagic activity were analyzed by western blot to detect the cleavage of GFP-fusion proteins. **f**, Ribophagic activity from (**b–e**) was quantified. **g**, The indicated yeast cells were treated with IAA for 2 h, then subjected to SD-N for 6 h, followed by performed the APEX-EM analysis. Scale Bar: 500 nm. **h, i**, The indicated yeast cells expressing Om45-GFP or Pex14-GFP were treated with IAA for 2 h, then subjected to SD-N for 0 or 8 h. Protein samples were analyzed by

western blot using an anti-GFP antibody. **j**, BY4741 cells, *atg1* $\Delta$  cells, or *atg39* $\Delta$  *atg40* $\Delta$  cells expressing with Sec63-GFP were subjected to SD-N for 0 or 8 h. ER-phagy activity was analyzed by western blot using an anti-GFP antibody. **k–m**, The indicated cells expressing Rpl3-GFP, Rpl25-GFP, or Rps25a-GFP were subjected to SD-N for 0 or 6 h. Ribophagic activity was analyzed by western blot using an anti-GFP antibody. Pgk1 served as a loading control. The data are representatives of three independent experiments unless specified in the legends. Statistical significance: \*\*\* $P < 0.001$ , \* $P < 0.05$ .  $P$  values were calculated by two-tailed Student's  $t$  tests (**f**) and the data are presented as mean  $\pm$  s.d. ( $n = 3$  biological replicates). Exact  $P$  values, source numerical data and unprocessed blots are provided in Source data.

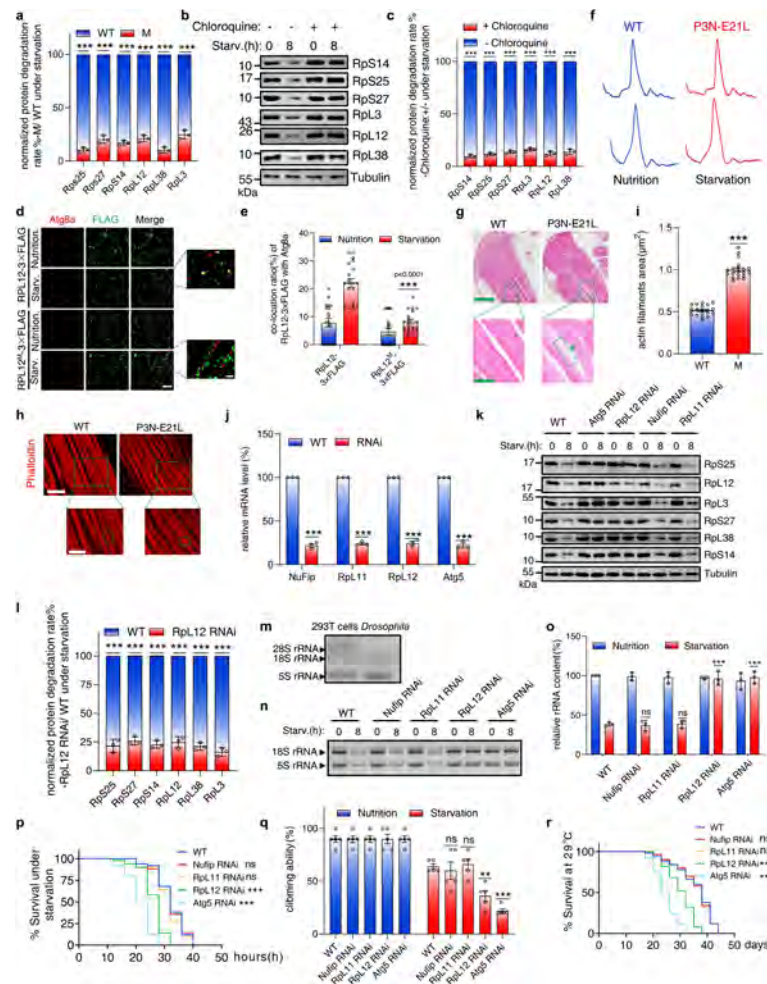


Extended Data Fig. 6 | See next page for caption.

**Extended Data Fig. 6 | The Rpl12 P3 and E21 residues are highly conserved across species and *rpl-12(sb7750[P3N-E21L])* mutations impair worm growth and development.**

**a**, Amino acid sequence alignment of the RPL12 protein across different species. **b**, GST pulldown assays were performed using His-TF-RPL-12 protein and GST-LGG-1 or GST-LGG-2 from *E. coli*. The samples were separated by SDS-PAGE and visualized using Coomassie blue staining. **c**, Wild-type or *cup-5* mutant worms were starved for 0 h or 24 h. Ribosomal protein levels were assessed by western blotting using the indicated antibodies, with Tubulin serving as a loading control. **d**, Degradation ratios of the indicated proteins from **(c)** were quantified and presented as mean  $\pm$  s.d. ( $n = 3$  biological replicates). two-tailed Student's *t* tests were used. **e**, Western blot analysis showing the expression levels of RPL-12-3 $\times$  FLAG and RPL-12<sup>P3N-E21L</sup>-3 $\times$  FLAG in the indicated worm strains. The data shown are representative of two independent experiments. **f**, Quantification of the number of normal adult worms per day for each strain ( $n = 10$ ). All values

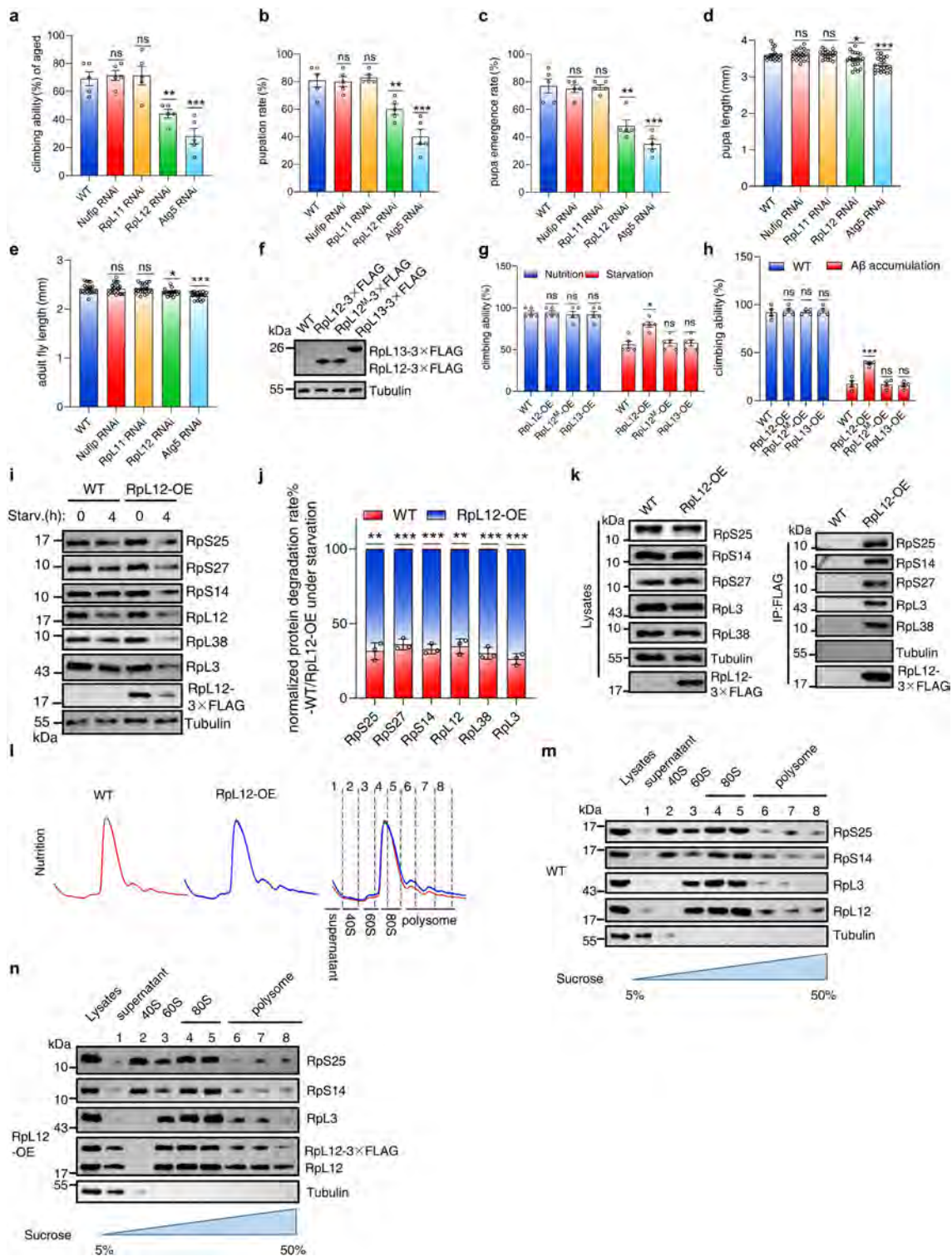
are presented as mean  $\pm$  s.d. ( $n = 3$  biological replicates). two-tailed Student's *t* tests were used. **g**, The percentage of embryos that hatched normally into larvae for each strain. ( $n = 3$  biological replicates, 1<sup>st</sup> repeat:  $N_2 = 722$ , *rpl-12(syb7750)* = 654, *atg-3(bp412)* = 436. 2<sup>nd</sup> repeat:  $N_2 = 479$ , *rpl-12(syb7750)* = 672, *atg-3(bp412)* = 346. 3<sup>rd</sup> repeat:  $N_2 = 615$ , *rpl-12(syb7750)* = 864, *atg-3(bp412)* = 490). Two-tailed Student's *t* tests were used. **h**, Lifespan analyses were performed for each strain at 20 °C. *P* values were calculated using the Log-rank (Mantel-Cox) test (*L4440* = 102, *atg-3 RNAi* = 66, *rpl-12 RNAi* = 100, *rpl-26 RNAi* = 90). **i**, RNAi efficiency was validated by RT-PCR. *ama-1* was used as an internal reference gene. Data are shown as mean  $\pm$  s.d. ( $n = 3$  biological replicates). two-tailed Student's *t* tests were used. Blots and gels are representatives of three independent experiments unless specified in the legends. Statistical significance: \*\*\**P* < 0.001, \*\**P* < 0.01, \**P* < 0.05, ns: no significance. Exact *P* values, source numerical data and unprocessed blots/gels are provided in Source data.



### Extended Data Fig. 7 | RPL12 is crucial for maintaining cellular homeostasis in *Drosophila*.

**a**, Degradation ratios from Fig. 6d were quantified. **b**, Ribosomal protein levels were analyzed after treated with chloroquine and starved for 8 h. **c**, The degradation ratios from (b) were quantified. **d**, Co-localization of Atg8a with Rpl12-3×FLAG or Rpl12<sup>P3N-E21L</sup>(M)-3×FLAG in muscle tissues. Scale bar: 3 μm (overview) and 1 μm (insets: magnified views). **e**, is the quantitation of **d** (n = 20). **f**, Ribosome profiling was analyzed in starved WT and Rpl12 P3N-E21L flies' thorax. **g**, Sections of fly muscle tissues were stained with hematoxylin and eosin (H&E). Muscle degeneration is indicated by an arrow. Scale bar: 120 μm (overview) and 30 μm (insets: magnified views). **h**, Actin networks in thorax tissues were analyzed using phalloidin-TRITC staining. Expanded Z-line is indicated. Scale bar: 12 μm (overview) and 7 μm (insets: magnified views). **i**, is the quantitation of (h) (n = 20). **j**, RNAi efficiency was validated. **k**, The levels of ribosomal proteins following starvation treatment. **l**, is the quantitation

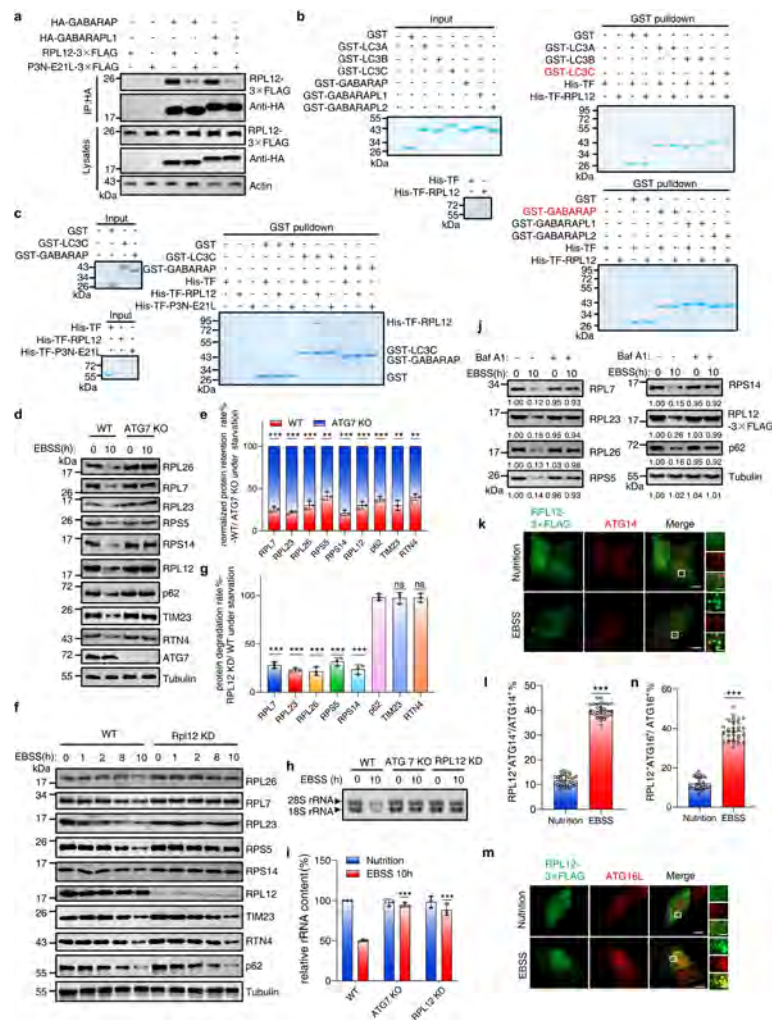
of (k). **m**, Total RNA from HEK293T cells or flies were analyzed. **n**, rRNA levels were assessed following starvation treatment. **o**, is the quantitation of (n). **p**, Starvation sensitivity of the indicated flies. n = 50. **q**, Climbing abilities of indicated flies under starvation condition (5 groups, n = 10 each). **r**, Lifespans of indicated flies at 29 °C. n = 50. Tubulin served as a loading control in immunoblot. MHC-Gal4 was used to drive the knockdown and expression of relevant genes in indirect flight muscle (d, j, k, m, p). Data in b, d, g, h, k, m, n are representative of three independent experiments, n = 15 for each replicate in a-c and k-n. P values were calculated by two-tailed Student's t tests (a, c, e, i, j, l, o, q) and data are shown as mean ± s.d. The Log-rank (Mantel-Cox) test (p, r) was used to analyze differences in survival rates. Statistical significance: \*\*\*P < 0.001, \*\*P < 0.01, ns: no significance. Exact P values, source numerical data, and unprocessed blots are provided in Source data.



Extended Data Fig. 8 | See next page for caption.

**Extended Data Fig. 8 | Overexpression of RPL12 promotes starvation-induced ribophagy in *Drosophila*.** **a**, Age-induced impairment of climbing ability was tested in WT, *RpL12*, *RpL11*, *Nufip*, and *Atg5* RNAi flies. Data are shown as mean  $\pm$  s.d. (5 groups,  $n = 10$  for each group). **b-e**, Pupation (**b**), pupa emergence rate (**c**), as well as lengths of pupa (**d**) and adult flies (**e**) were quantified in wild-type (WT), *RpL12*, *RpL11*, *Nufip*, and *Atg5* RNAi flies. Data are shown as mean  $\pm$  s.d. (**b, c**, 5 groups,  $n = 20$  each; **d, e**,  $n = 20$ ). **f**, Expression levels of RpL12-3 $\times$ FLAG, RpL12<sup>P3N-E21L</sup>(M)-3 $\times$ FLAG and RpL13-3 $\times$ FLAG proteins were analyzed by western blot. Data are representative of two independent experiments. **g**, Climbing abilities of the indicated flies were quantified under starvation conditions. Data are shown as mean  $\pm$  s.d. (5 groups,  $n = 10$  each). **h**, Overexpression of wild-type RpL12 mitigates the loss of climbing ability induced by A $\beta$ 42. Elav-Gal4 was used to drive overexpression of RpL12, RpL12 P3N-E21L and RpL13 in the fly central nervous system (CNS). Data are shown as mean  $\pm$  s.d. (4 groups,  $n = 20$  each). **i**, WT flies

and flies overexpressing RpL12-3 $\times$ FLAG were subjected to starvation for 0 or 4 h. Ribophagic activity was assessed by measuring ribosomal protein levels before and after starvation. **j**, Degradation ratios from (**i**) were quantified and presented as mean  $\pm$  s.d. **k**, Cell lysates were immunoprecipitated with anti-FLAG agarose beads and analyzed with the indicated antibodies. **l**, Ribosome profiling was performed in WT and RpL12-OE flies under nutrient-rich conditions. **m, n**, The fractions isolated from (**l**) were analyzed by western blot using the indicated antibodies. Tubulin served as a loading control in immunoblot. MHC-Gal4 was used to drive the expression of relevant genes in indirect flight muscle (**f, g, k**). Data in (**i-k, m, n**) are representative of three independent experiments,  $n = 15$  for each replicate in **f, i-k**. *P* values were calculated by two-tailed Student's *t* tests (**a-e, g, h, j**). \*\*\**P* < 0.001, \*\**P* < 0.01, \**P* < 0.05, ns: no significance. Exact *P* values, source numerical data, and unprocessed blots are provided in Source data.



**Extended Data Fig. 9 | RPL12 regulates ribosome turnover in mammalian cells.** **a**, HEK293T cells were co-transfected with hRPL12-3×FLAG or hRPL12<sup>P33N-E21L</sup>-3×FLAG, along with HA-GABARAP or HA-GABARAPL1. The cells were starved with EBSS for 1 h. Cell lysates were immunoprecipitated using anti-HA agarose beads and analyzed by western blot with an anti-FLAG antibody. **b**, GST pull-down assays were performed using His-TF and His-TF-hRPL12 proteins with GST, GST-LC3s, or GST-GABARAPs expressed in *E. coli*. **c**, GST pull-down assays were performed using purified His-TF, His-TF-hRPL12, or His-TF-hRPL12<sup>P33N-E21L</sup> proteins with GST, GST-LC3C, or GST-GABARAP proteins expressed in *E. coli*. **d**, WT and ATG7 KO HEK 293 T cells were starved with EBSS for 0 or 10 h. Western blot analysis assessed protein levels. **e**, Degradation ratios from (**d**) were quantified. **f**, WT and Rpl12 KD stable HEK293T cells were starved for 10 h, and ribophagy activity was assessed by western blot for ribosomal proteins degradation. **g**, Degradation ratios from (**f**) were quantified. **h**, The indicated cell lines were subjected to EBSS

starvation for 0 or 10 h, and total RNA was extracted for analysis. **i**, rRNAs levels from (**h**) were quantified and normalized to wild-type. **j**, RPL12 knockdown cells were transfected with the RPL12-3×FLAG plasmid and treated with EBSS alone or EBSS combined with Bafilomycin A1 for 0 or 10 h. Protein samples were analyzed by western blot. **k**, **m**, U2OS cells expressing RPL12-3×FLAG were stained with anti-FLAG and anti-ATG14 (**k**) or anti-ATG16L (**m**) antibodies after EBSS starvation for 0 or 1 h. Scale bar: 10 μm (overview) and 2 μm (insets: magnified views). **l**, **n**, Co-localization of RPL12-3×FLAG with ATG14 (**l**) or ATG16L (**n**) ( $n = 30$  cells) were quantified from (**k**) and (**m**). Actin and Tubulin served as the loading control. Blots, gels and imaging data are representatives of three independent experiments. Statistical significance: \*\*\* $P < 0.001$ , \*\* $P < 0.01$ , ns: no significance.  $P$  values were calculated by two-tailed Student's  $t$  tests (**e**, **g**, **i**, **l**, **n**) and the data are presented as mean  $\pm$  s.d. ( $n = 3$  biological replicates). Exact  $P$  values, source numerical data and unprocessed blots/gels are provided in Source data.



## Reporting Summary

Nature Portfolio wishes to improve the reproducibility of the work that we publish. This form provides structure for consistency and transparency in reporting. For further information on Nature Portfolio policies, see our [Editorial Policies](#) and the [Editorial Policy Checklist](#).

### Statistics

For all statistical analyses, confirm that the following items are present in the figure legend, table legend, main text, or Methods section.

n/a Confirmed

- The exact sample size ( $n$ ) for each experimental group/condition, given as a discrete number and unit of measurement
- A statement on whether measurements were taken from distinct samples or whether the same sample was measured repeatedly
- The statistical test(s) used AND whether they are one- or two-sided  
*Only common tests should be described solely by name; describe more complex techniques in the Methods section.*
- A description of all covariates tested
- A description of any assumptions or corrections, such as tests of normality and adjustment for multiple comparisons
- A full description of the statistical parameters including central tendency (e.g. means) or other basic estimates (e.g. regression coefficient) AND variation (e.g. standard deviation) or associated estimates of uncertainty (e.g. confidence intervals)
- For null hypothesis testing, the test statistic (e.g.  $F$ ,  $t$ ,  $r$ ) with confidence intervals, effect sizes, degrees of freedom and  $P$  value noted  
*Give  $P$  values as exact values whenever suitable.*
- For Bayesian analysis, information on the choice of priors and Markov chain Monte Carlo settings
- For hierarchical and complex designs, identification of the appropriate level for tests and full reporting of outcomes
- Estimates of effect sizes (e.g. Cohen's  $d$ , Pearson's  $r$ ), indicating how they were calculated

*Our web collection on [statistics for biologists](#) contains articles on many of the points above.*

### Software and code

Policy information about [availability of computer code](#)

#### Data collection

Detection of mass spectrometry samples using a Thermo EASY-nLC1200 integrated nano-HPLC system and a Thermo Q Exactive HF-X mass spectrometer.  
Olympus IX83, Zeiss LSM 800/900 and Tecnai G2 Spirit 120V were used to collect microscopic images.  
Shanghai Yuehe Biotechnology's upright fluorescence microscope YHF21 is used for observing HE-stained sections.  
Miniature Chemiluminescence Imaging System MiniChemi was used to scan blots.  
BIOCOMP 153 (an ISCO gradient collector) was used for detecting the absorbance at different positions in a sucrose solution.  
Clix Science Instruments's GenoSens 2100 was used to detect RNA content.  
ZSDICHUANG's Labmazewas used to detect behavior ability of *Drosophila melanogaster*.  
Peptide separation was performed using an Easy-nLC 1200 system coupled to a ThermoFisher Orbitrap Exploris 480 mass spectrometer.

#### Data analysis

Statistical analysis was performed using GraphPad Prism 8.  
Graph were generated by GraphPad Prism 8.  
Image processing and blot data analyzing was performed using the Fiji ImageJ software.  
Each mass spectrometry result underwent analysis using Thermo Xcalibur Qual Browser and Proteome Discovery for subsequent database searching.  
The ultraviolet absorption peak graph is displayed by the Flow Cell software(version 1.56A).  
Cross-linked peptides were identified using pLink2 software(version 2.3.11).  
The R package DESeq2 (version 1.34.0) was employed to identify components with different abundance in MS.

For manuscripts utilizing custom algorithms or software that are central to the research but not yet described in published literature, software must be made available to editors and reviewers. We strongly encourage code deposition in a community repository (e.g. GitHub). See the Nature Portfolio [guidelines for submitting code & software](#) for further information.

## Data

Policy information about [availability of data](#)

All manuscripts must include a [data availability statement](#). This statement should provide the following information, where applicable:

- Accession codes, unique identifiers, or web links for publicly available datasets
- A description of any restrictions on data availability
- For clinical datasets or third party data, please ensure that the statement adheres to our [policy](#)

The mass spectrometry proteomics data have been deposited to the ProteomeXchange Consortium (<http://proteomecentral.proteomexchange.org>) via the PRIDE repository 55,56 (<ftp://massive.ucsd.edu/v08/MSV000096540/> and <ftp://massive.ucsd.edu/v08/MSV000096542/>), with the dataset identifier MassIVE MSV000096540(or PXD058305) and MSV000096542(or PXD058307). The raw LC-MS-based untargeted metabolomics data files generated in this study are available at the National Genomics Data Center57 (<https://ngdc.cncb.ac.cn/omix/releaseList>) with the dataset identifier OMIX008012 and are publicly available. Source data are provided with this paper. All of the other data supporting the findings of this study are available from the corresponding author upon reasonable request.

## Research involving human participants, their data, or biological material

Policy information about studies with [human participants or human data](#). See also policy information about [sex, gender \(identity/presentation\), and sexual orientation](#) and [race, ethnicity and racism](#).

Reporting on sex and gender	<input type="text" value="n/a"/>
Reporting on race, ethnicity, or other socially relevant groupings	<input type="text" value="n/a"/>
Population characteristics	<input type="text" value="n/a"/>
Recruitment	<input type="text" value="n/a"/>
Ethics oversight	<input type="text" value="n/a"/>

Note that full information on the approval of the study protocol must also be provided in the manuscript.

## Field-specific reporting

Please select the one below that is the best fit for your research. If you are not sure, read the appropriate sections before making your selection.

- Life sciences       Behavioural & social sciences       Ecological, evolutionary & environmental sciences

For a reference copy of the document with all sections, see [nature.com/documents/nr-reporting-summary-flat.pdf](https://nature.com/documents/nr-reporting-summary-flat.pdf)

## Life sciences study design

All studies must disclose on these points even when the disclosure is negative.

Sample size	The chosen sample sizes were similar to those previously used by us and others in this field and make the data statistically significant. For example, n=20-35 cells from 3 experiments/dished were included when conclusions were based on immunofluorescent staining( Relevant literature:PMID: 37043189 ). Images of C.elegans (n=20-25) were analyzed( Relevant literature: PMID: 39511227).About 300 cells were counted when observing the image of yeast cells( Relevant literature:PMID: 34314677). In the Drosophila climbing assay, each cohort had at least 15 flies (n ≥ 15). When conclusions were based on Drosophila staining, at least 5 flies per genotype were included (Relevant literature: PMID: 38996009).
Data exclusions	No data was excluded.
Replication	Numbers of replicates were stated in the figure legends.
Randomization	All samples were randomly allocated to experimental. For example,In the worm and fly experiments, age-matched individuals with different genotypes were randomly assigned to experimental groups. For cell culture experiments, cells with different genotypes or treatments were randomly distributed into experimental groups. In the animal experiments, age-matched mice were randomly assigned to different experimental groups.
Blinding	Except for MS-based analysis, the investigators were not blinded to allocation during experiments and outcome assessment.

## Reporting for specific materials, systems and methods

## Materials & experimental systems

## Methods

n/a	Involved in the study
<input type="checkbox"/>	<input checked="" type="checkbox"/> Antibodies
<input type="checkbox"/>	<input checked="" type="checkbox"/> Eukaryotic cell lines
<input checked="" type="checkbox"/>	<input type="checkbox"/> Palaeontology and archaeology
<input type="checkbox"/>	<input checked="" type="checkbox"/> Animals and other organisms
<input checked="" type="checkbox"/>	<input type="checkbox"/> Clinical data
<input checked="" type="checkbox"/>	<input type="checkbox"/> Dual use research of concern
<input checked="" type="checkbox"/>	<input type="checkbox"/> Plants

n/a	Involved in the study
<input checked="" type="checkbox"/>	<input type="checkbox"/> ChIP-seq
<input checked="" type="checkbox"/>	<input type="checkbox"/> Flow cytometry
<input checked="" type="checkbox"/>	<input type="checkbox"/> MRI-based neuroimaging

## Antibodies

### Antibodies used

anti-Pgk1 (Nordic Immunology, NE130/7S; 1:10,000), anti-FLAG (Sigma, F1804; 1:2,500) for WB, anti-FLAG(TRAN, R10427; 1:600) for immunostaining, anti-HA (Abmart, M20003L; 1:3,000), anti-thiophosphate ester (Abcam, ab133473; 1:10,000), anti-GFP (Roche, 11814460001; 1:2,500), anti-His(Proteintech, Hrp-66005, 1:2000), anti-RPL12 (Proteintech, 14536-1-AP P, 1:2000), anti-RPL23 (Proteintech, 16086-1-AP, 1:2000), anti-RPL7 (Proteintech, 14583-1-AP, 1:2000), anti-RPS5 (Proteintech, 16964-1-AP, 1:2000), anti-RPL26 (Proteintech, 17619-1-AP, 1:2000), anti-RPS14 (Proteintech, 16683-1-AP, 1:2000), anti-Atg7 (Proteintech, 10082-2-AP, 1:5000), anti-Tubulin (Proteintech, 11224-1-AP, 1:10000), anti-TIM23 (Proteintech, 11123-1-AP, 1:3000), anti-RTN4 (Proteintech, 10950-1-AP, 1:3000), anti-p62/SQSTM1 (Proteintech, 18420-1-AP, 1:5,000), anti-LC3 (MBL, PM036, 1:1,000), anti-Cherry (Biodragon, B1026, 1:2000), anti-ATG14(Proteintech, 19491-1-AP, 1:100), anti-ATG16L(Proteintech, 29445-1-AP, 1:100), anti-Atg8a (millipore, ABC974; 1:2000 for WB; 1:600 for immunostaining), anti-Ape1 antibody was obtained from Dr. Zhiping Xie Lab (Shanghai Jiaotong University, China), anti-RPS-0, anti-RPL-5, and anti RPL-25-2 antibodies was obtained from Dr. Xiaochen Wang (IBP, Chinese Academy of Sciences, China), goat anti-mouse IgG1, human ads-HRP (SouthernBiotech, 1070-05; 1:10,000); goat anti-rabbit, human ads-HRP (SouthernBiotech, 4010-05; 1:10,000) Goat anti-Mouse IgG H&L Alexa Fluor® 488, ( Abcam, cab150113; 1:1000); Goat anti-Rabbit IgG H&L Alexa Fluor® 594 (Abcam, ab150080; 1:1000). Anti-Rps2, anti-Rps5, anti-Rpl12, anti-Rpl25, and anti-Rpl38 antibodies for *S. cerevisiae*; anti-RPS-2, anti-RPS-5, anti-RPS-13, anti-RPL-12, anti-RPL-26, and anti-RPL-27 antibodies for *C. elegans*; anti-RpS14, anti-RpS25, anti-RpS27, anti-RpL3, anti-RpL12, and anti-RpL38 for *D. melanogaster* were produced by Biodragon Company, China.

### Validation

anti-Pgk1 (Nordic Immunology, NE130/7S; 1:10,000)  
This antibody has been discontinued, and no relevant webpage information can be found.  
Publications: PMID: 29114050

anti-FLAG (Sigma, F1804; 1:2,500) for WB, anti-FLAG(TRAN, R10427; 1:600) for immunostaining,  
<https://www.sigmaaldrich.cn/CN/zh/product/sigma/f1804>  
Species specificity: Mouse  
Applications: WB, IP, IF, IHC  
Publications: PMID: 31176697

anti-HA (Abmart, M20003L; 1:3,000)  
<https://www.ab-mart.com.cn/page.aspx?node=%2059%20&id=%20963>  
Species specificity: Mouse  
Applications: WB, IF, IHC,IP/ ChIP, ELISA  
Publications: PMID: 38163844

anti-thiophosphate ester (Abcam, ab133473; 1:10,000)  
<https://www.abcam.cn/products/primary-antibodies/thiophosphate-ester-antibody-51-8-ab133473.html>  
Species specificity: Rabbit  
Applications: IP  
Publications: PMID: 33988507

anti-GFP (Roche, 11814460001; 1:2,500)  
<https://www.sigmaaldrich.cn/CN/zh/product/roche/11814460001>  
Species specificity: Mouse  
Applications: IP, WB, IF  
Publications: PMID: 21803848

anti-His (Proteintech, HRP-66005, 1:2000)  
<https://www.ptgcn.com/products/6-His-His-Tag-Antibody-HRP-66005.htm>  
Species specificity: Mouse  
Applications: WB, IP, CoIP, ELISA  
Publications: PMID: 32579975

anti-RPL12 (Proteintech, 14536-1-AP P, 1:2000)  
<https://www.ptgcn.com/products/RPL12-Antibody-14536-1-AP.htm>  
Species specificity: Rabbit  
Applications: WB, ELISA  
Publications: PMID: 32040547

anti-RPL23 (Proteintech, 16086-1-AP, 1:2000)  
<https://www.ptgcn.com/products/RPL23-Antibody-16086-1-AP.htm>  
Species specificity: Rabbit  
Applications: WB, IP, IHC, ELISA  
Publications: PMID: 27992407

anti-RPL7 (Proteintech, 14583-1-AP, 1:2000)  
<https://www.ptgcn.com/products/RPL7-Antibody-14583-1-AP.htm>  
Species specificity: Rabbit  
Applications: WB, IHC, IF/ICC, IP, ELISA  
Publications: PMID: 38302992

anti-RPS5 (Proteintech, 16964-1-AP, 1:2000)  
<https://www.ptgcn.com/products/RPS5-Antibody-16964-1-AP.htm>  
Species specificity: Rabbit  
Applications: WB, IHC, IF/ICC, ELISA  
Publications: PMID: 28759050

anti-RPL26 (Proteintech, 17619-1-AP, 1:2000)  
<https://www.ptgcn.com/products/RPL26-Antibody-17619-1-AP.htm>  
Species specificity: Rabbit  
Applications: WB, IF/ICC, ELISA  
Publications: PMID: 31792210

anti-RPS14 (Proteintech, 16683-1-AP, 1:2000)  
<https://www.ptgcn.com/products/RPS14-Antibody-16683-1-AP.htm>  
Species specificity: Rabbit  
Applications: WB, IHC, ELISA  
Publications: PMID: 22718973

anti-Atg7 (Proteintech, 10082-2-AP, 1:5000)  
<https://www.ptgcn.com/products/MATK-Antibody-10082-2-AP.htm>  
Species specificity: Rabbit  
Applications: WB, IHC, IF/ICC, ELISA  
Publications: PMID: 33524783

anti-Tubulin (Proteintech, 11224-1-AP, 1:10000)  
<https://www.ptgcn.com/products/TUBA1B-Antibody-11224-1-AP.htm>  
Species specificity: Rabbit  
Applications: WB, IHC, IF/ICC, FC (Intra), IP, ELISA  
Publications: PMID: 36593399

anti-TIM23 (Proteintech, 11123-1-AP, 1:3000)  
<https://www.ptgcn.com/products/TIMM23-Antibody-11123-1-AP.htm>  
Species specificity: Rabbit  
Applications: WB, IHC, IF/ICC, IP, ELISA  
Publications: PMID: 36477540

anti-RTN4 (Proteintech, 10950-1-AP, 1:3000)  
<https://www.ptgcn.com/products/RTN4-Antibody-10950-1-AP.htm>  
Species specificity: Rabbit  
Applications: WB, IHC, IF/ICC, FC (Intra), ELISA  
Publications: PMID: 28102736

anti-p62/SQSTM1 (Proteintech, 18420-1-AP, 1:5,000)  
<https://www.ptgcn.com/products/SQSTM1-Antibody-18420-1-AP.htm>  
Species specificity: Rabbit  
Applications: WB, IHC, IF/ICC, FC (Intra), IP, ELISA  
Publications: PMID: 30487606

anti-LC3 (MBL, PM036, 1:1,000)  
<https://www.mblbio.com/bio/g/dt/A/?pcd=PM036>  
Species specificity: Rabbit  
Applications: WB, IP, FCM, IC, IF  
Publications: PMID:18849965

anti-Cherry (Biodragon, B1026, 1:2000)  
<https://www.biodragon.cn/cn/goods/goodsView?GoodsId=1767>  
Species specificity: Rabbit  
Applications: WB, Elisa

anti-ATG14(Proteintech, 19491-1-AP, 1:100)  
<https://www.ptgcn.com/products/Barkor-Specific-Antibody-19491-1-AP.htm>  
Species specificity: Rabbit  
Applications: WB, IHC, IF/ICC, ELISA

Publications: PMID: 36481655

anti-ATG16L(Proteintech, 29445-1-AP, 1:100)  
<https://www.ptgcn.com/products/ATG16L1-Antibody-29445-1-AP.htm>  
 Species specificity: Rabbit  
 Applications: WB, IHC, IF/ICC, ELISA  
 Publications: PMID: 39261846

anti-Atg8a (millipore, ABC974; 1:2000 for WB; 1:600 for immunostaining)  
<https://www.sigmaaldrich.cn/CN/zh/product/mm/abc974>  
 Species specificity: Rabbit  
 Applications: WB  
 Publications: PMID: 37470098

anti-Ape1 antibody was obtained from Dr. Zhiping Xie Lab (Shanghai Jiaotong University, China)  
 This antibody was prepared by their laboratory and does not have any commercial information.  
 Publications: PMID: 36076954

anti-RPS-0, anti-RPL-5, and anti RPL-25-2 antibodies was obtained from Dr. Xiaochen Wang (IBP, Chinese Academy of Sciences, China)

The following antibodies were prepared by biological companies and finally passed the antibody titer test. The specific antibody against the target protein was obtained by pre-experiment :  
 Anti-Rps2, anti-Rps5, anti-Rpl12, anti-Rpl25, and anti-Rpl38 antibodies for *S. cerevisiae*; anti-RPS-2, anti-RPS-5, anti-RPS-13, anti-RPL-12, anti-RPL-26, and anti-RPL-27 antibodies for *C. elegans*; anti-RpS14, anti-RpS25, anti-RpS27, anti-RpL3, anti-Rpl12, and anti-Rpl38 for *D. melanogaster* were produced by Biodragon Company, China.

## Eukaryotic cell lines

Policy information about [cell lines and Sex and Gender in Research](#)

Cell line source(s)	HEK293T ATCC CRL3216 U2OS ATCC HTB-96 ATG7 KO HEK293T cells were donated by Prof. Sun Qiming from Zhejiang University. RPL12 KD HEK293T cells were constructed in our lab.
Authentication	The U2OS and HEK293T cell lines were authenticated by Procell Life Science&Technology Co.,Ltd (short tandemrepeat profiling). ATG7 KO HEK293T cells and RPL12 KD HEK293T cells were authenticated by Western blot.
Mycoplasma contamination	No test for mycoplasma contamination was performed. But when we do related experiments, we always add mycoplasma scavengers..
Commonly misidentified lines (See <a href="#">ICLAC</a> register)	NO commonly misidentified lines were used

## Animals and other research organisms

Policy information about [studies involving animals](#); [ARRIVE guidelines](#) recommended for reporting animal research, and [Sex and Gender in Research](#)

Laboratory animals	The method section of the article is introduced in detail, specifically, there are the following animals The following <i>C. elegans</i> strains were used in this study: N2, atg-3(bp412), rpl-12(syb7750) (PHX7750, SunyBiotech), daf-2(e1370), rpl-12(syb7750); daf-2(e1370), zacEx2240[rpl-12p::rpl-12 WT cDNA], zacEx2238[rpl-12p::rpl-12 P3N-E21L cDNA], Atg-3 RNAi, Rpl-12 RNAi, Rpl-26 RNAi. Transgenic lines zacEx2240[rpl-12p::rpl-12 WT cDNA], zacEx2238[rpl-12p::rpl-12 mutant cDNA].Experiments with <i>C. elegans</i> typically begin at the L4 stage. The following <i>D. melanogaster</i> strains were used in this study: Elav-Gal4, MHC-Gal4, Da-Gal4, UAS-Atg5 RNAi, UAS-Nufip RNAi, UAS-RPL11 RNAi, UAS-RPL12 RNAi, UAS-RPL13A-FLAG and RPL12(P3N-E21L) mutant flies. Experiments with flies typically begin three days after eclosion. The mice used are Male C57BL/6 mice. Mice were used in experiments starting at 6-8 weeks of age.
Wild animals	No wild animals were used.
Reporting on sex	The mice used in our experiments were all male, a factor considered during the experimental design. Male mice were chosen due to their more stable hormonal levels, which generally result in more consistent physiological and behavioral responses, thereby helping to reduce variability. Male mice were ordered, and their sex was confirmed by checking the anogenital distance. While we used male mice to ensure stability, the conclusions regarding ribosome studies are expected to be independent of sex.
Field-collected samples	No field-collected samples were used.
Ethics oversight	Our research complied with all of the relevant ethical regulations. All of the animal procedures were conducted according to the protocols approved by the Animal Care and Use Committee of the animal facility at Zhejiang University.

Note that full information on the approval of the study protocol must also be provided in the manuscript.

## Plants

### Seed stocks

*Report on the source of all seed stocks or other plant material used. If applicable, state the seed stock centre and catalogue number. If plant specimens were collected from the field, describe the collection location, date and sampling procedures.*

### Novel plant genotypes

*Describe the methods by which all novel plant genotypes were produced. This includes those generated by transgenic approaches, gene editing, chemical/radiation-based mutagenesis and hybridization. For transgenic lines, describe the transformation method, the number of independent lines analyzed and the generation upon which experiments were performed. For gene-edited lines, describe the editor used, the endogenous sequence targeted for editing, the targeting guide RNA sequence (if applicable) and how the editor was applied.*

### Authentication

*Describe any authentication procedures for each seed stock used or novel genotype generated. Describe any experiments used to assess the effect of a mutation and, where applicable, how potential secondary effects (e.g. second site T-DNA insertions, mosaicism, off-target gene editing) were examined.*